

Design and Analysis of Antenna for 5G Wireless Communicationn

*A thesis submitted in fulfilment of the requirements of the degree of
Doctor of Philosophy*

Submitted by
PARUL KANSAL
(2K20/PhDEE/16)

Under the Supervision of

Dr. Anup Kumar Mandpura

Assistant Professor
Department of Electrical Engineering
Delhi Technological University

and

Prof. Narendra Kumar

Professor
Department of Electrical Engineering
Delhi Technological University



**Electrical Engineering Department
Delhi Technological University
Delhi-110042, India
2024**

DECLARATION

I hereby certify that the work which is presented in this thesis entitled “**Design and Analysis of Antenna for 5G Wireless Communication**” submitted in partial fulfillment of the requirements for the award of the degree of Doctor of Philosophy in the Department of Electrical Engineering, Delhi Technological University, Delhi. This is an authentic record of my own work carried out under the supervision of Dr. Anup Kumar Mandpura and Prof. Narendra Kumar. The matter presented in this thesis has not been submitted elsewhere for the award of a degree.

Parul Kansal
(2K20/PhD/EE/16)


Place:
Date:

CERTIFICATE

This is to certify that the thesis entitled “**Design and Analysis of Antenna for 5G Wireless Communication**” being submitted by Ms. Parul Kansal for the award of the degree of **Doctor of Philosophy** in the Department of Electrical Engineering, Delhi Technological University, Delhi, is the record of student’s own work carried out by her under our supervision. The contents of this research work have not been submitted in part or fully to any other institute or university for the award of any degree.

Date:

Dr. Anup Kumar Mandpura
Assistant Professor
Department of Electrical Engineering
Delhi Technological University
Delhi-110042, India


Prof. Narendra Kumar
Department of Electrical Engineering
Delhi Technological University
Delhi-110042, India

ABSTRACT

The fifth generation (5G) technology for cellular communication utilizes three main frequency bands: low band (600-850 MHz), mid band (3.4-3.6 GHz), and high band (24-30 GHz). Each of these bands has some distinct advantages and disadvantages. For fast data communication, 5G networks utilize the mid band frequencies, which also necessitate smaller antenna components. In this thesis we explore Single-Input Single-Output (SISO) and Multi-Input Multi-Output (MIMO) microstrip patch antennas that meet the gain, band-width, efficiency and diversity parameters for 5G wireless technology. Further, simulation, analysis, and testing are conducted to achieve a highly efficient, low-profile MIMO antenna specifically designed for 5G applications.

A microstrip patch antenna for 5G communication with highly reflecting metasurface (MS), excited by a coplanar waveguide (CPW) feed is designed. This antenna is suitable for the frequency band 3.86 GHz to 4.49 GHz. The use of MS enables to achieve a higher gain, wider bandwidth, smaller return losses, and better efficiency. Also, a Fabry Perot cavity-based microstrip patch antenna for 5G communication is investigated to achieve higher gain. The Fabry Perot cavity based antenna used three techniques: a perfect electric conductor (PEC) sheet, high dielectric superstrate, and metasurface superstrate. The size of the PEC sheet needs to be kept large to reflect the radiation resulting in larger antenna size. A high dielectric superstrate provides better return loss and gain as compared to PEC, however it increases the antenna cost. Finally, metasurface superstrate is explored in the design microstrip patch antenna for 5G communication which has better gain, bandwidth and return loss as compared to PEC and dielectric superstrate antennas.

Further, simulation, analysis are also performed to design highly efficient, low-profile MIMO antenna tailored for 5G applications. A closely integrated MIMO patch antennas operating at 3.5 GHz with improved isolation is designed. This configuration comprises of two mirror-symmetrical single-feed patch antennas with a separation of $0.011 \lambda_0$ is implemented. A metasurface is employed as a decoupling structure that consists of pairs

of uniform cut wires. An enhanced isolation of 10dB to 35dB between the closely spaced antennas is achieved by employing the metasurface and gain of 3.85 dBi. Further to reduce antenna size, a two-port circularly polarized (CP) MIMO antenna operating at sub-6 GHz with a distinctive slot and a circular split ring resonator (SRR) at the ground plane is designed. A sequence of parasitic elements in the shape of 'h' is placed in the space between the two antenna elements for decoupling. The designed antenna has an impedance bandwidth of 3.3 to 3.6 GHz, axial ratio bandwidth of 3.35 to 3.51 GHz and minimum 20 dB isolation.

An innovative integrated dual-band MIMO antenna featuring unit cells arranged orthogonally and fed by a CPW is designed. By incorporating a curved design into the antenna's radiator elements, the antenna effectively operates in two resonant frequencies: 3.5 GHz (Wi-Max) and 5.5 GHz (WLAN). This design eliminates the need for additional isolation components while still achieving high isolation. Finally, a triple-band two-port MIMO antenna with self-isolation was designed for the frequency bands: 2.58 GHz to 2.84 GHz, 3.4 GHz to 3.9 GHz, and 4.3 GHz to 4.6 GHz. The gain enhancement, radiation pattern, radiation efficiency, MIMO diversity parameters using microstrip patch antenna and other key aspects are presented in the thesis.

ACKNOWLEDGEMENT

I wish to express my gratitude to **GOD** almighty for giving me the courage and the strength to carry out this project, which opened my doors of knowledge.

I would like to express my deep and sincere gratitude to my supervisors **Dr. Anup Kumar Mandpura** and **Prof. Narendra Kumar** for their valuable guidance and continuous monitoring of my research work. It was great honour for me to pursue my research work under their supervisions. **Prof. Narendra Kumar** has been the motivating and inspiring factor behind my research work. It's his Vigor and hunger to perform in adverse situations that has inspired me to strive for excellence. Continuous monitoring by **Dr. Anup Kumar Mandpura**, valuable guidance and input has always been a driving force to complete my research work. It is a life time experience to work under both of my supervisors and humbly acknowledge lifetime gratitude to them.

I would like to express my thanks to **Prof. Rachna Garg, HOD (EE)** for her kind support. I would like to thank the SRC members who has given me valuable guidance and advice to improve quality of my research work. I am extremely thankful to staff member of Lab **Mr. Mukesh Gupta** for providing me immense facility and assistance to carry out my research work. I would like to thank other office staffs, Central library and Computer Centre staff members, for their valuable co-operation and support.

I owe this moment of great satisfaction to **Dr. Jugal Kishor**, Associate Professor, Department of Electronics and Communication Engineering, ABES Engineering College, Ghaziabad, (India), for his everlasting support and guidance in my Ph.D. He has constantly inspired me to remain focused on achieving my goal. His interest, moral support, and excellent guidance throughout have brought this work to its final stage.

I would like to thank **Dr. Abhay Kumar Singh**, for his unconditional support during my thesis.

I would like to thank **Mr. Amit Kumar Saini**, Director, Cadre Design, India for his help in my research journey.

I am extremely grateful to my research group and friends **Mr. Brijendra sangar, Dr. Arvind Goswami, Mrs. Poonam Dhaka and Mr. Divyansh Shailly** valuable assistance, co-operation and great source of learning.

If I get any success today for my research work, the entire credit should go to my Mother **Smt. Kusum Kansal**, Brother **Mr. Ravi Shanker Kansal**, Sisters **Mrs. Neha Kansal & Mrs. Deepali Kansal** and Father **Shri. Prem Kumar Kansal**. I deeply convey my gratitude to my nephew **Avyukt & Anaya** who has endured me and my long hours spent in the laboratory with patience and encouraged me to carry out my research work.

I would like to thank other family members supporting me directly or indirectly to carry out my research work. Last, but not the least, I thank Mother Nature and Almighty God for providing me the opportunity for pursuing doctoral studies.

Date:

Place:

Parul Kansal
Roll No. 2K20/PHDEE/16

DEDICATED TO MY BELOVED PARENTS

Prem Kumar Kansal

&

Kusum Kansal

TABLE OF CONTENTS

ABSTRACT	i
ACKNOWLEDGEMENTS	iii
LIST OF FIGURES	ix
LIST OF TABLES	xiii
CHAPTER 1 Introduction & Literature Review	1
1.1 Evolution of Mobile Communication	2
1.1.1 1G Communication Systems	2
1.1.2 2G Communication Systems	2
1.1.3 2.5G Communication Systems	3
1.1.4 3G Communication Systems	3
1.1.5 4G Communication Systems	3
1.2 5G Technology	4
1.3 5G Expected Spectrum	5
1.4 Requirements of the Antennas for Future Wireless Technology	6
1.5 Multiple Input Multiple Output (MIMO) antenna	6
1.5.1 Design Factors	10
1.6 Literature Survey	12
1.6.1 Microstrip Antenna	12
1.6.2 High gain antenna	14
1.6.3 MIMO antenna	16
1.7 Motivation and Objective of the Thesis	21
1.8 Design Guidelines of the Antenna	23
1.8.1 Organization of Thesis	25
CHAPTER 2 CPW-Fed Microstrip Patch Antenna for 5G Applications	29
2.1 Introduction	29
2.2 Geometry of the Proposed Antenna	30
2.2.1 Design Procedure CPW-Fed Microstrip Patch Antenna	30
2.2.2 Design of Composite CPW-Fed Microstrip Patch Antenna with Superstrate	31
2.3 Parametric Analysis	32
2.4 Simulated and Analysis of Results	33
2.4.1 S- Parameter	33

2.4.2 Realized Gain	34
2.4.3 Radiation Pattern	34
2.4.4 Beam Scanning	36
2.5 Comparative Performance Analysis of Proposed Antenna with Existing Design	36
2.6 Conclusions	38
CHAPTER 3 High Gain Microstrip Patch Antenna with Fabry-Perot Cavity for 5G Communication	39
3.1 Introduction	39
3.2 Design Procedure of Microstrip Patch Antenna	40
3.2.1 Design Procedure of Metasurface Unit Cell	40
3.2.2 Design Procedure of Microstrip Patch Antenna	41
3.2.3 Design of Proposed Microstrip Patch Antenna with Three Configuration	42
3.4 Parametric Analysis	43
3.5 Results and Analysis of the Antenna	45
3.5.1 S- Parameter	45
3.5.2 Realized Gain	45
3.5.3 Radiation Pattern	46
3.5.4 Efficiency	47
3.6 Comparative Performance Analysis of Proposed Antenna with Existing Design	48
3.7 Conclusions	49
CHAPTER 4 Metasurface Decoupling for Closely Spaced 5G MIMO Antennas	50
4.1 Introduction	50
4.2 Design Procedure of Proposed Antenna	51
4.2.1 Metasurface Design and Analysis	51
4.2.2 Design of Microstrip MIMO Antenna	52
4.2.3 Design of Microstrip MIMO Antenna with a Metasurface	53
4.3 Parametric Analysis	56
4.4 Simulated and Measured Results	59
4.5 Conclusions	64
CHAPTER 5 High-Isolation Circularly Polarized MIMO Antenna for Sub-6 GHz Application	65
5.1 Introduction	65
5.2 Design Procedure of Proposed Antenna	66

5.3 Parametric Analysis	68
5.4 Proposed MIMO Antenna Design	69
5.5 Result and Analysis of the Proposed 2-port CP MIMO Antenna	71
5.5.1 Radiation Characteristics	72
5.6 Diversity Parameter of the MIMO Antenna	75
5.7 Conclusions	79
CHAPTER 6 Dual-Band CPW-Fed MIMO Antenna for 5G Applications	80
6.1 Introduction	80
6.2 Antenna Design	81
6.2.1 Procedures for Designing a Single Unit Antenna	81
6.2.2 Suggested Four-Port Configuration	85
6.3 Simulated and Measured Results	88
6.4 MIMO System Evaluation	92
6.5 Conclusions	96
CHAPTER 7 Triple Band Self-Decoupled MIMO Antenna Pair for 5G Communication	97
7.1 Introduction	97
7.2 Antenna Design and Decoupled Structure	98
7.2.1 Triple-Band Antenna Design	98
7.2.2 Parametric Analysis	100
7.2.3 Proposed Self-Decoupled Antenna Pair	101
7.2.4 Decoupling analysis	102
7.3 Simulated and Measured Results	104
7.3.1 Radiation Pattern	107
7.3.2 Peak Gain & Efficiency	109
7.3.3 Diversity Performance Analysis	110
7.4 SAR Analysis	113
7.5 Conclusions	115
CHAPTER 8 Conclusion and Future Scope	117
8.1 Conclusion of the Presented Work	117
8.2 Future Scope of the Presented Work	119
Publications	121
References	122

LIST OF FIGURES

Figure 1.1: Evolution of wireless technology	4
Figure 1.2 Multiple antennas configuration	8
Figure 1.3 MIMO antennas configuration	9
Figure 1.4 Basic structure of a microstrip patch antenna	12
Figure 1.5 Various geometry of microstrip antenna	14
Figure 1.6 Design methodology of the proposed antennas	24
Figure. 2.1 Microstrip patch antenna dimensions with CPW feed	30
Figure 2.2 Proposed antenna with (a) metasurface superstrate (b) top view of metasurface superstrate	32
Figure 2.3. Effects of varying the parameter ‘a’ of the antenna. (a) S-parameter (b) realized gain.	33
Figure 2.4. Comparison of the s-parameter without metasurface & with metasurface.	33
Figure 2.5. Comparison of the realized gain without metasurface & with metasurface	34
Figure 2.6. 3D radiation pattern with metasurface superstrate.	35
Figure 2.7 Demonstrates a different phi cut in a 2D pattern at 4 GHz.	35
Figure 2.8. Comparison of beam scanning without metasurface & with metasurface upto -4	36
Figure 3.1 Reflection phase characteristics of metasurface (a) unit cell (b) Phase.	41
Figure 3.2 Dimensions of the microstrip patch antenna. [Dimensions in mm $L_g = 40$, $W_g = 40$, $L_p = 35$, $W_p = 20$, $L_f = 11.67$]	41
Figure 3.3 Proposed antenna with (a) PEC sheet (b) high dielectric superstrate (c) metasurface superstrate (d) side view of the proposed metasurface superstrate antenna.	43
Figure 3.4 Parametric analysis of the antenna. (a) S-parameter (b) Realized gain.	44
Figure 3.5 Comparison of the s-parameter with a simple patch, superstrates, and PEC sheet.	45

Figure 3.6 Comparison of realized gain with a simple patch, superstrates, and PEC sheet.	46
Figure 3.7 3D radiation pattern (a) Simple patch (b) with PEC sheet (c) with dielectric superstrate (d) with metasurface superstrate	46
Figure 3.8 Radiation pattern of the proposed antenna at 3.5 GHz.	47
Figure 3.9 Simulated efficiency of the antenna	47
Figure 4.1 (a) Unit cell with cut wire (b) Permeability characteristics of metasurface	52
Figure 4.2 (a) Geometry (b) Simulated & Measured S-parameter of MIMO antenna	53
Figure 4.3 (a) Proposed MIMO antenna with metasurface (b) top view (c) side view	54
Figure 4.4 Simulated magnitude of electric field distribution (a) without metasurface (b) with metasurface	56
Figure 4.5 Parametric analysis of proposed MIMO antenna (a) $ S_{11} $ with H (b) $ S_{11} $ with L (c) $ S_{21} $ with H (b) $ S_{21} $ with L	58
Figure 4.6 Simulated and Measured (a) S-parameter of the proposed antenna and (b) Gain with and without metasurface.	60
Figure 4.7 (a) S-parameter measurement by VNA (b) Radiation pattern measurement setup (a) $\Phi=0$ Simulated with & without metasurface (b) $\Phi=90$ Simulated with and without metasurface (c) $\Phi=00$ Measured & Simulated with metasurface (d) $\Phi=900$ Measured & Simulated with metasurface.	63
Figure 5.1 Schematics of the single-element antenna to showing step by step design (a) Ant. 1 (b) Ant. 2 (c) Ant.	66
Figure 5.2 (a) Simulated S-parameter of Ant.1 to Ant.3 (b) Surface current density distribution of (i) Ant.2 (ii) Ant.3	67
Figure 5.3 Parametric analysis of proposed antenna (a) $ S_{11} $ with Y (b) $ S_{11} $ with X	68
Figure 5.4 Schematics (a) Top View (b) Bottom View (c) S-parameters with & without strip of the proposed 2-port CP MIMO antenna.	70
Figure 5.5 (a) S-parameters (b) Measurement setup of S-parameter by VNA (c) Simulated and Measured axial ratio plot (d) Simulated and Measured gain of the proposed 2-port CP MIMO antenna	72

Figure 5.6 Radiation pattern measurement setup (a) Front view (b) Back view (c) E-Plane (d) H-Plane of proposed 2-port CP MIMO antenna	74
Figure 5.7. Measured diversity parameters (a) ECC (b) DG (c) TARC (d) CCL (e) MEG of the proposed 2-port CP MIMO antenna	76
Figure 6.1 Single antenna design	82
Figure 6.2 Single antenna developments.	83
Figure 6.3 The surface current distributions at (a) 3.5 GHz and (b) 5.5 GHz	84
Figure 6.4 (a) Geometric arrangement (b) physical prototype of MIMO antenna	86
Figure 6.5 Measurement setup (a) reflection coefficient in dB (b) radiation pattern	87
Figure 6.6 S-parameters of the MIMO antenna (Simulated and tested)	88
Figure 6.7 S-parameters (simulated and tested) of the MIMO antenna at (a) port-1(b) other ports	89
Figure 6.8 Radiation characteristics of the designed antenna at (a) 3.5 GHz and (b) 5.5 GHz	90
Figure 6.9 Simulated and tested (a) Gain and (b) Efficiency of the proposed MIMO antenna	91
Figure 6.10 (a) ECC (b) DG (c) MEG (d) TARC (e) CCL of proposed 4-port MIMO	94
Figure 7.1 Evolution of the microstrip-fed monopole antenna (a) Antenna_1 (b) Antenna_2 (c) Antenna_3	99
Figure 7.2 Simulated S-parameter of single antenna	100
Figure 7.3 Parametric analysis of single antenna	100
Figure 7.4 Layout and design of self-decoupled MIMO antenna, (a) top view (b) bottom view	101
Figure 7.5 Simulated Smith chart showing the feeding distance $D_o=10\text{mm}$ and the CM and DM reflection coefficients	102
Figure 7.6 Self-decoupled antenna pair's vector current distributions at 3.6GHz (a) CM fed. (b) DM.	104
Figure 7.7 Self-decoupled MIMO antenna pair (a) S11 & S21 (b) S22 & S12 simulated and measured results (c) experimental test bench setup	106

Figure 7.8 Radiation patterns of self-decoupled MIMO antenna (a) at 2.7GHz (b) at 3.6GHz (c) at 4.5GHz (d) Measurement in anechoic chamber	108
Figure 7.9 Self-decoupled MIMO antenna pair (a) Peak gain (b) Radiation efficiency	109
Figure 7.10 Self-decoupled MIMO antenna measured (a) ECC (b) DG (c) TARC (d) CCL (e) MEG	113
Figure 7.11 SAR of the proposed antenna	114

LIST OF TABLES

Table 2.1: Design Parameter of Proposed Antenna with CPW feed	31
Table 2.2: Comparison of different type of existing antenna and proposed antenna	37
Table 3.1 Comparison with different existing structures	48
Table 4.1 Dimensions of the metasurface (Units: mm)	55
Table 4.2 Comparison of the proposed and other decoupling techniques	64
Table 5.1: Different parameters of the proposed 2-port CP MIMO antenna	71
Table 5.2: Comparison of the proposed 2- port CP MIMO Antenna with other MIMO Antennas	78
Table 6.1 The dimensions of the single unit dual band antenna.	82
Table 6.2 Comparing the MIMO antenna presented here with previously documented MIMO antenna designs.	95
Table 7.1 Comparisons of the decoupled antenna pair for recent Literature	114

Chapter 1

Introduction and Literature Review

The fifth-generation (5G) wireless technology represents the next phase in cellular communication development. 5G operates across three primary frequency bands: low (600-850 MHz), mid (3.4-3.6 GHz), and high (millimeter wave, 24-30 GHz). Each band has distinct advantages and disadvantages. The mid-band spectrum provides a wider coverage area than the high-band millimeter wave spectrum and is also capable of penetrating walls. It offers faster speeds and greater capacity compared to the low-band spectrum. In the millimeter wave range, frequencies such as 24 GHz, 28 GHz, 38 GHz, and 60 GHz are designated for 5G use; however, they face the challenge of high propagation loss. Given these limitations, most early 5G services are expected to operate within the 3.3-3.8 GHz and sub-6 GHz bands. Antennas with low gain, broad bandwidth, and beam steering capabilities were utilized in earlier wireless technologies to guide signal transmission and reception. However, 5G technology requires antennas with high gain for extensive network coverage and beam-steering capabilities (efficient coverage), high speed for signal transmission (high-speed data rate), and compactness to occupy less space.

To attain the high gain required for 5G communications at millimeter-wave frequencies, beamforming technology is crucial. Various large network structures are employed for beamforming, including Butler matrices, Rotman lenses, and phased array antennas, which are crucial for beam steering. However, these methods often add complexity, weight, and cost to the design. Disruptive beamforming offers a solution to these challenges by eliminating the need for phase shifters and power dividers to steer beams. Instead, it utilizes structures like artificial magnetic conductors (AMCs), metasurfaces, superstrates, and RF absorbers to achieve high gain, wide bandwidth, and beam steering.

This chapter provides a quick overview of 5G technology and outlines the anticipated spectrums. Subsequently, the specifications for antennas in the next wireless technologies are also explained. In conclusion, several kinds of periodic structures are also investigated

for beam steering and gain augmentation. The groundwork required to understand and value the work done in this thesis is laid forth in this introduction.

1.1 Evolution of Mobile Communication

Mobile communication technologies have evolved and improved in performance across numerous generations, which may be categorized as follows:

1.1.1 1G Communication Systems

The initial generation of mobile phones was analogue and solely utilized for voice communications, hence we might refer to this period as the analogue generation. In Europe, various first-generation communication systems were in use, such as TACS (Total Access Communication System), which operated at 900 MHz and had a channel bandwidth of 25 kHz and a data rate of 2 kbps. The most well-known system in the United States of America was called AMPS (Advanced Mobile Phone System), and it operated on the 800 MHz band with a 30 kHz channel bandwidth and a 10-kbps data rate. Because the technologies utilised in the various systems are incompatible, users of TACS and AMPS were unable to call one another (Rappaport, 2009).

1.1.2 2G Communication Systems

The second generation started when the communication networks were switched from analogue to digital. More services, such as brief message, data transfers, authentication, and data encryption, are made possible in addition to voice traffic. Among 2G communication systems, GSM (Global System Mobile) is the most well-known. The majority of the world's population uses it at 900 MHz and 1800 MHz, whereas the USA, Canada, Mexico, and certain nations in South America use it at 850 MHz and 1900 MHz (WorldTimeZone.com). It employed FDMA, which divides the channel's bandwidth into non-overlapping subchannels, and time division multiple access (TDMA), which divides the time frame into eight slots per channel, to achieve a 64 kbps data rate. Other 2G systems exist, such as the digital advanced mobile phone system.

1.1.3 2.5G Communication Systems

The circuit switch network architecture was utilised by the 1G and 2G systems. Whether or not the channel was utilised in this technique, it was formed between the transmitter and receiver and could not be used by other callers until the conversation between the transmitter and receiver was terminated. A system improvement was made possible in 2.5G by using a packet switch network architecture, which increased the data rate to 144Kbps. In this technique, a packet containing addressing data is used to transmit the information data. By delivering their packets to the location indicated in the addressing data, several users can use the channel. This generation includes a number of technologies, including general packet radio service (GPRS), high speed circuit switch data (HSCSD), and increasing the GSM evolution's data rate (GSM). All of these technologies are thought to represent improvements to the GSM system and a transitional phase between 2G and 3G communication systems (Rappaport, 2009).

1.1.4 3G Communication Systems

The preceding generations have undergone a true revolution that is based on Internet Protocols and supports both the circuit switch network and the packet switch network (IP). This function facilitates the globalisation of 3G systems and boosts data rates to 2 Mbps. Applications for multimedia have been supported, including full-motion video and video conferencing. The main 3G systems are based on the Universal Mobile Telecommunication System (UMTS). It is a development of the GSM system that utilises the wideband code division multiple access (WCDMA) standard, which offers a faster data rate and more capacity than GSM (Rappaport, 2009).

1.1.5 4G Communication Systems

The primary objective of any enhancement for any communication system is to increase the system data rate. In addition to the 3G capabilities, 4G systems offer a high data rate of up to 100 Mbps and add Multimedia Messaging Services (MMS), Digital Video Broadcasting (DVB), and improved clarity for watching. The main 4G technology for

television is called Long Term Evolution (LTE), and it offers more data security, higher bandwidth, and better quality of services (QoS) than prior generations.

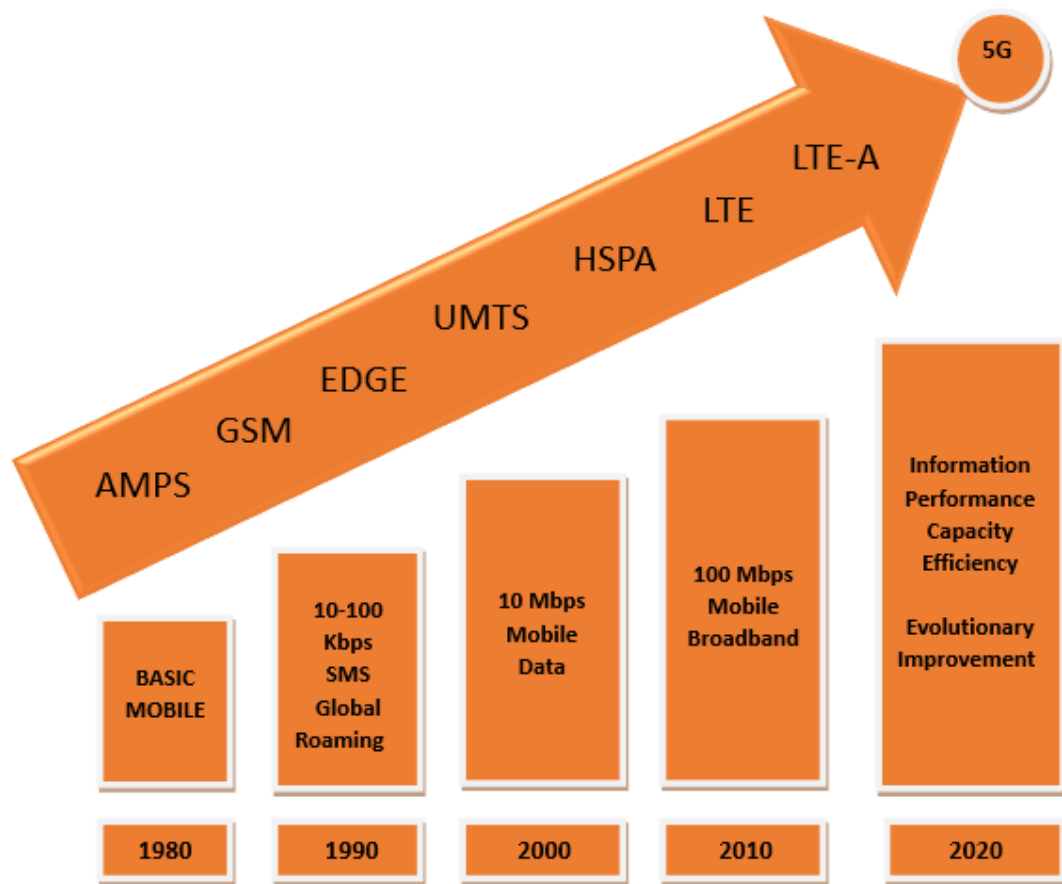


Figure 1.1: Evolution of wireless technology

1.2 5G Technology

The next fifth-generation (5G) wireless technology is a new worldwide wireless standard that follows 1G, 2G, 3G, and 4G. More connection is expected to be provided by 5G compared to previous technologies. 5G promises to only enhance cellular capabilities by increasing broadband power and mobile capacity and data speeds. Actually, compared to previous generations, 5G cellular networks are 10–50 times quicker. 5G technology may be used to develop new applications including the Internet of Things (IoT), Machine to

Machine (M2M) communications, Device to Devices (D2D), and the Internet of Vehicles (IoV) [1].

1.3 5G Expected Spectrum

In order to fulfill the future demands of cutting-edge, soon-to-be 5G wireless technology, more spectrums must be investigated for 5G services. Clearing prime bands should be given priority as 5G will need a significant quantity of additional, harmonised spectrum to fulfill market demand. Three sections comprise the 5G spectrum:

- i) Lower Band
- ii) Mid-band
- iii) Higher Band

i) Lower Band: The sub-1 GHz spectrum facilitates extensive coverage, including indoors, as well as in rural, suburban, and urban areas. Increasing low-band capacity is crucial for reducing the digital divide and ensuring more equitable broadband access between urban and rural regions.

ii) Mid-band: It offers an excellent balance of capacity and coverage benefits. Most commercial 5G networks operate in the 3.3–3.8 GHz band of frequencies. Long-term maintenance of 5G service quality and meeting growing demand would need more spectrum (e.g., 3.3-4.2 GHz, 4.8 GHz and 6 GHz).

iii) Higher Band: The GSMA advises supporting the 40 GHz, 66-71 GHz, 28 GHz, and 26 GHz bands for mobile devices.

Implementing connection quality standards at mm-wave frequencies presents additional challenges:

- At sub-6 GHz, impairments are not a concern; but, at mm-wave frequencies, they become more troublesome.

- Wider channel bandwidths at mm-wave frequencies are anticipated, which affects baseband and RF designs due to common signal impairments.
- 5G radio solutions address these issues by employing beam steering and multi-antenna spatial diversity on base stations and mobile devices [2].

1.4 Requirements of the Antennas for Future Wireless Technology

According to the IEEE definition, "An antenna is a transitional structure between free space and a guiding device that allows radio waves to be transmitted or received" [3]. As the demand for effective signal transmission and reception in wireless communication technologies—such as satellite communication, cell phones, and laptops—continues to grow, the role of the antenna becomes increasingly critical. Antennas are essential for transmitting and receiving signals in all wireless communication systems, converting electrical signals into electromagnetic waves and vice versa. Future advancements in wireless technology will greatly benefit from antennas that offer high gain, wide bandwidth, low ohmic losses, and high radiation efficiency.

To cover extensive network areas, 5G technology requires antennas that offer high-speed transmission, high gain, and compact size. Beamforming antennas are essential for mobile carriers utilizing 5G New Radio (NR) as they play a critical role in network capacity. Developing beamforming technology is key to achieving high-gain antennas, as it enables the creation of highly directional antenna patterns, particularly those that can be electronically steered. Unlike conventional antennas used in earlier wireless technologies, which only broadcast and receive based on fixed radiation patterns, beamforming antennas dynamically adjust their beam directions—both main and null—according to the location of connected users. This dynamic capability enhances signal direction, reduces interference, and improves the signal-to-interference-plus-noise ratio (SINR) [4].

1.5 Multiple Input Multiple Output (MIMO) Antenna

In the new era of modern wireless communication, it requires an errorless channel capacity with lower error rate, bonded with high-speed data rates. However, these features are hindered due to co-channel interference and multipath fading occurring in the communication systems. Multipath fading occurs as a result of signal being reflected by

various paths getting distorted and signal weakened. Co-channel interference occurs as a result of same frequency signals travelling on the same path get interfered on each other. In order to avoid all these errors, we use multiple antennas in transmitter and receiver side. While increasing the channel capacity, these errors are minimized and codes are developed for multiple antenna system. A variety of antenna strategy is utilized for radio correspondence which is planned by M number of sending and N number of getting antennas to concentrate on as far as possible on the information pace of various antenna framework in a Rayleigh blurring climate. The primary center was to utilize an equivalent number of antenna cluster components at both the transmitter and collector to build the channel limit. Further, space-time codes for transmission were acquainted which used various types of antennas without the necessity of any criticism from the recipient to the transmitter [5].

(MIMO is one of the smart antenna technologies employed in modern wireless communication systems. In this technique, channel capacity is being increased with the existing power and bandwidth without the need for modifying the bandwidth of the system. Here, channel capacity is increased by implementing multiple antennas in both transmitter and receiver sides, hence the name MIMO. They can be characterized into various forms as shown in Figure 1.2.

MIMO (Multiple-Input Multiple-Output) essentially integrates various multiple antenna techniques, including:

- SISO (Single-Input Single-Output): This is a traditional system where both the transmitter and receiver are equipped with a single antenna each.
- SIMO (Single-Input Multiple-Output): In this system, there is one transmitting antenna and multiple receiving antennas.
- MISO (Multiple-Input Single-Output): This configuration features multiple transmitting antennas and a single receiving antenna.

MIMO builds on these concepts by utilizing multiple antennas at both the transmitter and receiver ends to enhance communication performance.

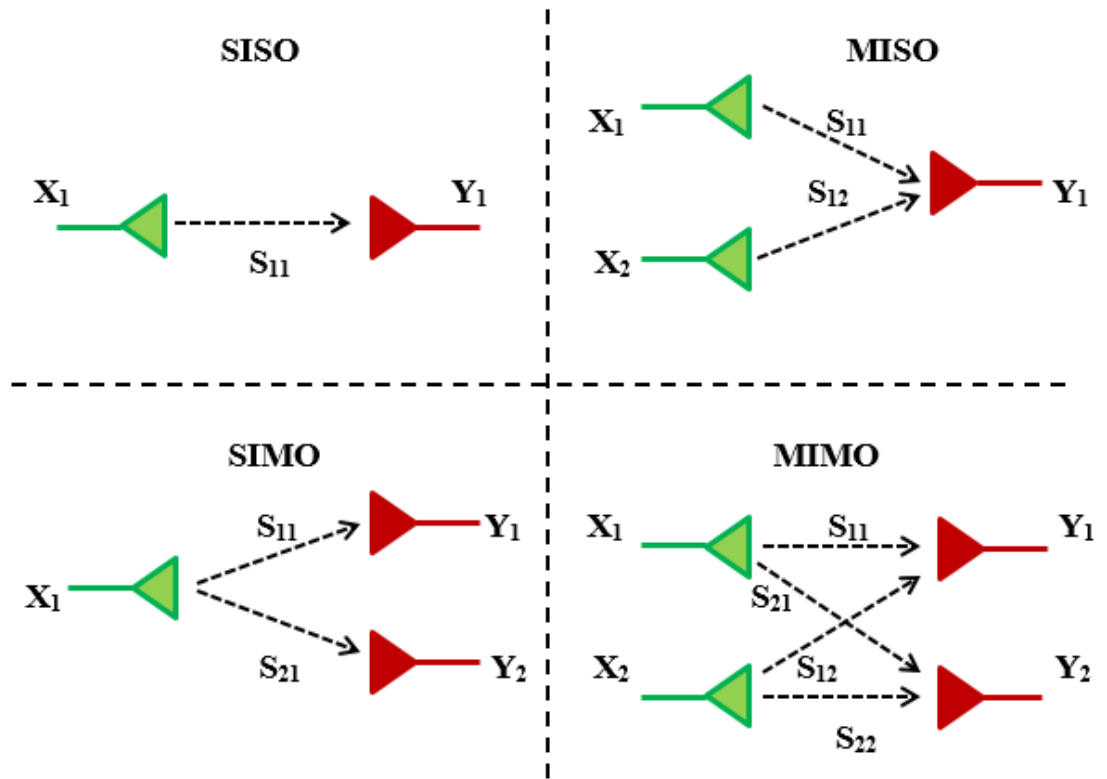


Figure 1.2 Multiple antennas configuration

MIMO innovation has attracted interest in latest wireless correspondence frameworks. An imperative expand in channel limit is accomplished without the need of additional bandwidth or sending power by sorting out numerous antennas for transmission to achieve an exhibit advantage and variety of advantages, consequently recuperating the unearthly effectiveness and dependability[6]. The high decoupling mechanism needs between antenna advancements and a smaller size for application in versatile gadgets in MIMO antenna framework. Figure 1.3 shows the configuration of MIMO system.

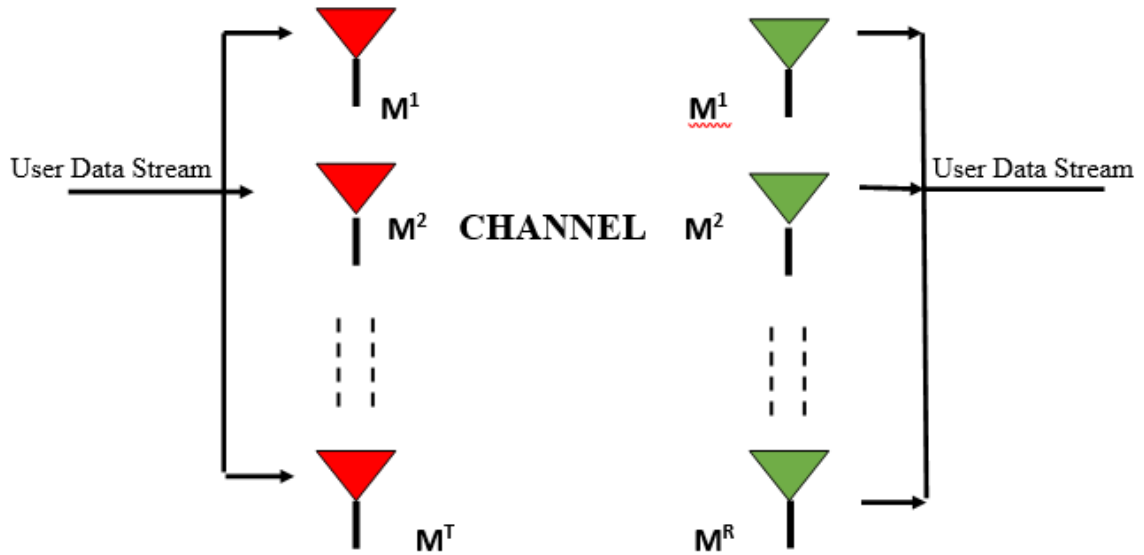


Figure 1.3 MIMO antenna configuration

In Figure 1.3, the transmitter section is designed with the M^T number of transmit antennas, and the receiver section is designed with M^R number of receiving antennas. The MIMO system is designed with the following equation.

$$y = Hx+n \quad (1.1)$$

Whereas,

y is the receive vector;

x is the transmit vector;

H is the channel vector;

n is the noise vector;

Diversity is multiple links between transmitter and receiver. It is used to combat the fading nature of the antenna system. If one of the links between the transmitter and receiver is attenuated or damaged, there is other link present for the communication between them. The antenna system with diversity will have low 3D cross correlation [7].

The performance of good antenna diversity can be achieved by following three methods:

(a) Spatial Diversity

This type of diversity is used to improve the reliability of the communication system. In this, same amount of data are sent across different path or propagation or parallel transmission of the data. This aims to improve the data rate of antenna system known as spatial multiplexing. In this type of diversity, the correlation between the antennas should be as low as possible.

(b) Beam Diversity

The antenna has different gains in different directions.

(c) Polarization Diversity

This diversity is basically the easiest form for achieving any diversity with small MIMO antenna communication system. In this type of diversity, multiple antennas radiate in a specified direction and the polarization between them should be orthogonal.

With respect to the above types of diversity, no antenna will give a perfect diversity system. Generally, it is a combination of different types of diversity, even if polarization diversity effect is strongest. The best choice of any antenna diversity system is the propagation of the signal between transmitter and receiver. In designing the MIMO antenna system, propagation of the signal is generally defined by pattern diversity. Pattern diversity is the placement of the antenna to give the pattern. Polarization diversity and pattern diversity will generally affect the performance of the MIMO antenna. So, when four or more antennas are placed, all types of diversity factors should be included in designing the MIMO system [8].

1.5.1 Design Factors of the MIMO Antenna

For the MIMO Antenna For good diversity of MIMO antenna, the following factors should be included in antenna design:

- Antenna should have some type of directivity in the system so that it can be controlled
- The cross polar discrimination between the antennas should be considered.

- The mutual coupling between the antenna elements must be as low as possible.
- Antenna must have the property of directed spatial radiation.
- MIMO antenna or multiple antennas should be more efficient than single antenna (SISO) having all types of diversity.
- The size of antenna should be as low as possible.
- Impedance matching of the antenna should be high.

The imperfect cross-polarization of the antenna element will create a high correlation between the antennas at the receiver side. This will reduce the gain in the diversity system. So, this effect should be considered, while designing the MIMO antenna. When signal correlation increases the cross-polarization will reduce the diversity gain of the system. So, coupling between the antenna elements becomes the deciding factor for any designer to design a good MIMO antenna for communication [9].

For the reduction of antenna coupling, the following factors should be considered:

- **Current produced in the common ground plane**

This type of problem in the antenna is very likely. These are basically due to the coupling of antenna elements together. Defected Ground Structure (DGS) and Meta material are commonly used here to reduce the current induced in the common ground plane. This will basically enhance the isolation between antenna elements.

- **Direct radiation between two antennas**

These are generally created when the antennas lie in each other with near field regions.

- **Scattering from nearby things**

This can be reduced by careful design of the antenna (whole device). This issue can be mitigated through careful antenna design. By considering the placement of the antenna relative to other components and using techniques like shielding, engineers can minimize reflections and improve overall performance. [10].

1.6 Literature Survey

1.6.1 Microstrip Patch Antenna

In 1953, Deschamps initiated the primary idea of microstrip antenna (Deschamp 1953). Unfortunately, the fabrication of the microstrip antenna was not be possible for the researchers at that time due to the unavailability of appropriate substrate material and printing technology. After two decades of microstrip antenna fabrication, the first realistic microstrip antenna was developed in 1972. After that, widespread investigations were done on the advancement of microstrip antenna and arrayed antenna, for utilizing their abundant advantages like lower cost, easy to configure, lesser weight, lower volume, more compatible with integrated circuits.

As this technology gained more popularity for microwave and millimeter wave applications in the early 1970s, with terrific growth in modern communications and wireless technology applications. The printed circuit board utilized for low-frequency electronic circuit notion can equivalently be compared with the fundamental configuration of microstrip. The copper film is coated on both sides of the low-loss thin substrate. The copper-clad surface is utilized as a ground plane and the printed transmission lines, patches, etc. are cut out from another side. A quasi - Transverse Electric and Magnetic (TEM) wave generated and permitted to spread in between the radiating patch antenna and the ground plane.

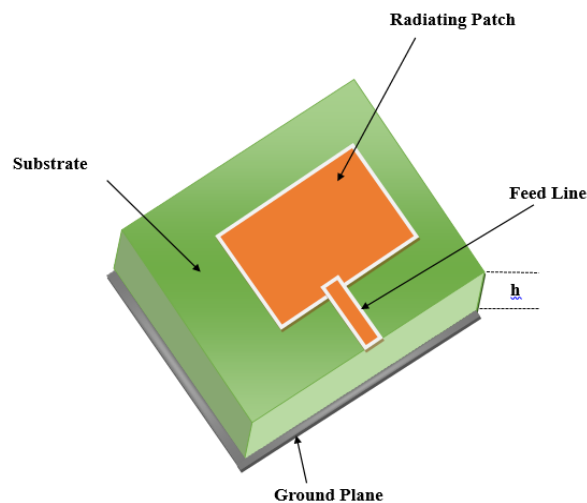


Figure 1.4 Basic structure of a microstrip patch antenna

As shown in Figure 1.4, the basic structure of microstrip patch antenna encloses the radiator patch or radiating element and ground plane in one and other sides of the substrate respectively. The thicknesses of these layers are approximately $t \ll \lambda$, where λ is the wavelength in free space. On the two layers of metal, the dielectric substrate is placed. Normally gold and copper is used to make a metallic layer.

The width and length of the microstrip patch antenna are given as,

$$W = \frac{c}{2f_o \sqrt{\frac{\epsilon_r + 1}{2}}} \quad (1.2)$$

$$L = L_{eff} - 2\Delta L \quad (1.3)$$

whereas,

f_o is the operating frequency (2.4 GHz)

$$L_{eff} = \frac{c}{2f_o \sqrt{\epsilon_{ref}}} \quad (1.4)$$

$$\epsilon_{ref} = \frac{\epsilon_{r+1}}{2} + \frac{\epsilon_{r-1}}{2} \left(1 + 12 \frac{h}{w}\right)^{-\frac{1}{2}} \quad (1.5)$$

A wide range of dielectric constants as $2.2 \leq \epsilon_0 \leq 12$ and thickness in the range of $0.003 \lambda \leq h \leq 0.05 \lambda$ are available for the antenna's substrate and the antenna's performance is affected by the substrate thickness such as bandwidth, gain etc. The different structure or geometry can be selected for design requirements such as ring sector, hexagonal, dipole, square, circular, rectangular, circular ring, elliptical and triangular and as illustrated in Figure 1.5.

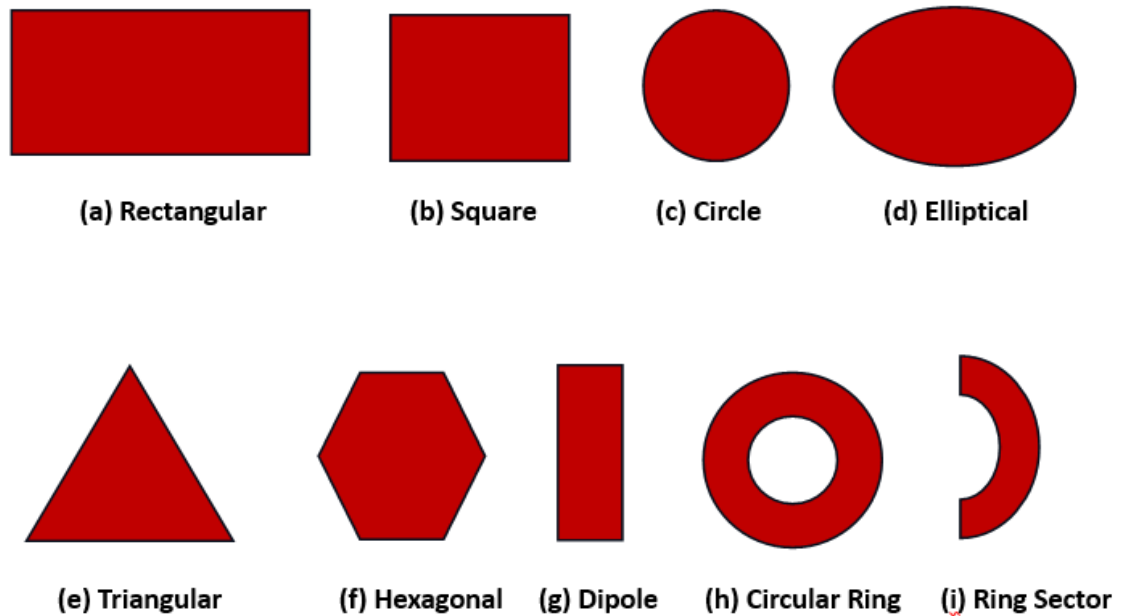


Figure 1.5 Various geometry of microstrip antenna

This structure offers several unique advantages, including a low profile, lightweight design, ease of fabrication, low production costs, and straightforward integration with RF circuits. Additionally, it is well-suited for conforming to curved surfaces. These benefits have made microstrip technology appealing since its early development. As a result, microstrip antennas have become a preferred choice for various applications such as satellite communication, spacecraft, mobile communication, telemetry, missile guidance, and biomedical applications. However, despite these advantages, microstrip antennas also face limitations such as narrow bandwidth, low radiation efficiency, high Q factor, poor isolation, and low polarization purity (Balanis 2005). Recent research has focused on developing advanced technologies to address and mitigate these constraints.

1.6.2 High Gain Antenna

In today's world, the demand for high-speed data transmission is there in the wireless communication systems [10]. Because of their lightweight and low cost with excellent performance, wideband microstrip antennas play an important role to fulfil these needs [11-13]. The research of broadband antenna design for 5G applications has gained prominence in recent years. The primary focus of researchers is on developing antennas

with wideband properties. Recently, Microstrip Patch Antennas (MPAs) have gained significant attention, particularly for low-power wireless communication applications [14-15]. The main challenge in designing these antennas is achieving a compact size while ensuring wide impedance bandwidth and excellent radiation patterns across the entire band [16]. Due to their low profile, small size, lightweight nature, and ease of manufacturing, microstrip patch antennas have garnered considerable interest for mobile communications, radar applications, and other uses.

This paper explores radio frequency designs suitable for 5G operations in the 4 GHz band and the 3-4 GHz range [17]. Various feeding methods are discussed, including probe-fed, microstrip line-fed, edge-fed, inset-fed, and Coplanar Waveguide (CPW) feeding. The CPW feeding method is particularly advantageous due to its wideband properties, as it uses a central strip for signal transmission and side-plane guiding ground. Consequently, CPW-fed slot antennas are considered among the most promising and effective for wideband applications [18-19].

Next-generation wireless technologies for 5G and beyond require high gain antennas with wide bandwidth. The 3.5 GHz frequency band has shown promising results in the implementation of 5G. The deployment speed of the 5G network in the mid-bands e.g. 3.5 GHz is significantly faster due to its propagation characteristics. There have been efforts to implement 5G communication systems in the 3.5 GHz band [20]. A microstrip patch antenna is broadly used over conventional antennas because of its size, cheap cost, and lightweight [21-22]. The metasurface-enabled conformal antenna consists of two components with an operating frequency from 2.36-2.4GHz gain is 6 dBi [23-35]. The EBG-based dual-layer patch multi-antenna structure for MIMO applications operates at 2.45 GHz, has a gain of 3.26 dBi, and has a 59.68 % efficiency [26]. Whereas, 6.3dBi gain is reported in [27] where a finite-size small high impedance surface (HIS) antenna is used to create a highly directional antenna for a smartwatch with an operating frequency is 2.4 GHz and an efficiency of 46 %. However, the RF antenna filter achieved 4.7 % of bandwidth which covered 4.06 - 4.2 GHz band and a maximum gain of 4.3 dBi [28-30]. Based on the Theory of Characteristic Modes (TCM), a wideband is created with a

consistent omnidirectional radiation pattern [31-33]. Microstrip patch antenna with partial substrate removal shows 5 % impedance bandwidth and 7 dBi gain [34]. Whereas the metamaterial-based lens antenna was reported in [35] which achieved a 6 dBi gain.

1.6.3 MIMO antenna

In the past few years, as wireless communication has swiftly advanced and its user base has expanded significantly, the need for elevated data rates and dependability has become crucial. The increased demand has led to a focus on Multiple-input-multiple-output (MIMO) systems among researchers, given their notable advantages in channel capacity and reliability [37-38]. A MIMO antenna engineer's goal is to design antennas that provide High isolation. Various researchers have proposed to improve port isolation between different components trying to attempt to reduce correlation. In [39-41] Decoupling networks, negative group delay lines, and neutralization are used in this process, along with the inclusion of parasitic components [42], metamaterial [43], meta-surface antenna array decoupling (MAAD) [44], a blend of these methods [45] or metasurface [46]. However, it has been documented a shared coupling is used between two antennas [47-48].

In [49] used potential for the decrease in ρ to enhance isolation might unintentionally and the radiation patterns of the antenna array [50]. Consequently, although these techniques reduce coupling between the MIMO antenna's components, increasing radiation efficiency, it is uncertain how they may affect channel correlation. In [51] that uses genuine articulation, it is conceivable that the decrease in ρ happened because the design set for isolation improvement unintentionally wound up shifting the radiation antenna elements [52]. Hence, the previously stated techniques, even while they increase the MIMO antenna's radiation efficiency by reducing coupling between its components, do not guarantee a definite impact on channel correlation.

In [53] DGS was used for separating two dual-band antenna arrays and isolation [54] was achieved by cutting in the ground plane. The dual-band achieved by L slot in the patch and element spacing is $0.023\lambda_0$ and decoupling is obtained by cross-shaped metal strips shorted to the ground plane [55]. The isolation is achieved greater than 15 dB by a V-slot

loaded in an antenna and spacing is 0.057λ [56]. To enhance the isolation in closely spaced inverted-F MIMO antennas dual band with a separation of approximately 0.115λ , two decoupling mechanisms were used. These include a meandering resonant branch and an etched ground plane with an inverted T-shaped slot [57].

To enable the new era of the internet of everything, the 5G mobile network system is a new global wireless framework that is designed to provide ubiquity connectivity to everyone and everything at once, including machines, objects, and devices, in a way that is incredibly reliable and reasonably priced [58]. MIMO systems efficiently take advantage of the multipath environment to boost wireless system performance as a whole. Systems using 5G MIMO considerably increase speed and capacity while delivering low latency and excellent dependability. Strong mutual coupling between antenna elements caused by compact MIMO antenna design may lead to a decline in the performance of system diversity overall and inter-element isolation. It is allowed for the 5G sub-6GHz MIMO system to have an isolation level of 10 dB. To improve MIMO performance, however, lower bound isolation of at least 15 dB should be needed. When compared to their linearly polarized (LP) counterparts, circularly polarized MIMO antennas provide several advantages, including the prevention of multipath interference, fading, and quality of service (QoS) [59-61]. In addition to the aforementioned, CP antennas, as compared to LP antennas, also aid in overcoming the orientation issue between the transmitter and receiver, greater mobility due to suppressed multipath interference, and better weather penetration [62]. Circularly polarized MIMO antennas have so been discussed in the literature in recent years. A compact CP MIMO antenna design in [63] using two truncated corner square patches with parasitic periodic metallic plates. It requires costly Taconic substrate, increasing manufacturing costs. A MIMO antenna proposed in [64] has employed an inexpensive FR-4 substrate to reduce production cost and to improve the performance of the antenna applying an eyebrow-shaped strip, however, it has a very big dimension of 85 mm×73 mm. The spatial diversity method has been used by [65] to increase the isolation between nearby antenna components (adjacent elements are separated by a distance of 13.75 mm). According to [66], the low-profile, microstrip-fed

MIMO antenna with the isolation of more than 17 dB, it is noteworthy that the gap between the two antenna elements, measured from centre to centre, is just 0.16, and isolation of up to 18.50 dB can be attained without the use of any extra decoupling structures. A dual port dielectric resonator-based CP antenna is also suggested for 5G communication [67]. Controllable CP, compact size, superior isolation, and simple geometry are this antenna's main benefits. Compact CP array antennas with minimal mutual coupling have been constructed in [68]. The broad impedance bandwidth of this antenna is 36%, and the CP BWs are around 23%. Additionally, there is a low envelope correlation coefficient and a large diversity gain (DG). A small two-port CP MIMO antenna for 5G outdoor applications was created in [69]. This CP MIMO antenna has left-hand circular polarization and covers the future 5G range between 3.3GHz and 3.8GHz. With a total footprint of $37 \times 30 \times 0.8$ mm³, for use at sub-6 GHz, a four-port small MIMO antenna with a built-in isolator has been developed. The circular isolator that was integrated into the device eliminates the need for any decoupling components and conserves space between individual antenna elements [70]. The goal of [71] is to achieve CP bandwidth with enhanced isolation employing a new ground structure and asymmetric Z-shaped radiating patch. This antenna geometry is extremely small thanks to the innovative ground construction. Different antenna design methodologies are presented [72-73] to achieve good mutual coupling between the antenna parts while also reducing the antenna's geometry. These papers will address several methods for achieving excellent isolation and compact dimensions.

According to reference [74], a MIMO antenna with a single split ring resonator on the top side and a defective ground structure on the bottom is designed to cover both the mid 5G band and C-band. The suggested antenna offers more than 15 dB isolation between antenna parts without the use of any decoupling mechanisms, as well as circular polarization at the second band useful for satellite applications. A two-element slotted octagon-shaped antenna for use in the sub-6 GHz range is described in [75]. A T-shaped structure that is positioned at the ground plane helps to provide isolation of more than 20 dB. The design and optimization of a five-port MIMO antenna system with polarization

and pattern diversity for the n79-5G band. Four end fire linearly polarized monopole antennas are merged with a broadside circularly polarized antenna [76]. The same dual-band MIMO antenna is designed in [77] to operate in the 3.3-3.8 GHz and 4.3-5.7 GHz frequency bands. In [78], two-shaped and one rectangular defect have been introduced into the ground plane to ensure wideband isolation [79] across the operating frequency range. In [80], a two-arm monopole antenna incorporating a coplanar waveguide feed line operate between 3.2 GHz and 4.12 GHz, with proper isolation.

MIMO systems utilize multiple transmitting and receiving antennas, capitalizing on the effects of signal propagation via various paths [81-83]. Nevertheless, the efficiency of antennas and the performance of MIMO systems can be compromised due to heightened mutual interaction when multiple antennas are positioned near [84-85]. This issue has emerged as a significant challenge requiring attention. Substantial endeavors have been devoted to alleviating this mutual interference.

To tackle the above issue and accommodate the constrained space within smartphones, a solution involves integrating 2 or 4 closely positioned or shared-radiator MIMO antenna elements. This approach effectively reduces the overall spatial requirement through spatial reuse [86]. In one instance [87-88], the method of using neutralization lines is employed to mitigate mutual interference among four closely positioned open-slot antenna elements covering the frequency band of 5G. This results in a compressed antenna size for a four-antenna unit. In another study [89], two gap-coupled loop antennas, which are mirror images of each other and function in the frequency range of 5G mid-band, are integrated to create a unique self-decoupled module. Through innovative methods [90], Utilizing grounded strips and distributed coupling capacitances for closely spaced loop antennas. Further advancement is seen in [91], by skilfully combining parallel and series LC tanks, a novel compact module housing four antennas is devised to function. In an array of research [92], an inventive orthogonal-mode strategy is introduced to naturally achieve high isolation across the frequency band [93] or shared radiator [94] obviating the need for supplementary decoupling structures. Recently, researchers have been more interested in using coplanar waveguides (CPW) feeding techniques to enhance antenna functionality

and achieve multiband capabilities. In the existing literature, antennas employing CPW feeding exhibit several benefits compared to alternative methods such as microstrip and coaxial probe feeding. These advantages encompass cost-effectiveness, reduced dispersion, favourable omnidirectional patterns, minimal surface wave propagation, and streamlined integration with both passive and active components [95-96]. Due to the appeal of these advantageous attributes, the choice has been made to employ CPW for crafting the antennas presented in this study.

The double-antenna or 4-antenna modules, characterized by their high integration and effective isolation, represent significant advancements in reducing the spatial requirements of MIMO antenna systems. Nevertheless, the limited bandwidth decoupling capability inherent in these design approaches could present a challenge as the global 5G New Radio (NR) industry progresses [97]. In the context of 5G mobile devices, there is a need to incorporate approximately MIMO antenna components working within the sub-6 GHz. This must be accomplished within the constraints of a compact environment and alongside existing 2G/3G/4G antennas. A straightforward strategy involves physically separating individual antenna elements and achieving partial decoupling through spatial distancing [98-99].

The intended frequency operating range is achieved with the structure of the single-element antenna. The antenna design results in resonance at 3.5 GHz and 5.9 GHz. The MIMO antenna [100-103] is tested where good agreement is achieved between overall results. The MIMO antenna design suggested in reference [104] comprises four identical radiating elements in an octagonal shape. These elements are arranged orthogonal to each other. The antenna possesses the capability to reject signals in two frequency bands, namely 3.5 GHz and 5.5 GHz, which align with the Wi-MAX and WLAN bands. [105-108]. The parametric analysis including variations in length, widths of patches, varying sizes of DGS, Interlaced Lozenge Structure (ILS) are considered for surface wave radiations suppression. This results in better mutual coupling between radiators [109-112]. The design aspects of a compact four-port MIMO antenna with proper isolation for different application like Internet of Things (IoT) are explored in [113-119].

Different types of MIMO antennas are proposed in [120-126] to reduce mutual coupling between antenna radiators. MIMO systems, which take advantage of multipath propagation, employ multiple transmitting and receiving antennas [127-128]. However, the reduced efficiency of the antennas and the performance of MIMO caused by the increased mutual coupling that arises from positioning several antennas close to one another make this a critical issue to overcome.

To enhance the level of integration for MIMO antennas and to facilitate the upcoming requirements of the broad-spectrum 5G NR sector, a pair of self-decoupled MIMO antennas connected by a common radiator can be utilized. Even though two antenna components are combined to create a paired antenna sharing a common radiator, sufficient isolation is attained without the need for additional decoupling methods. A mode-cancellation method (CM) constructed around a new understanding of common mode (CM) and differential mode (DM) cancellation has been introduced to analyse the actual workings of the self-decoupling phenomena. The combination of CM and DM currents might mimic the current mode delivered via a single port, as outlined by the MCM. Consequently, half of the existing current in the shared radiator is overlapped. While the current in the other half is negated, resulting in a natural self-decoupling feature [129-131]. Because it gives a clear design route for tackling the mutual coupling issue, recently MIMO antenna designs have used the approach of even-mode and odd-mode [132-135]. In this part, antennas with closely spaced feed points can be examined. Around antenna feed points, electromagnetic fields or currents tend to congregate [136-139] and significant electromagnetic fields or currents can be created at additional feed sites when one feed point is energized. As a result, achieving a high level of isolation in this situation is challenging [140].

1.7 Motivation and Objective of the Thesis

The sub-6 GHz band is a crucial component of 5G networks due to its balance of coverage,

capacity, and compatibility with existing infrastructure, making it essential for widespread and reliable 5G deployment.

The literature survey indicates that numerous research groups are actively exploring 5G antenna design and have achieved varying degrees of success. Building on these advancements, our research focuses on enhancing key features such as gain, isolation, and bandwidth through the use of different periodic structures, which are examined in detail. The following challenges serve as motivating factors for our research in the field of 5G antennas:

- Conventional microstrip patches antennas for 5G applications have the problem of low gain, high Sidelobe Level (SLL).
- Investigation is needed to design a novel antenna having superior radiation characteristics (radiation pattern, gain, directivity and efficiency) and easy to integrate with the 5G system.
- To overcome the challenges of 5G wireless communication there is a need to design dual-band and multi-band antenna for different applications such as radar & satellite communications, and vehicle radars.
- MIMO antenna design is required for higher link reliability, data speeds, high throughput, low latency & high channel capacity without requiring additional power or spectrum.

Based on the factors mentioned, the primary objective of this thesis is to design and analyze MIMO and microstrip patch antennas, with a focus on achieving high isolation and enhancing MIMO parameters.

The main objectives of this thesis are listed below:

- To design a microstrip patch antenna for 5G wireless communication with improved gain.
- To design and fabricate a novel microstrip patch antenna having superior radiation characteristics for 5G wireless communication.
- To design a multiband antenna for 5G wireless communication.

- To design a MIMO antenna having high isolation and superior radiation characteristics for 5G wireless communication.
- To design MIMO antenna with improved gain and for 5G wireless communication.

1.8 Design Guidelines of the Antenna

Figure 1.6 shows the overall work is divided into the following steps:

Step 1: Based on the literature review identification of the requirements of the 5G antenna.

Step 2: Design and simulation of the antenna and performance analysis of the antenna in virtual or simulation mode.

Step 3: Once satisfied with the results of the simulation, prototyping, or fabrication of the antenna.

Step 4: After the fabrication of the antenna again the performance measurement of the antenna parameters in the real environment.

Step 5: If the performance of the designed antenna is up to the mark, the overall work needs to be documented in terms of a research article.

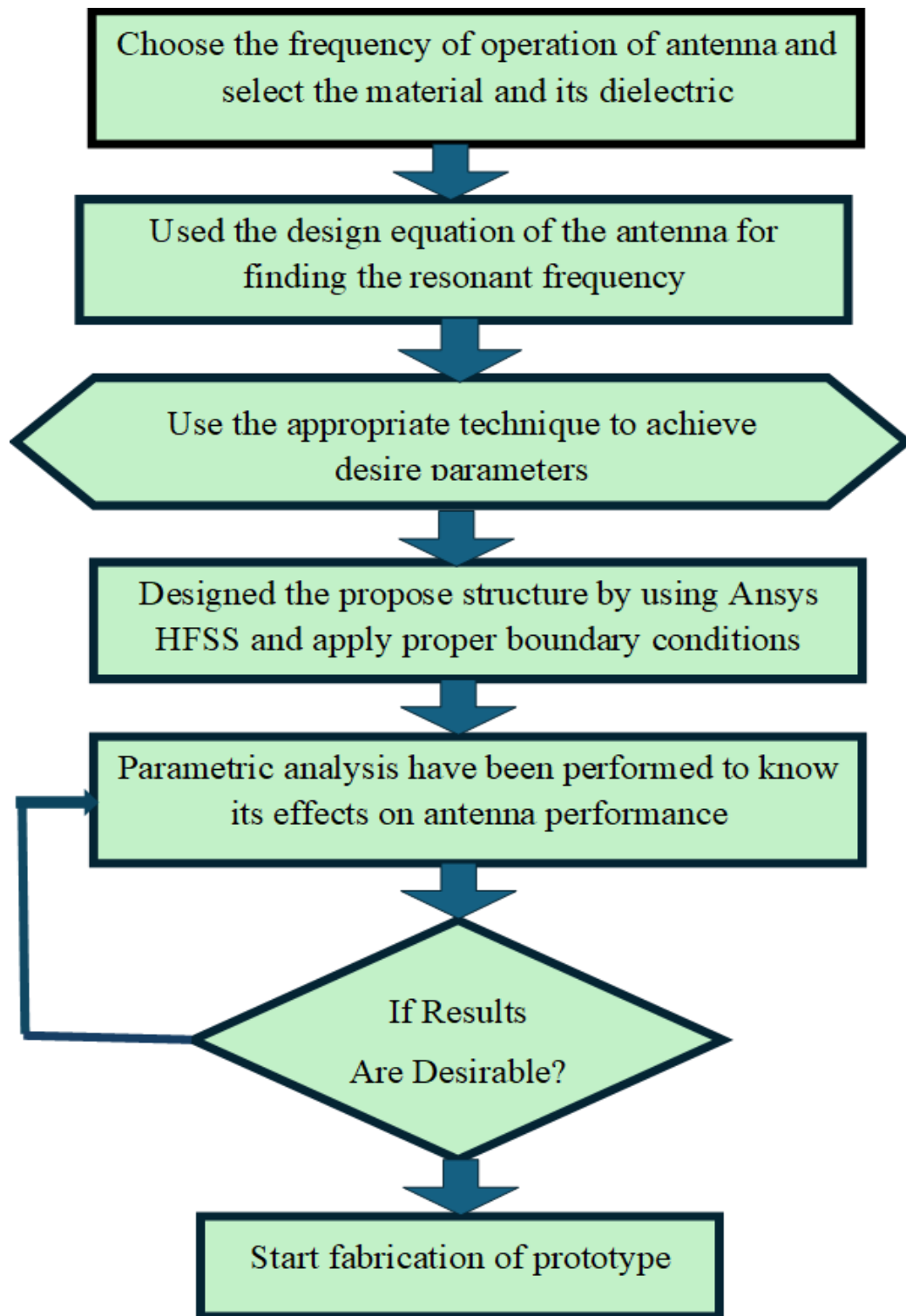


Figure 1.6 Design methodology of the proposed antennas

1.8.1. Organization of the Thesis

The thesis is organized into eight chapters, outlined as follows:

Chapter 1: This chapter provides an overview of 5G technology, including the anticipated frequency spectrums. It also discusses the future requirements for antennas in wireless technology and explores methods for enhancing gain and optimizing MIMO antennas. This introductory chapter establishes the necessary background to understand and appreciate the research presented in the subsequent chapters.

Chapter-2: This second chapter introduces a Coplanar Waveguide (CPW)-fed microstrip patch antenna designed for 5G communication. To enhance antenna performance, a highly reflective metasurface is integrated. The antenna operates in the 3.86 to 4.49 GHz frequency range and is fabricated on a FR-4 substrate. The CPW-fed configuration is employed to improve bandwidth and gain compared to traditional feeding methods. The core innovation lies in the incorporation of a metasurface superstrate above the antenna, which significantly enhances gain and enables beam scanning. Simulation results using Ansys HFSS demonstrate the effectiveness of the proposed design, achieving a substantial gain of 6.06 dBi, a wide bandwidth of -10 dB, high efficiency of 92%, and a scanning capability of -4 degrees. These results highlight the potential of the CPW-fed metasurface-enhanced antenna for advanced 5G applications.

Chapter 3-: This third chapter presents a microstrip antenna design optimized for 5G communication. To enhance antenna performance, we explored the integration of a Fabry-Perot cavity structure. Conventional techniques using PEC sheets or high dielectric superstrates faced challenges in terms of size and cost, respectively. This study introduces a metasurface superstrate as a promising alternative. By strategically placing the metasurface above the antenna, we create a resonant cavity that significantly boosts gain and bandwidth. Simulation results using Ansys HFSS demonstrate the effectiveness of the proposed design, achieving a substantial gain of 6.8 dBi, a bandwidth of -10 dB covering

3.44-3.61 GHz, and an efficiency of 69%. These findings underscore the potential of metasurface-enhanced antennas for reliable and efficient 5G communication systems.

Chapter- 4: This fourth chapter presents an approach to enhance the performance of closely integrated MIMO patch antennas operating at 3.5 GHz. The proposed design employs a pair of mirror-symmetrical patch antennas with an exceptionally small separation distance of $0.011\lambda_0$. To address the critical challenge of isolation between these closely spaced antennas, a metasurface-based decoupling structure is introduced. This structure, composed of uniform cut wires, effectively mitigates signal interference, leading to a substantial improvement in isolation levels. Simulation and experimental results corroborate the effectiveness of the proposed design. The metasurface not only significantly enhances isolation from 10 dB to 35 dB but also contributes to a gain increase from 1.85 dBi to 3.85 dBi. These findings underscore the potential of the metasurface-based decoupling structure as a promising solution for improving the performance of closely coupled MIMO patch antennas. While this study focuses on a two-element antenna array, the concept holds promise for future applications involving larger antenna systems. The developed MIMO patch antenna exhibits exceptional characteristics, making it a suitable candidate for 5G wireless communication systems. By addressing the critical issue of isolation in closely spaced antennas, this research contributes to the advancement of antenna technology and paves the way for more efficient and reliable wireless communication.

Chapter-5: This chapter fifth presents a novel approach to antenna design for 5G sub-6 GHz applications through the development of a two-port circularly polarized MIMO antenna. The proposed design incorporates a unique combination of a patch antenna, a circular slot, and a circular split ring resonator to achieve optimal performance. By carefully integrating these elements and introducing parasitic elements for isolation, we have designed an antenna that exhibits impedance bandwidth of 3.3 to 3.6 GHz with impedance matching better than 10 dB and has an axial ratio bandwidth of 3.35 to 3.51

GHz. The proposed 2-port CP MIMO antenna design with insect fed gives good diversity performance with ECC 0.004, DG 10 dB, CCL 0.40 b/s/Hz, MEG 1.03 dB, and TARC 10 dB. The results that the proposed antenna surpasses existing MIMO systems in terms of channel capacity loss and diversity performance. With a wide impedance bandwidth, stable radiation patterns, and robust diversity characteristics, this research contributes significantly to the advancement of antenna technology for 5G communication systems.

Chapter -6: This sixth chapter introduces an integrated dual-band MIMO antenna designed for global systems for mobile communications applications. The proposed antenna's unique orthogonal arrangement of unit cells eliminates the need for additional isolation components, simplifying the fabrication process. By incorporating a curved form into the radiator elements, the antenna achieves dual-band operation at 3.5 GHz (Wi-Max) and 5.5 GHz (WLAN) frequencies. The compact four-port MIMO antenna demonstrates impressive performance, exhibiting isolation exceeding 18 dB for both frequency bands and a low envelope correlation coefficient. Experimental results align closely with simulations, validating the effectiveness of the proposed design. This research contributes significantly to the advancement of MIMO antenna technology by offering a compact, efficient, and high-performance solution for dual-band wireless communication systems.

Chapter – 7: This seventh chapter introduces a two-port MIMO antenna designed for 5G mobile phones, featuring a unique self-isolation mechanism that eliminates the need for additional decoupling components. By employing a mode-cancellation technique, the antenna achieves exceptional isolation of approximately 22 dB across the crucial triple-band spectrum of 2.58-2.84 GHz, 3.4-3.9 GHz, and 4.3-4.6 GHz. The proposed antenna demonstrates impressive performance with a respectable overall gain across all bands and exceptional diversity metrics, including ECC and DG. These characteristics, combined with its compact design and simple structure, make it highly suitable for integration into modern 5G devices. This research contributes significantly to the advancement of MIMO

antenna technology by offering a promising solution for enhancing wireless communication performance and user experience.

Chapter – 8: In conclusion, eighth chapter provides a summary of the overall findings and outlines future research directions. This thesis involved designing a variety of antennas, including microstrip patch antennas with microstrip and CPW feeding, metasurface-based MIMO antennas, single-band, double-band, and triple-band MIMO antennas. The goal was to achieve high gain, excellent isolation, and improved diversity parameters for 5G applications. These antennas are designed to support 5G applications operating in mid-band sub-6 GHz frequency ranges.

Chapter 2

CPW-Fed Microstrip Patch Antenna for 5G Applications

This chapter introduces a CPW-fed microstrip patch antenna for 5G. A metasurface enhances the antenna's performance, resulting in increased gain, wider bandwidth, lower losses, and better efficiency. The antenna operates at 3.86-4.49 GHz and is simulated using Ansys HFSS.

2.1 Introduction

The escalating demand for high-speed wireless data transmission has driven the need for efficient antenna solutions. Wideband microstrip antennas, renowned for their lightweight, low cost, and exceptional performance, have emerged as key components in fulfilling these requirements. Research into broadband antenna design for 5G applications has intensified in recent years. Microstrip Patch Antennas (MPAs) have emerged as a popular choice for low-power wireless communication systems. However, designing compact antennas with broad impedance bandwidth and consistent radiation patterns remains a significant challenge.

In the literature, the low profile, lightweight construction, and ease of manufacturing of MPAs make them attractive candidates for mobile communication, radar, and other applications [18]. This chapter introduced radio wire plans appropriate for 5G works in the 4 GHz band and in (3-4 GHz). Feeding methods include probe fed, microstrip line fed, edge fed, inset fed, and Coplanar Waveguide (CPW) [20]. The CPW is the signal feeder, with the side-plane guiding ground and the signal carried by the centre strip. The wide band properties of a CPW fed slot antenna are one of its advantages. As a result, the CPW fed slot antenna is the most promising and effective antenna for wideband distance applications [21].

The proposed antenna has a high impedance transmission capacity and radiation. Because of their low profile, tiny size, lightweight, and ease of manufacture, microstrip patch antennas have gained a lot of interest in wireless communications, mobile

communications radar applications, and other applications. Coaxial probe fed, microstrip line fed, edge fed, inset fed, and CPW fed are some of the feeding techniques available. The CPW is the signal feed, with the side-plane conductor serving as ground and the signal carried by the centre strip. The wide band properties of the CPW fed slot antenna are an advantage. As a result, the most effective and promising antenna for wideband wireless applications is the CPW fed slot antenna. They do, however, have some drawbacks, such as limited bandwidth and low gain. In this work, a novel design for a broadband planar antenna with CPW-fed technology is proposed for WLAN applications, consisting of a rectangular-shaped patch embedded with two slots.

2.2 Geometry of the Proposed Antenna

2.2.1 Design Procedure CPW Fed Microstrip Patch Antenna

This section outlines the antenna design methodology. Typically, the goal of constructing a wideband antenna is to create a compact, basic antenna with a broad bandwidth and low distortion. The design of a 4 GHz resonant frequency metasurface superstrate-based microstrip patch antenna with CPW feed is described. The design parameters of the proposed antennas are presented in Table 1.

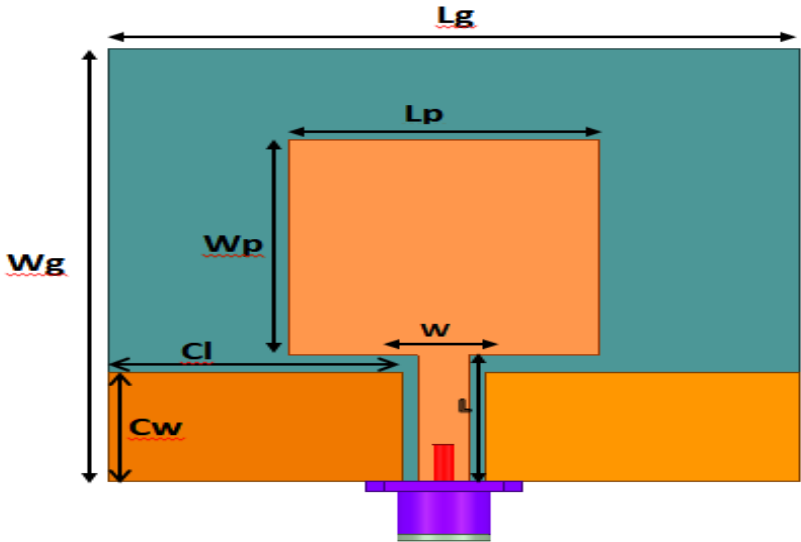


Figure. 2.1 Microstrip patch antenna dimensions with CPW fed

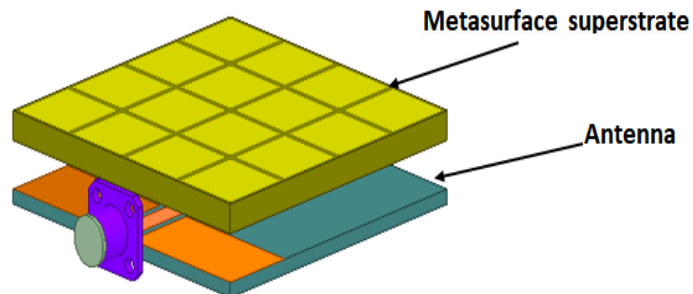
Table 2.1: Design Parameter of Proposed Antenna with CPW feed

S.No.	Proposed (40×40) Antenna
L _g	40
W _g	40
L _p	20
W _p	18
Cl	17
Cw	10
L	11.7
W	3
a	9.38
h	1.6

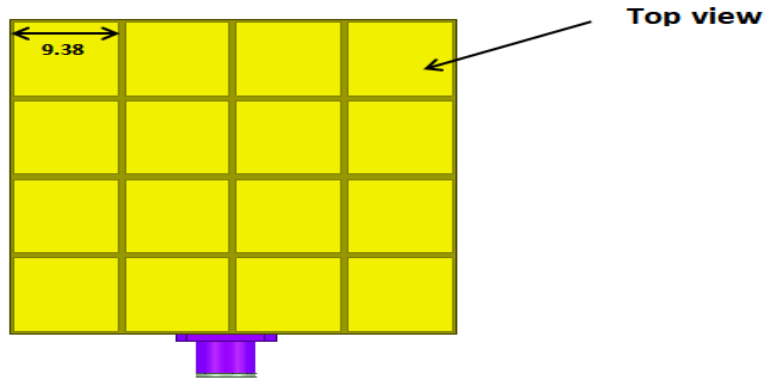
The geometry of the proposed CPW fed slot antenna is shown in Figure 2.1 with all dimensions in mm given in Table 2.1. The above figure shows the basic design of the antenna with CPW feed with all dimensions.

2.2.2 Design of Composite CPW Fed Microstrip Patch Antenna with Superstrate

In the proposed antenna design Figure 2.2 (a) the unit cell has a 10 mm periodicity and the metasurface contains a 4×4 grid of square metallic patches with a dimension of 9.38 mm. as shown in Figure 2.2 (b). The work was done on a FR4 substrate with a height of 1.6 mm and a permittivity of 4.4. At 4 GHz, the proposed metasurface superstrate is designed. The metasurface superstrate and antenna are separated by 5.2mm.



(a)

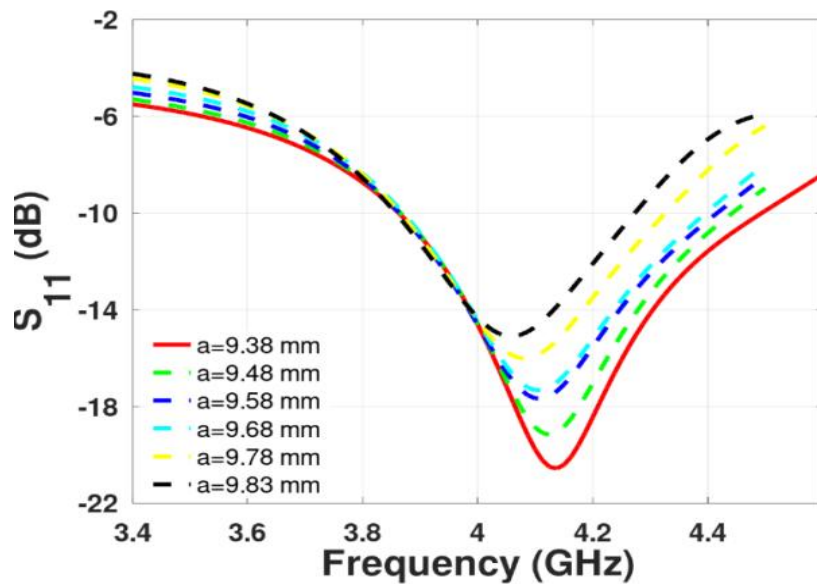


(b)

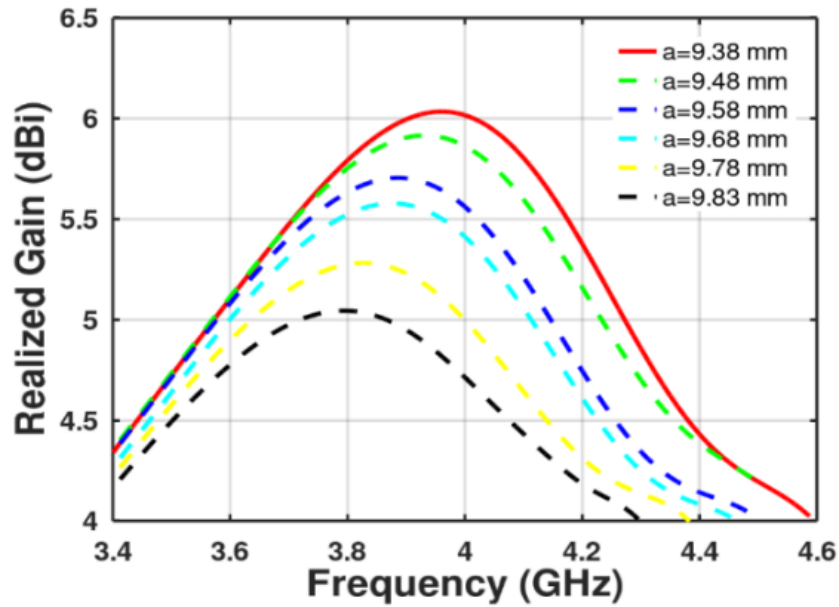
Figure 2.2 Proposed antenna with (a) metasurface superstrate (b) top view of metasurface superstrate

2.3 Parametric Analysis

The antenna design was simulated over the operational band and the antenna structure's design parameter was optimized using Ansys HFSS. Parametric study of the parameter size of the unit cell of the metasurface superstrate is used to determine the antenna's dimensions. The influence of 'a' on the s-parameter shows in Figure 2.3 (a) & (b).



(a)



(b)

Figure 2.3. Effects of varying the parameter ‘a’ of the antenna. (a) S-parameter (b) realized gain.

2.4 Simulated and Analysis of Results

2.4.1 S- Parameter

Figure 2.4 compares the simulation results of reflection coefficient of the design without metasurface and with metasurface superstrate. The metasurface superstrate improves the antenna return loss, as can be shown in Figure 2.4.

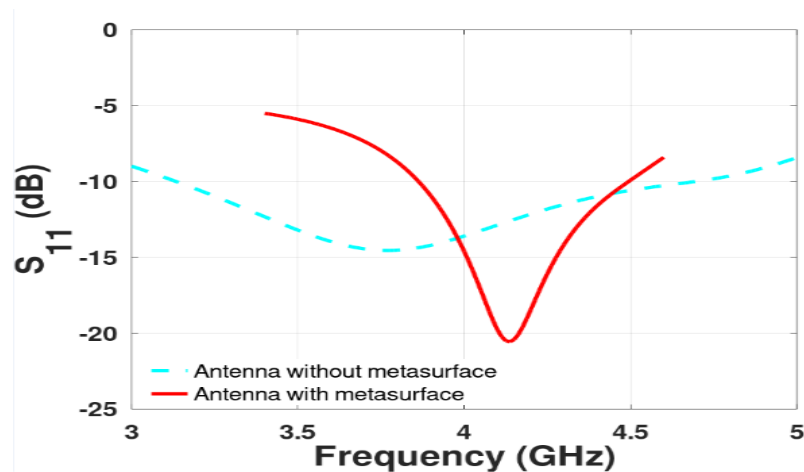


Figure 2.4 Comparison of the s-parameter without metasurface & with metasurface.

2.4.2 Realized Gain

Figure 2.5 illustrates the design's achieved gain with and without metasurface superstrate. The antenna gain is improved to 6.06 dBi by using a metasurface superstrate.

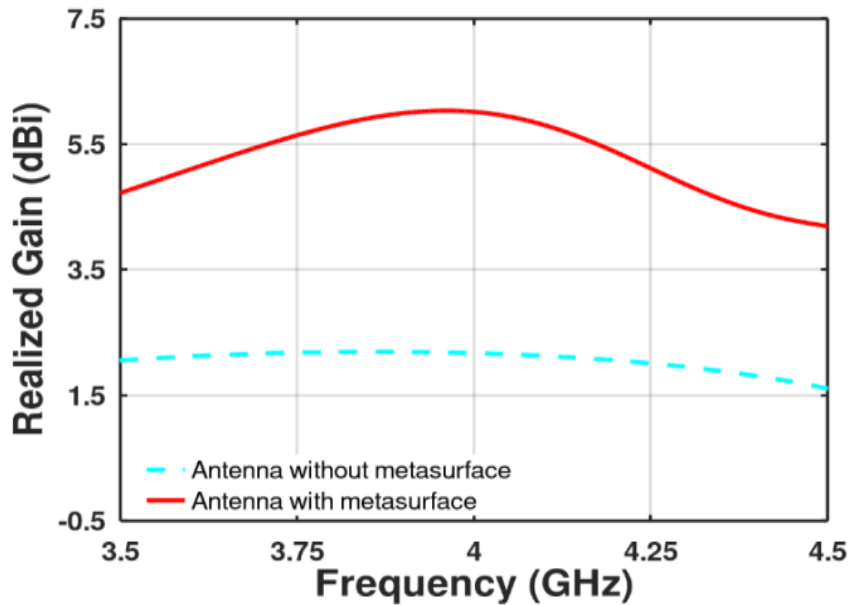


Figure 2.5 Comparison of the realized gain without metasurface & with metasurface

2.4.3 Radiation Pattern

Figure 2.6 illustrates the antenna gain was enhanced by increasing the forward radiation in the 3D radiation pattern of the antenna with metasurface superstrate. Figure 2.7 Radiation pattern of the proposed antenna at 4 GHz.

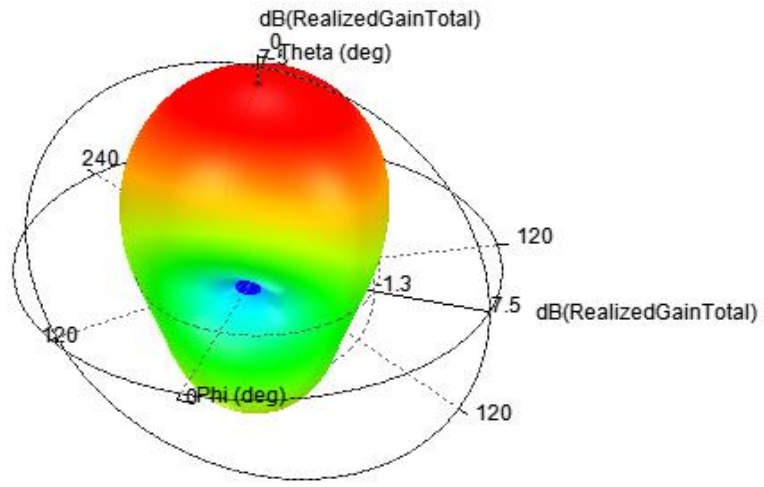


Figure 2.6 3D radiation pattern with metasurface superstrate.

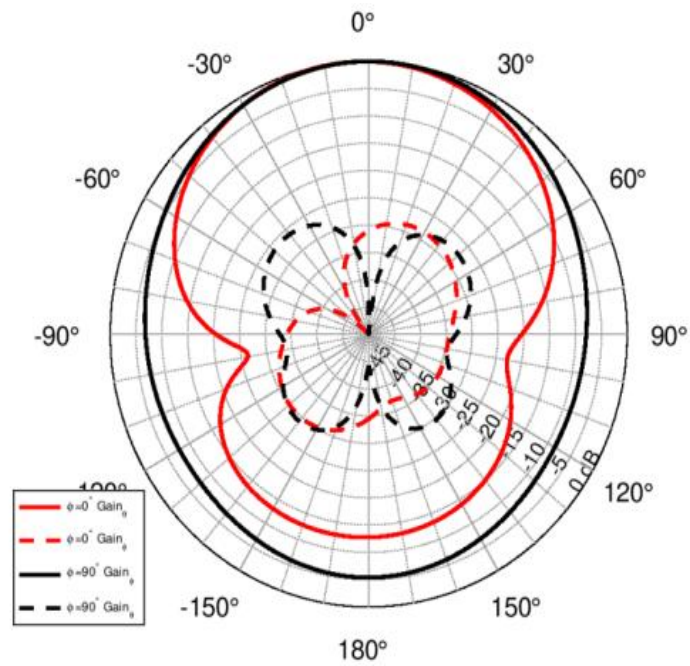


Figure 2.7 demonstrates a different phi cut in a 2D pattern at 4 GHz.

2.4.4 Beam Scanning

The beam scanning of the metasurface superstrate antenna is -4 degrees, as shown in Figure 2.8. The metasurface superstrate antenna, on the other hand, has a higher gain than the other designs, making it more appropriate for application.

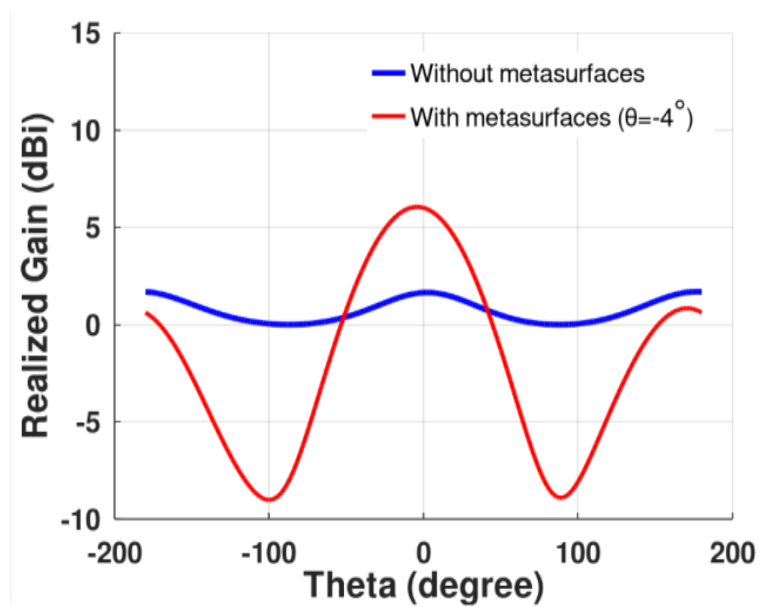


Figure 2.8. Comparison of beam scanning without metasurface & with metasurface upto -4

2.5 Comparative performance analysis of proposed antenna with existing design

This section provides a comparative analysis of the proposed antenna's performance against existing designs. Such as gain, size, feeding method, substrate and permittivity, and operating frequency band are considered.

Table 2.2 – Comparison of different type of existing antenna and proposed antenna

S.No	References	Operating frequency band	Size (mm)	Substrate & Permittivity	Gain (dBi)	Feeding method
1.	Pan et al. [16]	2.01-4.27 GHz & 5.06-6.79 GHz	48x58	Teflon (2.65)	2	Microstrip feed
2.	Karli & Ammor [17]	2.72-2.76 GHz & 6.62-7.5GHz	60x70	FR-4	-	Microstrip feed
3.	Jen-Yea Jan, et al. [18]	3.3-3.8 GHz, 3.2-4.2 GHz	50x50	FR-4(4.4)	5.3	CPW-fed
4.	D. Wen, Y. Hao [19]	1.85-2.9 Ghz	80x40	FR-4(4.4)	2	Coaxial fed
5.	J. Joubert [20]	2.4 Ghz	125x100	Rogers	5.3	CPW-Fed
6.	A.Bagwari, R.Tiwari [21]	2.51-3.96GHz & 5.2- 5.9GHz GHz	35x39	FR-4(4.3)	3.67	CPW-Fed
7.	Proposed Antenna	3.86-4.49 GHz	40x40	FR-4 (4.4)	6.06	CPW-Fed

As evident from the Table 2.2, the proposed antenna exhibits superior gain, wider bandwidth compared to the existing designs. Additionally, the proposed antenna's compact size, low profile, simple structure. Furthermore, a detailed discussion of the factors contributing to the performance improvement of the proposed antenna is presented.

2.6 Conclusions

The CPW-fed approach was created to improve the antenna's properties. We're utilizing CPW-fed to increase bandwidth and gain. A metasurface-based patch antenna for 5G that is CPW-fed and enabled by a metasurface superstrate above the antenna is shown in the proposed work. The metasurface superstrate is positioned above the antenna and reflects the antenna's radiation in phase, resulting in increased gain and scanning. The realized antenna has a -10 dB bandwidth (3.86-4.49 GHz), 6.06 dBi realized gain, 92 percent efficiency, and a -4-degree scanning capability. The suggested research demonstrates that the antenna may be utilized for 5G connectivity.

Chapter 3

High Gain Microstrip Patch Antenna with Fabry-Perot Cavity for 5G Communication

This chapter explores techniques to enhance gain of a Fabry-Perot cavity-based microstrip antenna for 5G. We investigate PEC sheets, high-dielectric, and metasurface superstrates. While PEC increases gain, it enlarges the antenna. High-dielectric superstrates are costly and less accessible. This chapter lays groundwork for a practical high-gain antenna solution.

3.1 Introduction

Next-generation wireless technologies for 5G and beyond require high gain antennas with wide bandwidth. The 3.5 GHz frequency band has shown promising results in the implementation of 5G. The deployment speed of the 5G network in the mid-bands e.g 3.5 GHz is significantly faster due to its propagation characteristics. There have been efforts to implement 5G communication systems in the 3.5 GHz band. A microstrip patch antenna is broadly used over conventional antennas because of its size, cheap cost, and lightweight.

In the literature, the metasurface-enabled conformal antenna consists of two components with an operating frequency from 2.36-2.4GHz gain is 6 dBi [24]. Whereas, 6.3dBi gain is reported in [2] where a finite-size small high impedance surface (HIS) antenna is used to create a highly directional antenna for a smartwatch with an operating frequency is 2.4 GHz and an efficiency of 46 %. However, RF antenna filter achieved 4.7 % of bandwidth which covered 4.06 - 4.2 GHz band and a maximum gain of 4.3 dBi [26]. Based on the Theory of Characteristic Modes (TCM), a wideband is created with a consistent omnidirectional radiation pattern [27].

In this chapter, design a metasurface superstrate-based antenna. Instead of employing multiple elements, a single element antenna is design using a metasurface superstrate. The gain of the antenna is increased by a perfect electric conductor (PEC) sheet, high dielectric

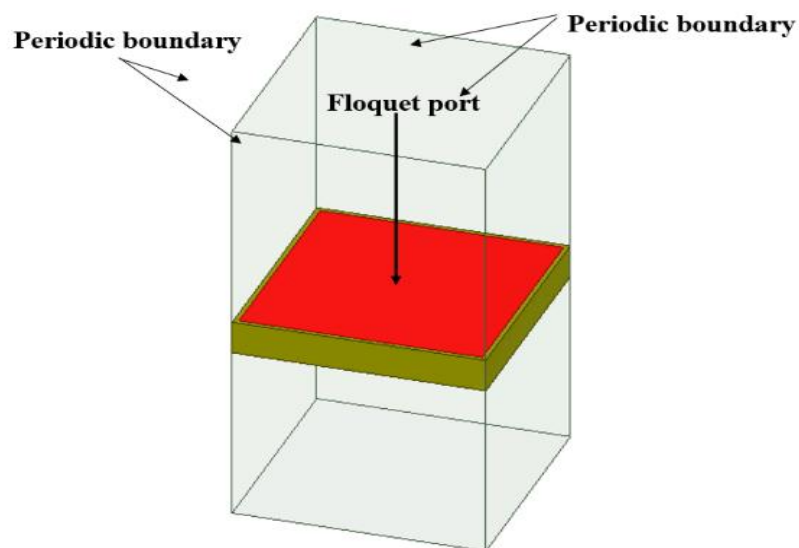
superstrate, and metasurface superstrate. A comparison of performance among the three antennas and previous work is also presented to determine the most efficient design. Finally, the proposed metasurface-based antenna achieved better results as compared to the PEC sheet and high dielectric superstrate-based antenna.

3.2 Design of the Proposed Antenna

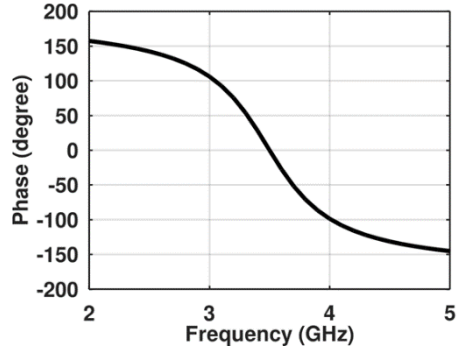
The design of the metasurface superstrate-based microstrip patch antenna is described which has a resonant frequency of 3.5GHz.

3.2.1 Design Procedure of Metasurface Unit Cell

The design and phase reflection characteristic of metasurface superstrate is shown in Figure 3.1. The metasurface comprises of 4×4 grid of square metallic patches with a size of 9.83 mm and the unit cell has a 10 mm periodicity. The dielectric used in work is FR4 substrate of height is 1.6 mm and permittivity 4.4. The proposed metasurface superstrate is designed at 3.5 GHz.



(a)



(b)

Figure 3.1 Reflection phase characteristics of metasurface (a) unit cell (b) Phase.

3.2.2 Design Procedure of Microstrip Patch Antenna

A microstrip patch antenna with microstrip fed as shown in Figure 3.2. The antenna geometry is defined by its length (l) and width (W) and is fed via a 50Ω SMA connector. Fabricated on an FR4 substrate ($\epsilon_r = 4.4$, $\tan \delta = 0.02$) with a thickness of 1.6 mm, the antenna dimensions are as follows: $L_g = 40$ mm, $W_g = 40$ mm, $L_p = 35$ mm, $W_p = 20$ mm, $L_f = 11.67$ mm (all dimensions in millimeters).

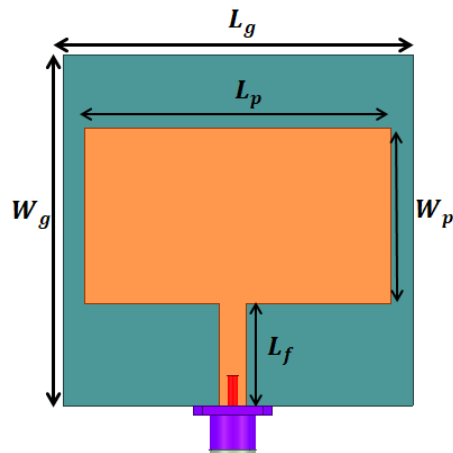
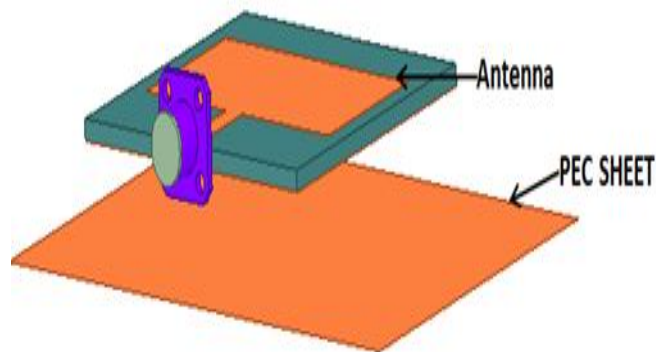


Figure 3.2 Dimensions of the microstrip patch antenna. [Dimensions in mm $L_g = 40$, $W_g = 40$, $L_p = 35$, $W_p = 20$, $L_f = 11.67$]

3.2.3 Design of Proposed Microstrip Patch Antenna with Three Configurations

In the first design, the antenna gain is increased by a PEC sheet placed below the antenna at 5.6 mm far away which acts as a reflector as shown in Figure 3.3 (a) and reflects the radiations from the antenna at 180° phase shift and increase the forward radiation. The limitation of the PEC sheet acquires large space and alignment with the center of the antenna is complicated which may affect the performance of the antenna. In the second design, the gain of the antenna is also enhanced by using a 1.6 mm high dielectric superstrate with permittivity of 40 as shown in Figure 3.3 (b). The limitation of high permittivity substrate is not easily available and the cost of the design increases also. In the third design, the metasurface works as Fabry Perot cavity formed between the antenna and metasurface superstrate which decides the gain after multi transmission and reflection is presented in Figure 3.3 (c). The antenna gain is drastically enhanced as compared to PEC and high dielectric superstrate. The side view of the metasurface-based microstrip patch antenna is shown in Figure 3.3 (d) where g_p (11.8mm) is the gap between metasurface superstrate and the antenna.



(a)

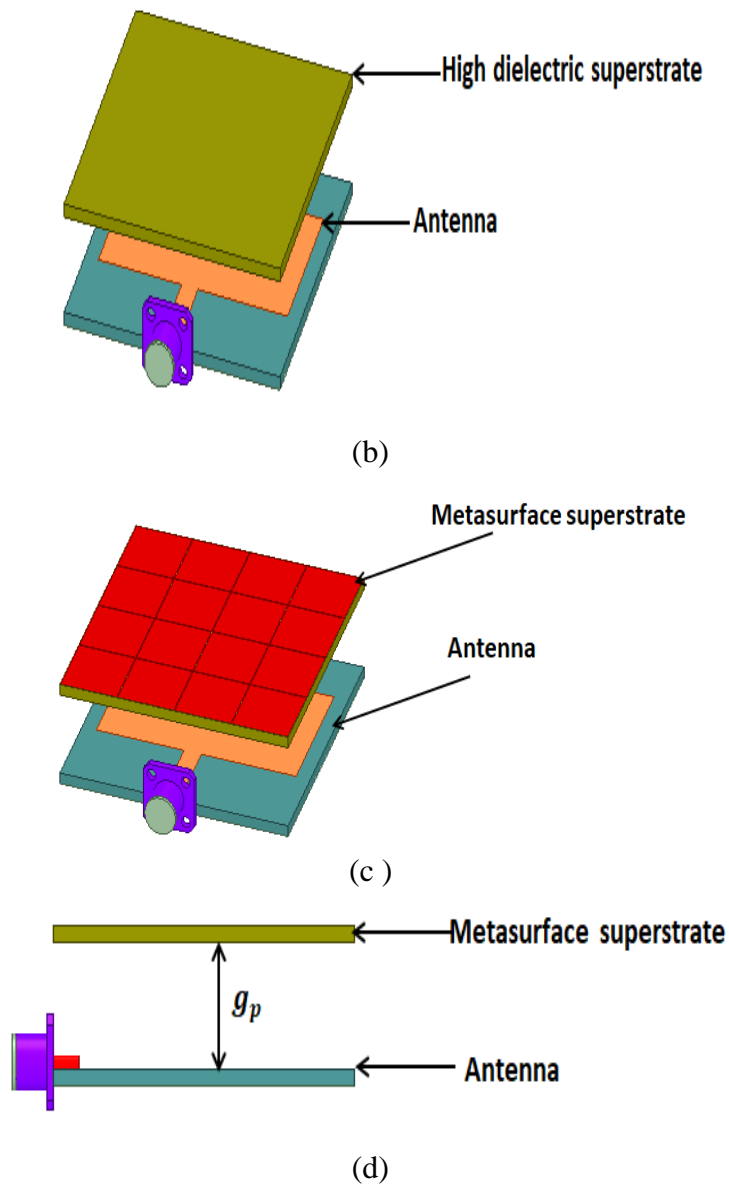
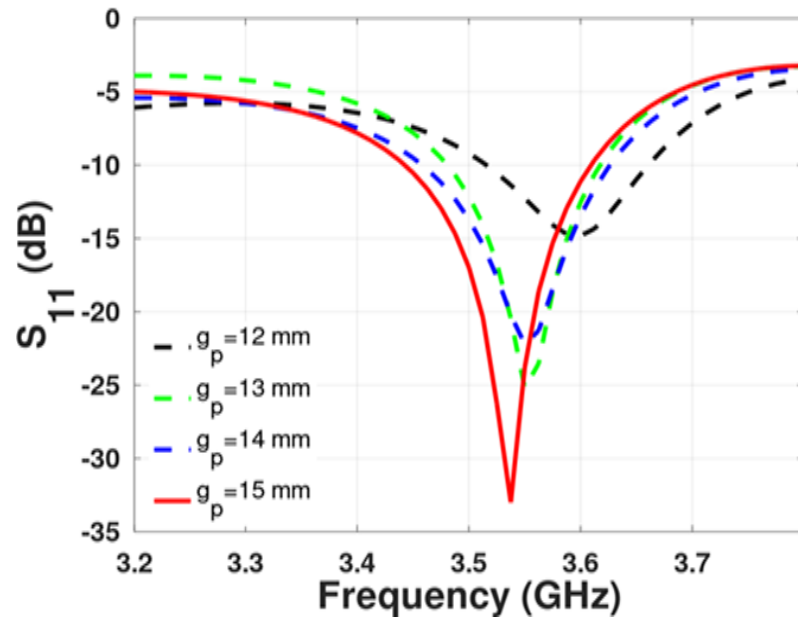


Figure 3.3 Proposed antenna with (a) PEC sheet (b) high dielectric superstrate (c) metasurface superstrate (d) side view of the proposed metasurface superstrate antenna.

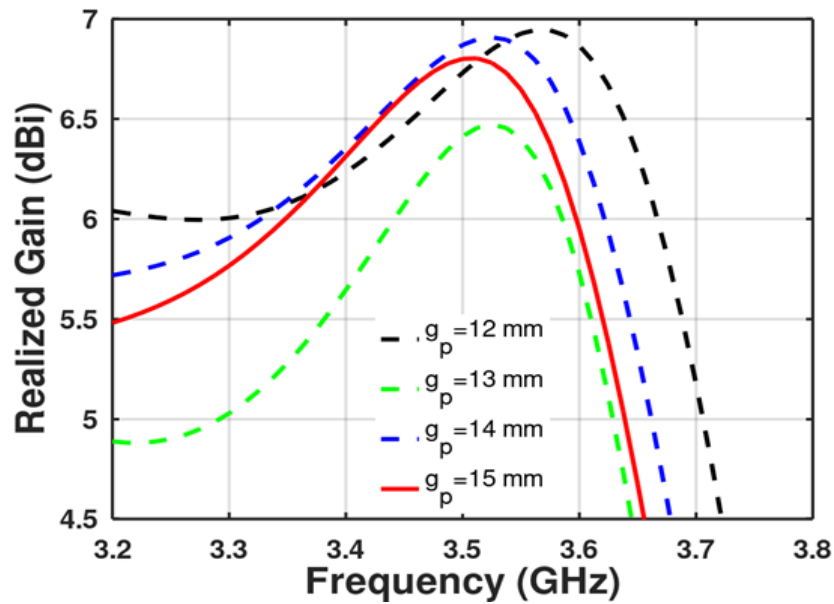
3.4 Parametric Analysis

Using Ansys HFSS, the antenna design over the operated band was simulated and design parameter of the antenna structure was optimized. The dimensions of the antenna are obtained by performing parametric analysis on the parameter g_p gap between the antenna and metasurface superstrate. The effect of ' g_p ' on the s-parameter is studied in Figure 3.4

(a). The value of ' g_p ' is varied from 12 to 15 mm. It is observed that the optimized value of $g_p = 15$ mm which provides desired bandwidth and good return loss. In the case of realized gain, the variation of g_p is given in Figure 3.4 (b). The optimized value of $g_p=15$ mm provides better gain with a high return loss.



(a)



(b)

Figure 3.4 Parametric analysis of the antenna. (a) S-parameter (b) Realized gain.

3.5 Results & Analysis of the Antenna

3.5.1 S- Parameter

Figure 3.5 shows the s-parameter of the design with the PEC sheet, high dielectric superstrate, and metasurface superstrate. It can be observed that the metasurface superstrate (Fabry-Perot cavity) increases the bandwidth and also improves the antenna return loss.

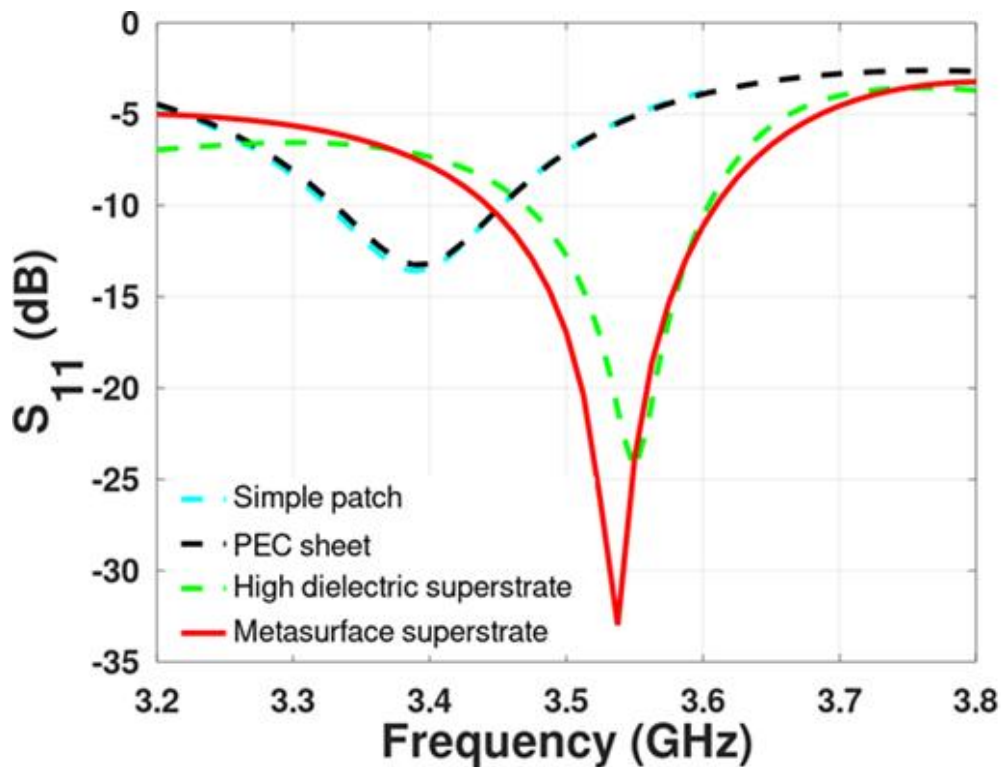


Figure 3.5 Comparison of the s-parameter with a simple patch, superstrates, and PEC sheet.

3.5.2 Realized Gain

The multiple reflections and transmissions between the antenna and metasurface (Fabry-Perot cavity) increase the gain of the antenna. The wave coming out after multiple reflections and transmissions are in phase which results in gain enhancement. It is observed from Figure 3.6, that a gain of the metasurface superstrate structure is improved as compared to the PEC sheet and high dielectric superstrate antenna.

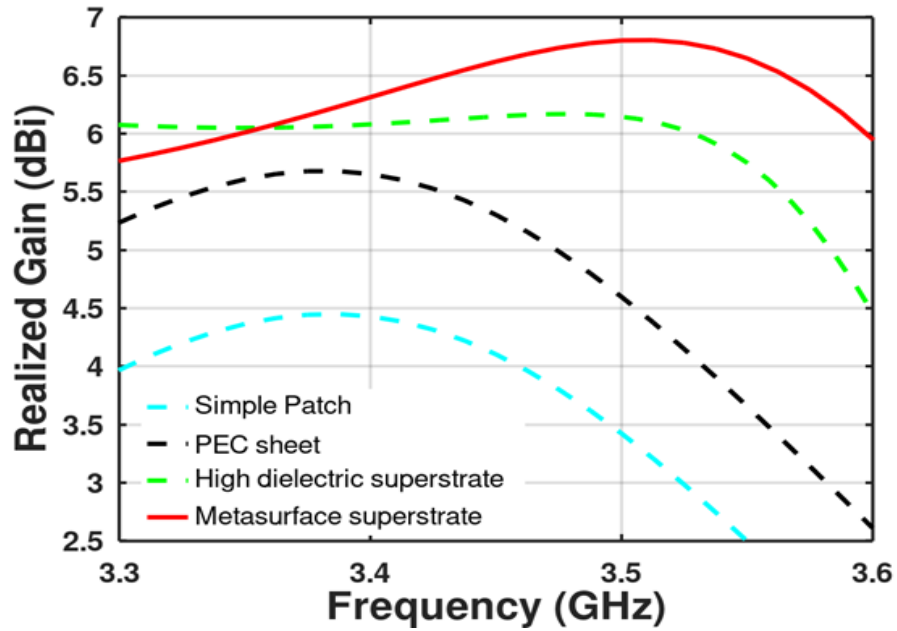


Figure 3.6 Comparison of realized gain with a simple patch, superstrates, and PEC sheet.

3.5.3 Radiation Pattern

Figure 3.7 shows the 3D radiation pattern of the antenna with a simple patch, PEC sheet, dielectric superstrate, and metasurface superstrate. It shows that the metasurface superstrate-based antenna increased more forward radiation among PEC sheet and high dielectric superstrate which increased the antenna gain. Figure 3.8 demonstrate 2D pattern at 3.5 GHz with different phi cuts.

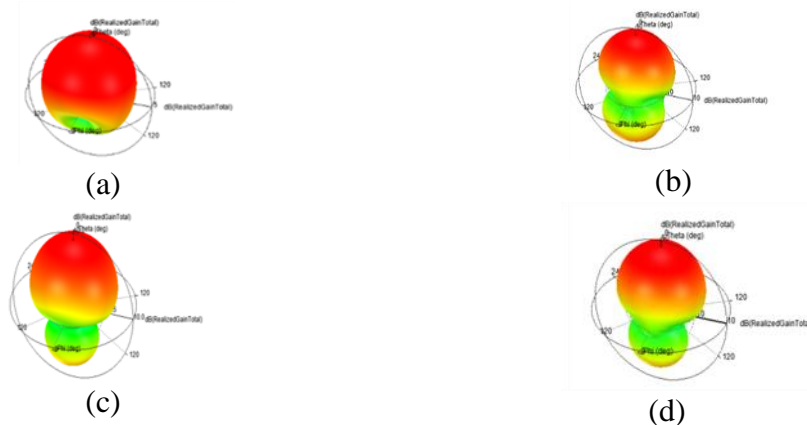


Figure 3.7 3D radiation pattern (a) Simple patch (b) with PEC sheet (c) with dielectric superstrate (d) with metasurface superstrate

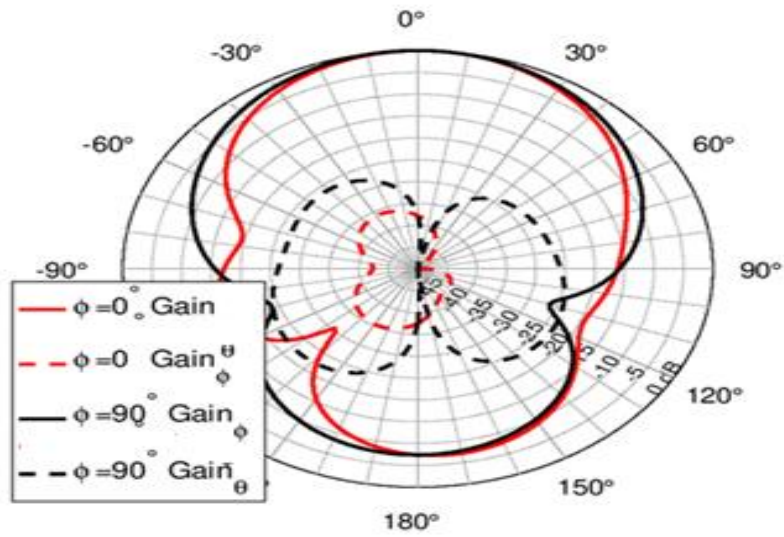


Figure 3.8 Radiation pattern of the proposed antenna at 3.5 GHz.

3.5.4 Efficiency

Figure 3.9 illustrates that the efficiency of the metasurface superstrate antenna is more than the PEC sheet-based antenna but slightly less than the high dielectric superstrate antenna. However, the gain of the metasurface superstrate antenna is high as compared to the other two structures which makes it more suitable to use.

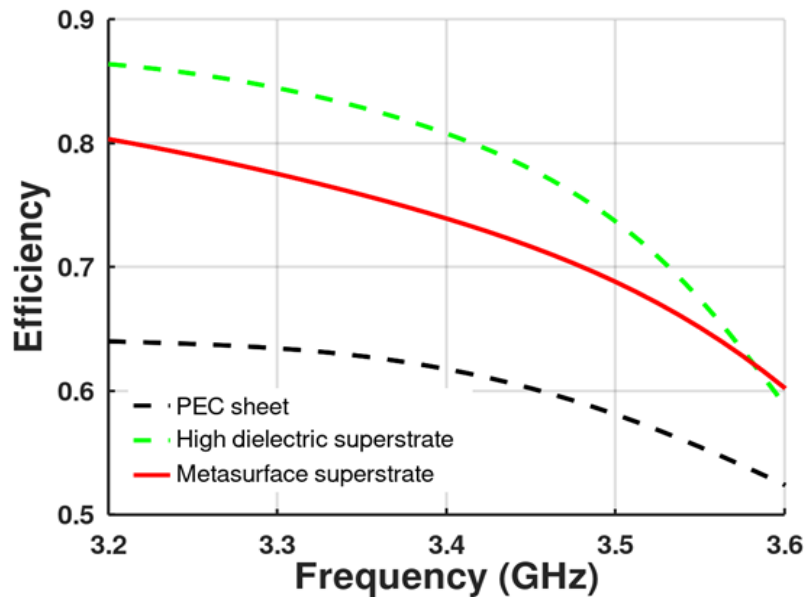


Figure 3.9 Simulated efficiency of the antenna

3.6 Comparative Performance Analysis of Proposed Antenna with Existing Design

The proposed design's comparisons are shown in Table 3.1 in terms of size, bandwidth, gain, and efficiency with existing work, reported in the literature. The proposed work shows better results as compared to other antennas.

Table 3.1 Comparison of different existing structures

Ref no.	Antenna Type	Dimension (λ_0)	Frequency band (GHz)	Gain (dBi)	Efficiency (%)
[23]	Metasurface-enabled conformal	0.5×0.3×0.02 8	2.36-2.4	6.2	-
[24]	Dual layer EBG	0.17×0.17×0. 5	2.45	3.26	59.68
[25]	HIS	0.30×0.30×0. 24	2.4	6.3	46
[26]	RF antenna filter	30×20×1.6 (mm)	4.06-4.26 (3.95)	4.3	-
[27]	Wide band	0.49×0.24×0. 004	1.85-2.9	2	-
This Work	Metasurface MSA	0.467×0.467× 0.175	3.44- 3.61(4.9%)	6.8	69

3.7 Conclusions

The proposed work demonstrates a metasurface-based patch antenna for 5G, which is enabled by a metasurface superstrate over the antenna which works as a Fabry Perot cavity. The metasurface superstrate is placed above the antenna which reflects the radiation in phase from the antenna which increases the gain as well as bandwidth. The realized antenna achieved - 10 dB bandwidth which covers (3.44-3.61 GHz), 6.8 dBi realized gain and 69 % efficiency. The proposed work shows that the designed antenna can be used for 5G communication.

Chapter 4

Metasurface Decoupling for Closely Spaced 5G MIMO Antennas

This chapter introduces a compact MIMO antenna array operating at 3.5 GHz. To enhance isolation between closely spaced patch antennas, a metasurface-based decoupling structure is proposed. Simulation and measurement results demonstrate a significant improvement in isolation from 10 dB to 35 dB, while also increasing antenna gain by 2 dB. The proposed design offers a promising solution for high-performance MIMO systems.

4.1 Introduction

In recent years, the wireless communication landscape has undergone rapid evolution, characterized by a burgeoning user base and escalating demands for enhanced data rates and reliability. To address these challenges, Multiple-Input-Multiple-Output (MIMO) systems have emerged as a focal point of research due to their inherent advantages in channel capacity and link robustness. A primary objective for antenna engineers in MIMO system design is to achieve superior isolation between antenna elements. To this end, considerable research efforts have been directed towards mitigating correlation and improving port isolation.

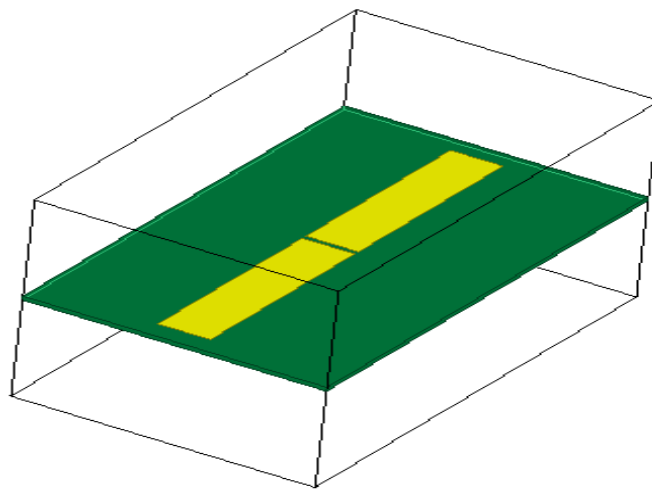
In the literature, [50-51] used the potential for the decrease in ρ to enhance isolation unintentionally and the radiation patterns of the antenna array [52-54]. Consequently, although these techniques reduce coupling between the MIMO antenna's components, increasing radiation efficiency, it is uncertain how they may affect channel correlation. In [56-57] the previously stated techniques, even while they increase the MIMO antenna's radiation efficiency by reducing coupling between its components, do not guarantee a definite impact on channel correlation.

A metasurface based decoupling method (MDM) consists pair of non-uniform cut wires with different lengths reducing mutual coupling dual-band two-element MIMO antenna array closely coupled with a distance of only 0.008 and achieved isolation is 25 dB[24]. This paper introduces a rectangular microstrip MIMO antenna operating at 3.5 GHz with decoupling structures. It has a 1 mm ($0.011 \lambda_0$) spacing between antennas, and a metasurface is employed as the decoupling structure. A metasurface made up of two uniform cut wires is placed as a superstrate above the antennas, achieving a substantial 35 dB isolation at 3.5 GHz.

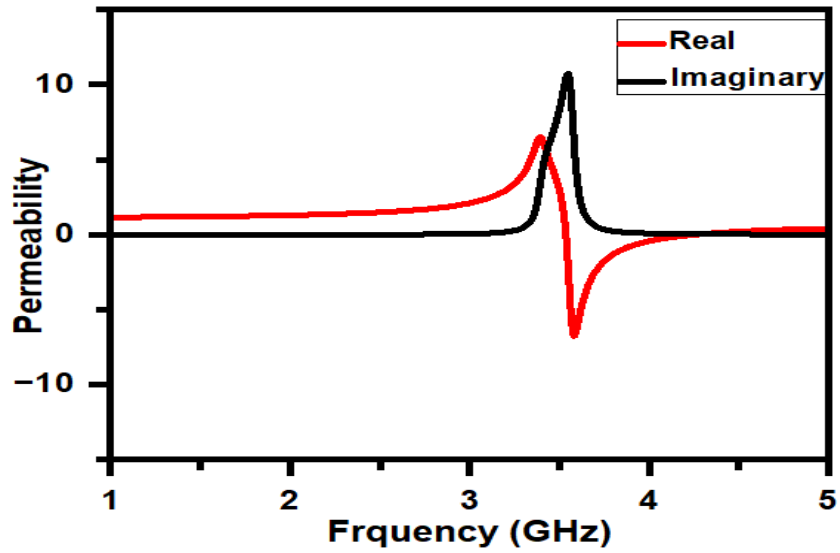
4.2 Design Procedure of Proposed Antenna

4.2.1 Metasurface Design and Analysis

The design and reflective index characteristics of the metasurface unit cell are shown in Figure 4.1. The metasurface consists of two cut wires with a size of 58 mm width and 45 mm length. The FR-4 substrate with a height of 0.8mm and a dielectric constant of 4.4. The proposed metasurface is designed for 3.5 GHz and the real part of permeability is negative.



(a)

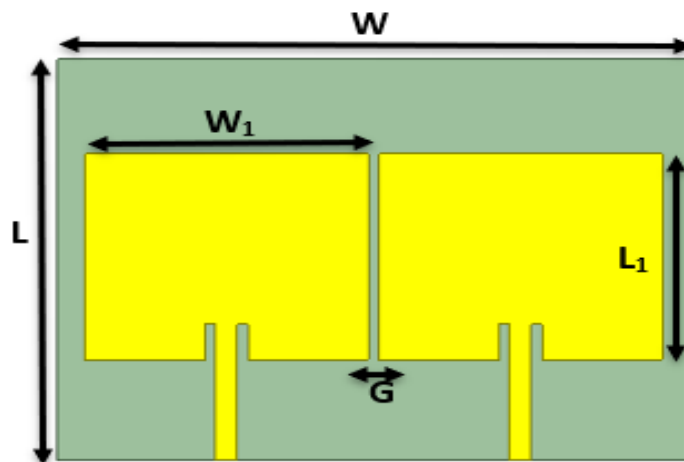


(b)

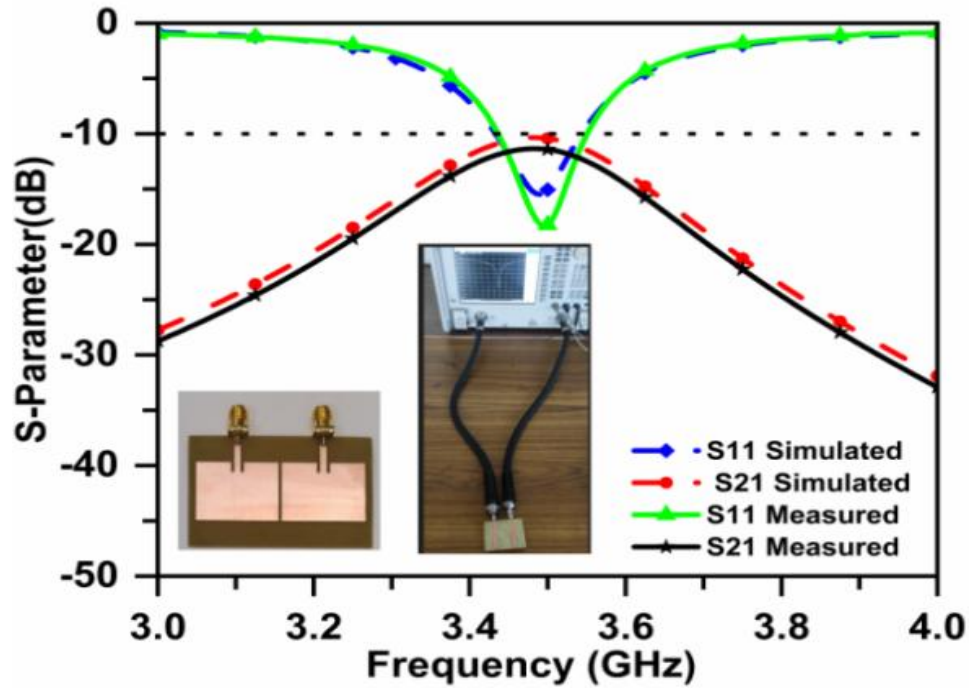
Figure 4.1 (a) Unit cell with cut wire (b) Permeability characteristics of metasurface

4.2.2 Design of Microstrip MIMO Antenna

The geometry of two antennae with a separation of 1mm is shown in Figure 4.2(a). The FR-4 substrate with a dielectric constant of 4.4 is used for the fabrication of both antennas. The overall size of the two-element antenna array is 40 mm (width) \times 58 mm (length). The dimensions are: $W=58$ mm, $L=40$ mm, $W_1=26$ mm, $L_1=20.55$ mm and $G=1$ mm . Figure 4.2(b) shows the simulated and measured S-parameter of 2- Port MIMO antenna where isolation is -10dB at 3.5GHz and S_{11} is well below -10 dB.



(a)



(b)

Figure 4.2 (a) Geometry (b) Simulated & Measured S-parameter of MIMO antenna

4.2.3 Design of Microstrip MIMO Antenna with a Metasurface

To improve the isolation a metasurface with two cut wires on the top of the mimo antenna with a certain height has been incorporated in Figure 4.3. The key variables of Metasurface for improving the isolation of MIMO antennas are Wire length, Wire Gap, and Height of Metasurface. Due to the metasurface superstrate inevitably influencing the initial matching condition, adjustments are made to the antenna geometry and feed structure after successfully decoupling the two antennas to meet the matching specifications. The final optimized dimensional of the MIMO antenna is given in Table 4.1. The simulated and measured S-parameters with the metasurface are presented in Figure 4.6(a). Using metasurface the isolation between two antennas improved by 35 dB for the frequency range of 3.42 GHz to 3.62 GHz.

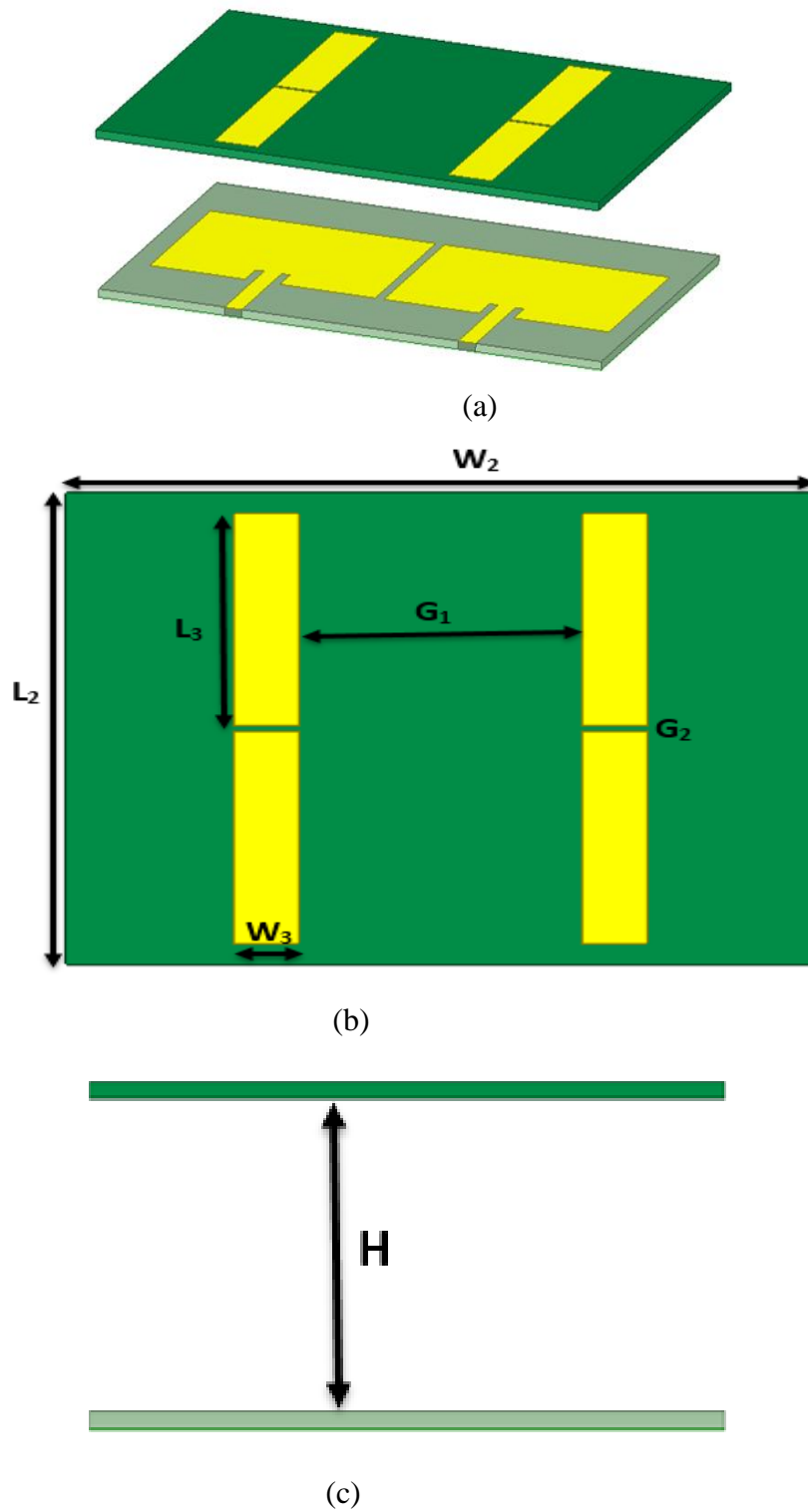
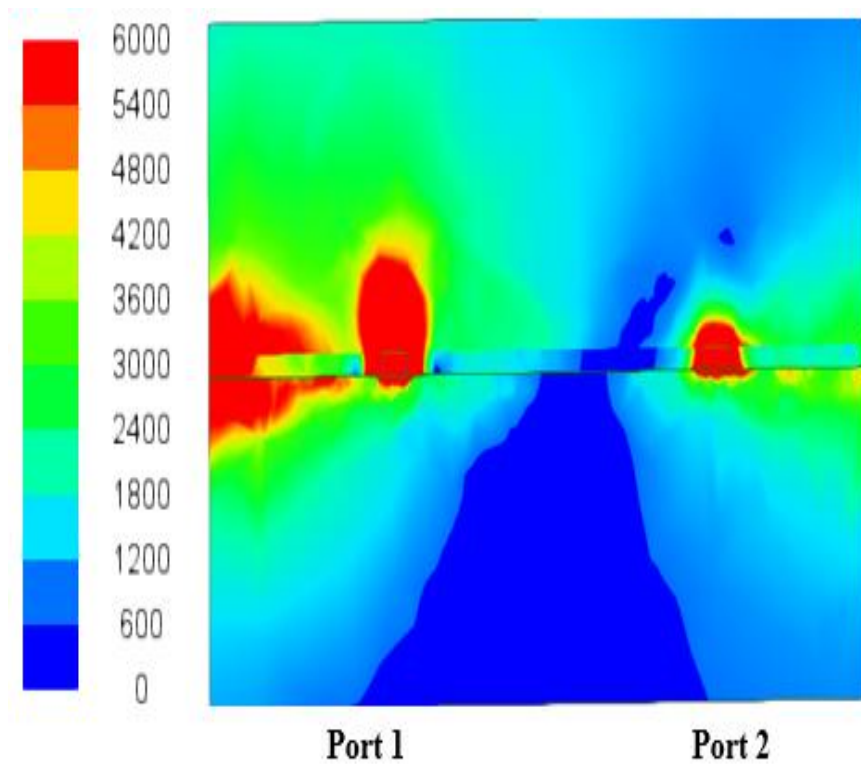


Figure 4.3 (a) Proposed MIMO antenna with metasurface (b) top view (c) side view

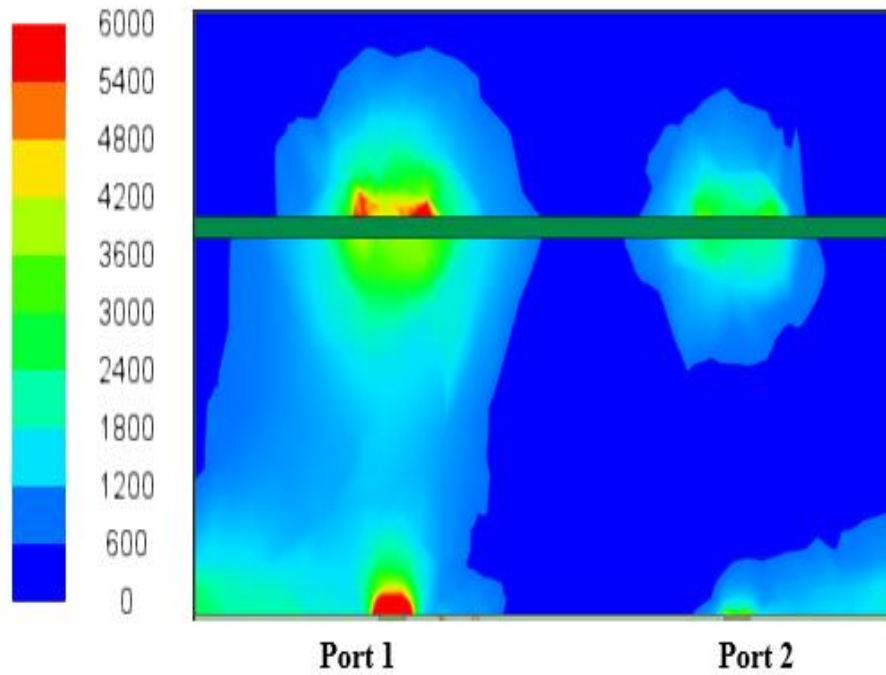
Table 4.1 Dimensions of the metasurface (Units: mm)

W_2	L_2	W_3	L_3	H	G_1	G_2
58	45	5	20.25	15	22	0.5

Figure 4.4 shows the electric field current distribution with and without metasurface at 3.5GHz. When the metasurface superstrate is not present, a noticeable concentration of the electric field occurs around antenna2. Upon introducing the metasurface, the distribution of the electric field around antenna2 decreases significantly. Instead, the electric field is strongly concentrated on the metasurface, forming shielding zones for antenna2.



(a)

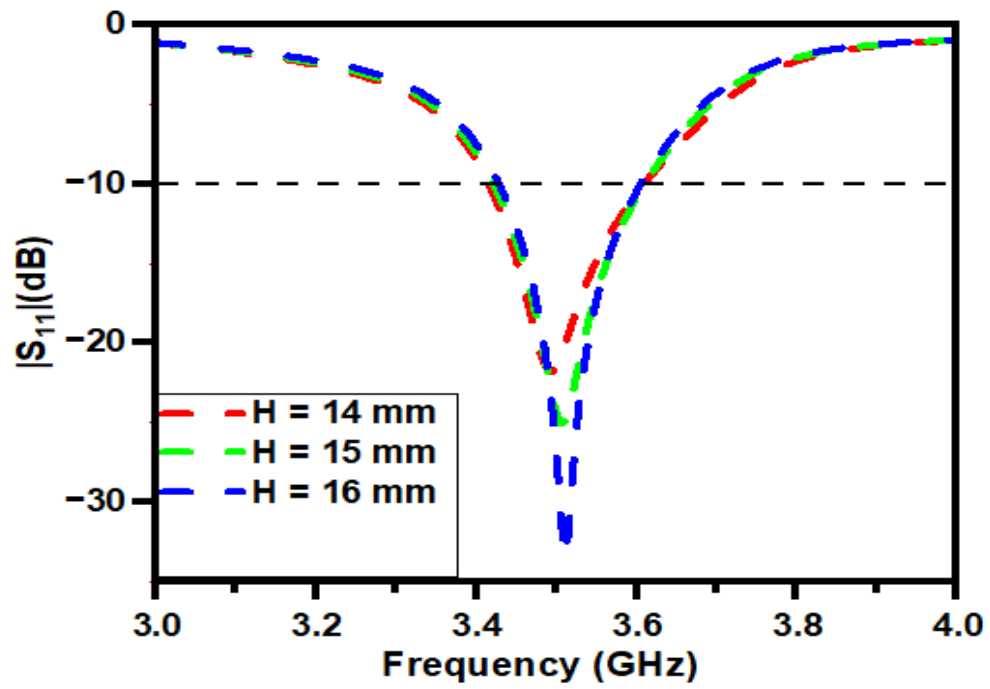


(b)

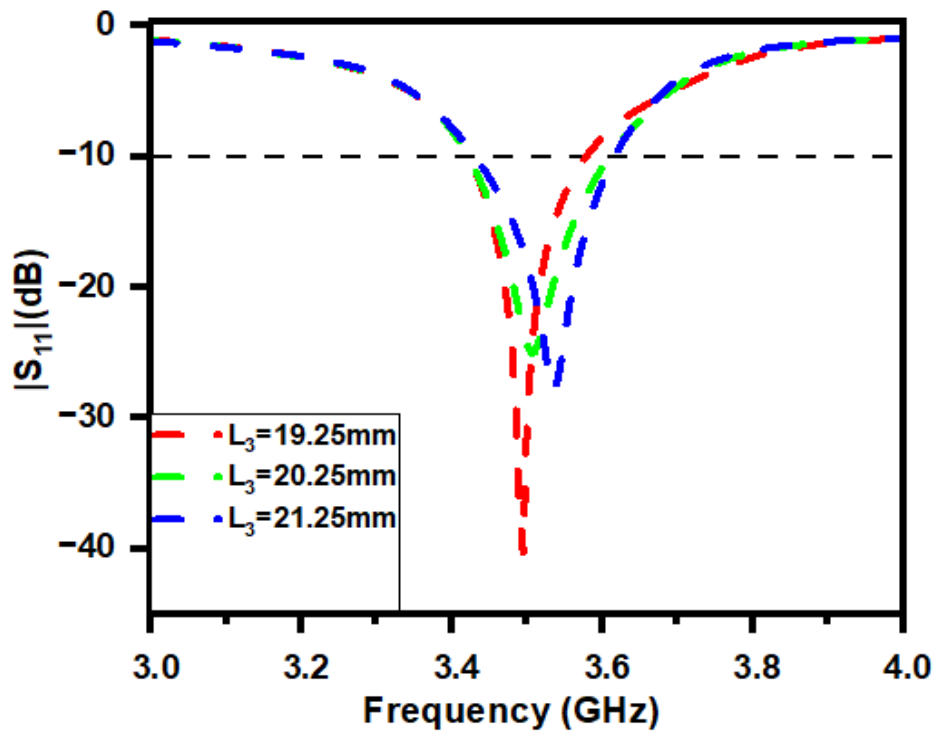
Figure 4.4 Simulated magnitude of electric field distribution (a) without metasurface (b) with metasurface

4.3 Parametric Analysis

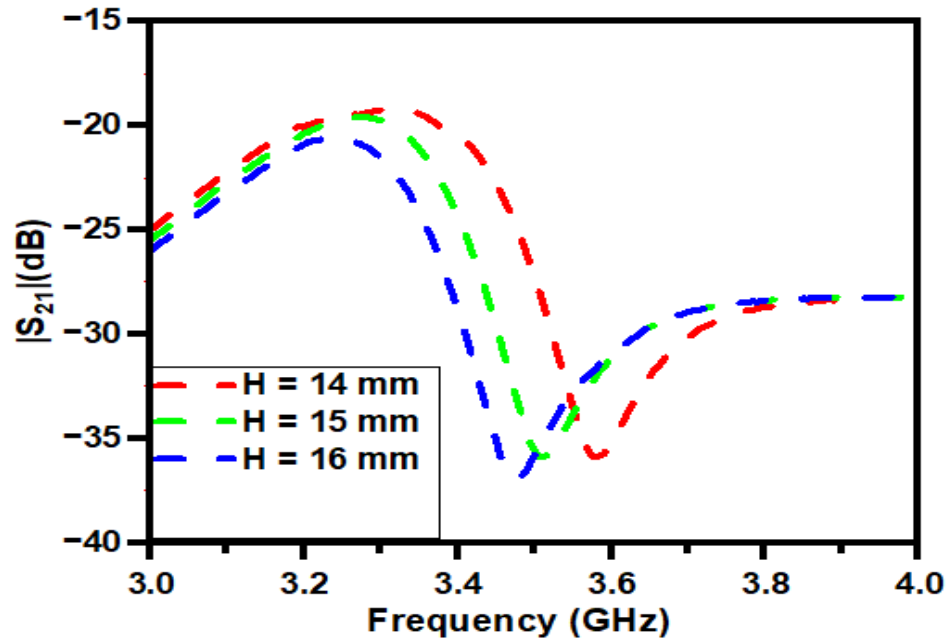
Using Ansys HFSS, the simulation of the antenna design across the operational frequency range was conducted, and the design parameters for the antenna structure were fine-tuned. The antenna's dimensions were determined through a parametric analysis involving the metasurface height (parameter H) and the length of cut wires (parameter L₃). The impact of H and L₃ on the S₁₁ and S₂₁ parameters is illustrated in Figure 4.5. The H varied between 14 and 16 mm, while L₃ ranged from 19.25 to 21.25 mm. The optimized values were identified as H = 15 mm and L₃ = 20.25 mm, resulting in the desired favourable return loss.



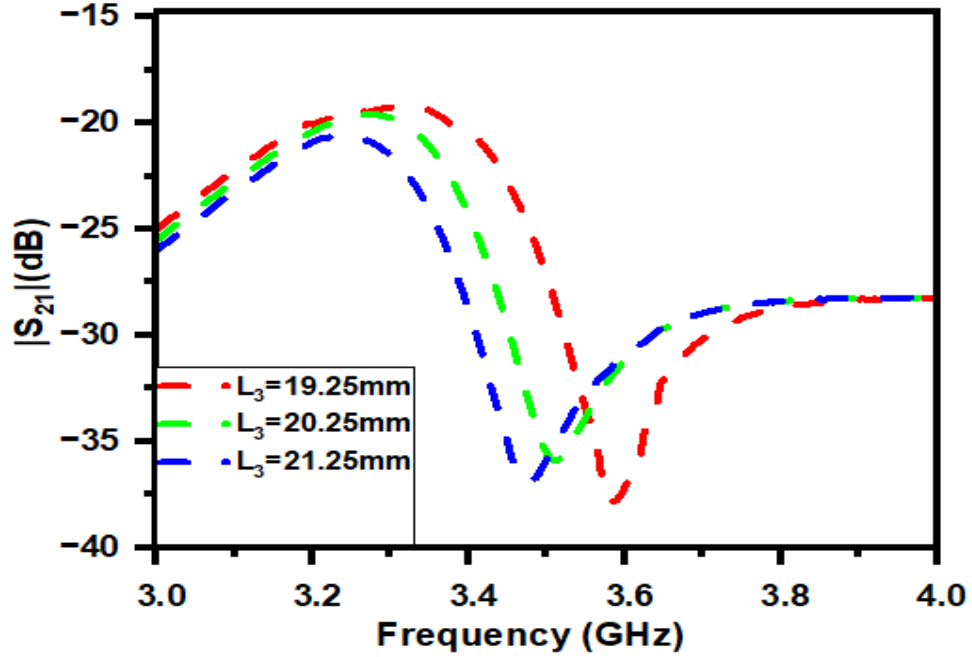
(a)



(b)



(c)

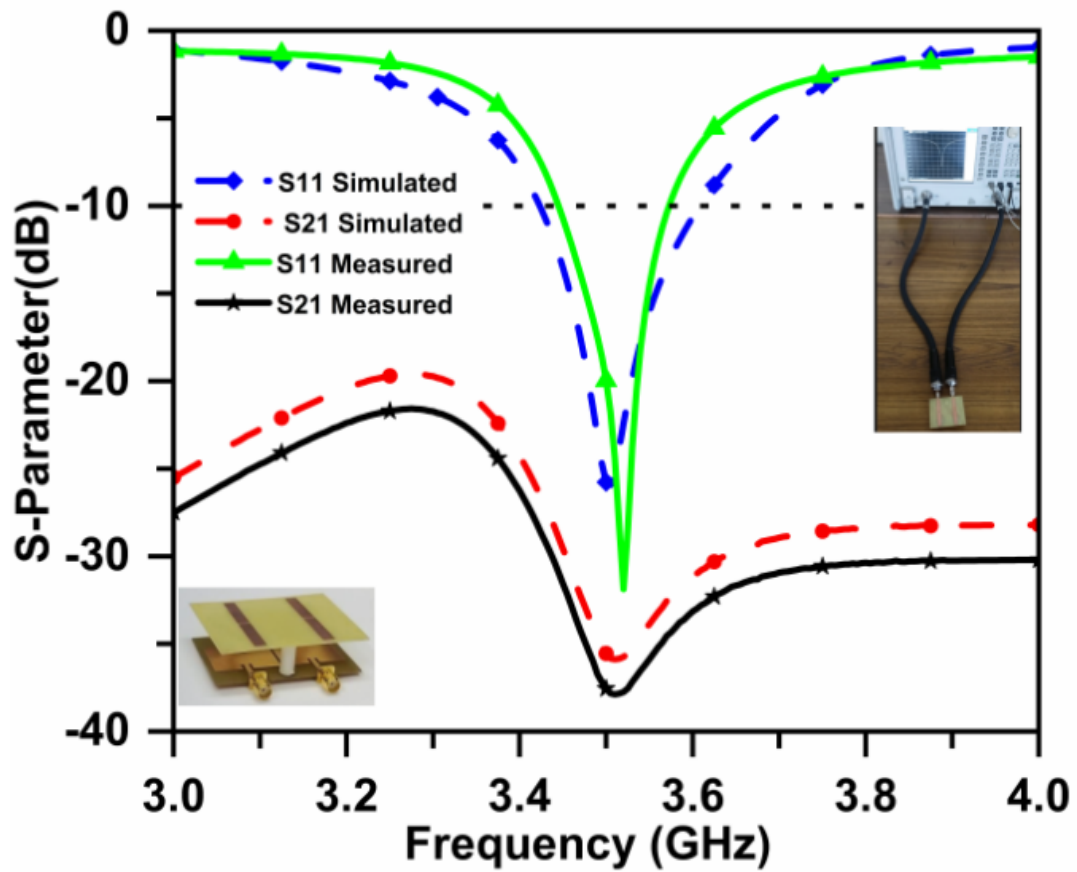


(d)

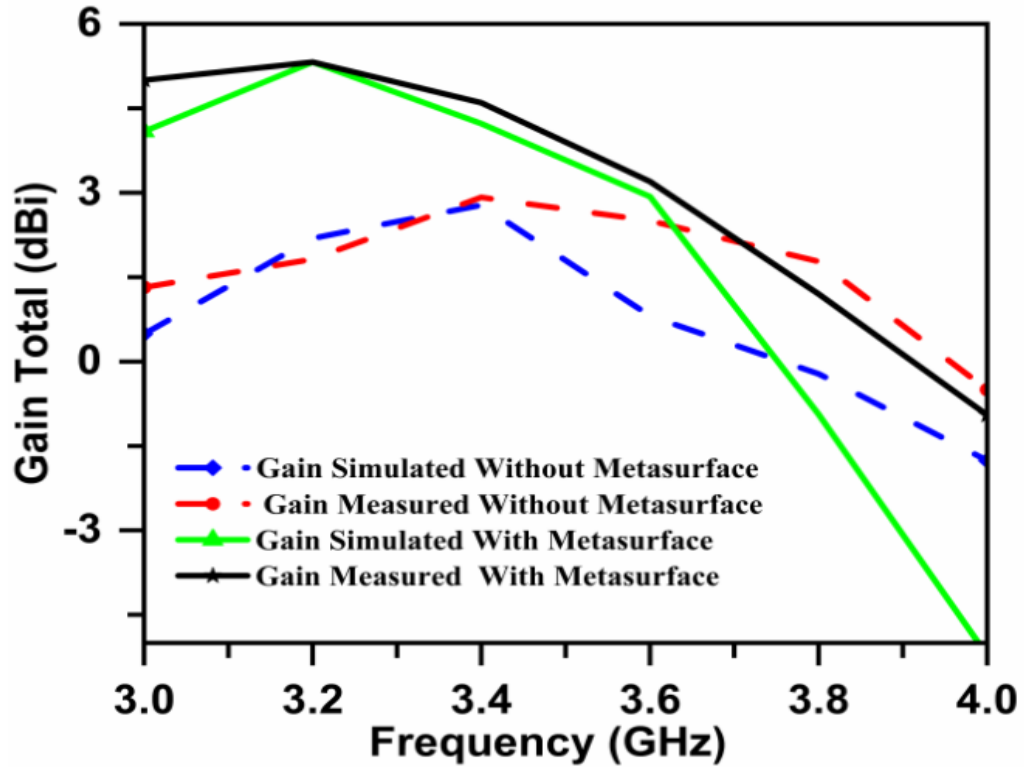
Figure 4.5 Parametric analysis of proposed MIMO antenna (a) $|S_{11}|$ with H (b) $|S_{11}|$ with L
 (c) $|S_{21}|$ with H (d) $|S_{21}|$ with L

4.4 Simulated and Measured Results

The simulated and measured S-parameters of the suggested antenna are presented in Figure 4.6(a). The measured findings confirm the effective suppression of the mutual coupling between the antennas. Figure 4.6(b), shows that the proposed antennas with the metasurface exhibit an enhanced peak gain in contrast to the original antennas without metasurfaces at 3.5 GHz, the gain has been increased from 1.82 dBi to 3.85 dBi.



(a)



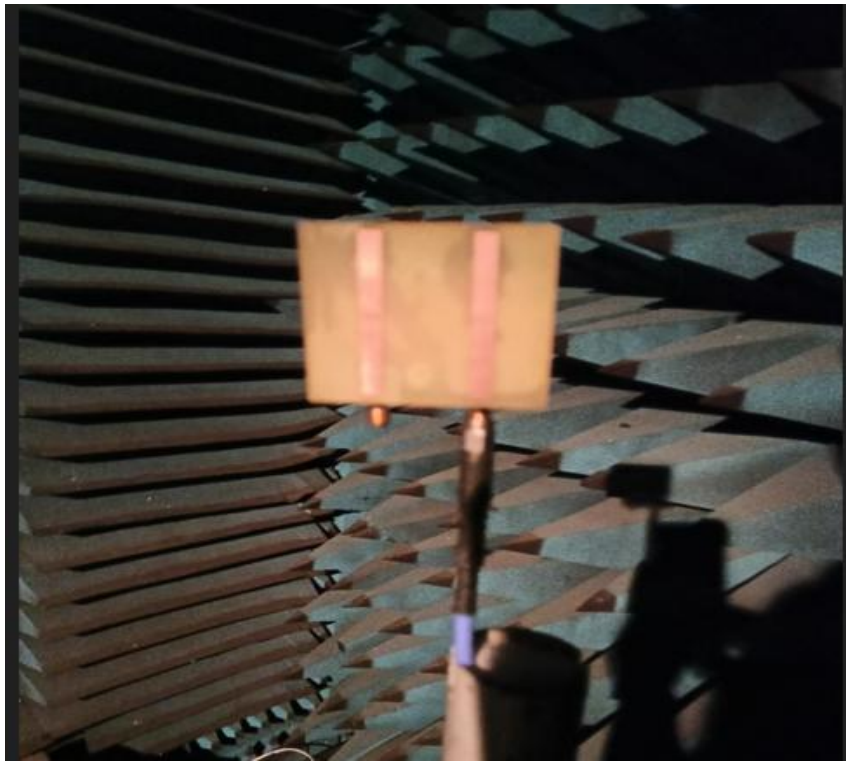
(b)

Figure 4.6 Simulated and Measured (a) S-parameter of the proposed antenna and (b) Gain with and without metasurface.

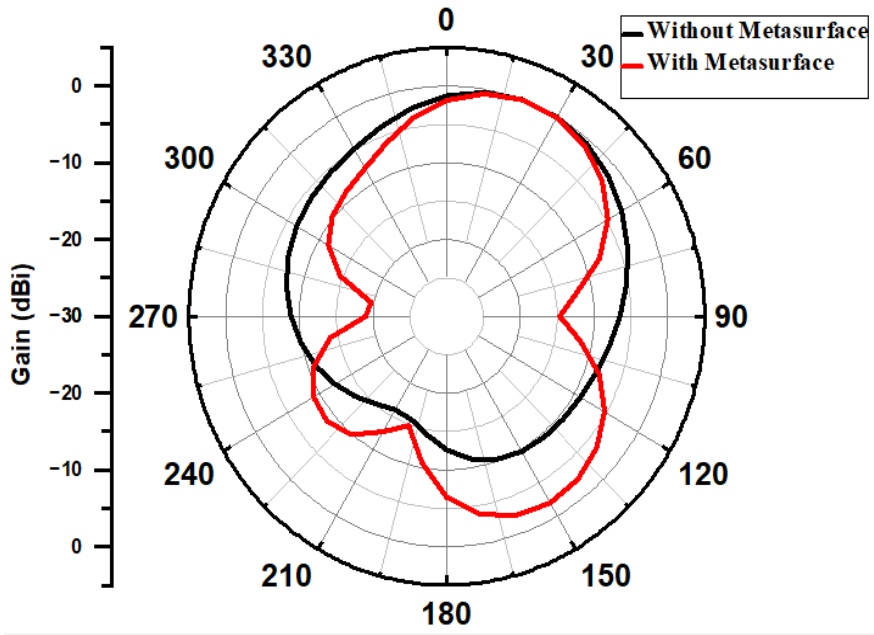
Figure 4.7(a) illustrates S-parameter measurement by VNA & Figure 4.7(b) shows anechoic chamber measurement of the radiation pattern, fabricated antenna samples and the test antenna, each antenna is independently stimulated, with the other antenna terminated by a matched load. To validate the simulated radiation patterns, a comparison is made between antennas without a metasurface and with a metasurface at 3.5 GHz, depicted in Figure 4.7(c) and (d). Additionally, Figures 4.7(e) and (f) present a comparison between the measured and simulated results with the metasurface.



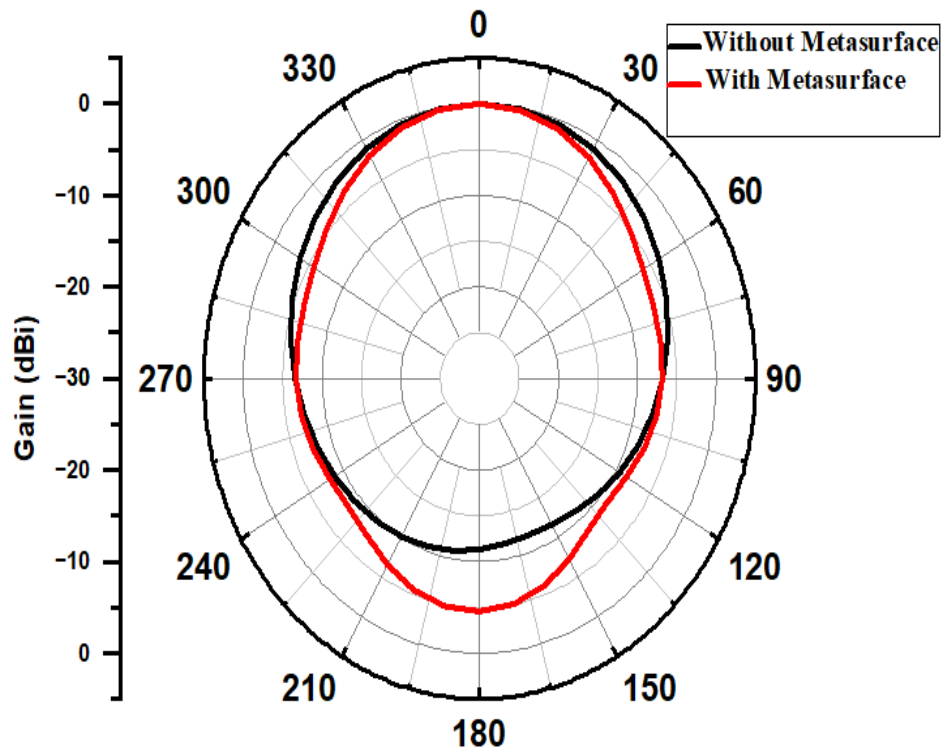
(a)



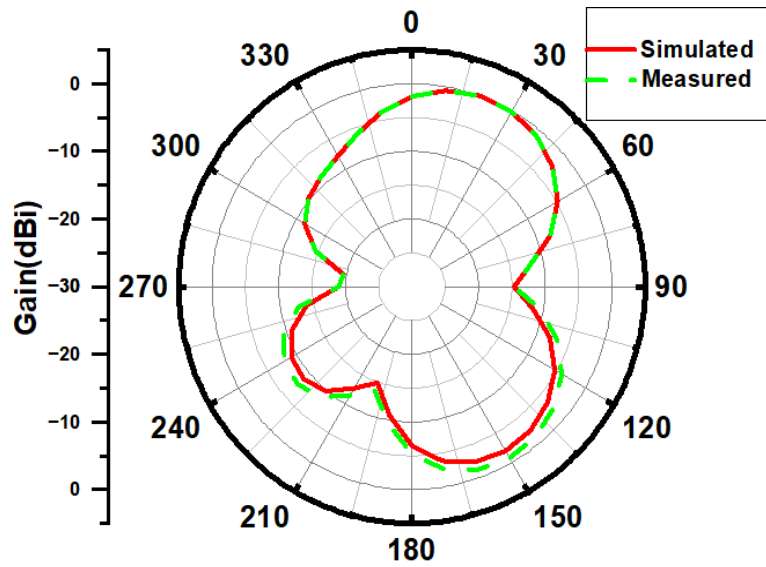
(b)



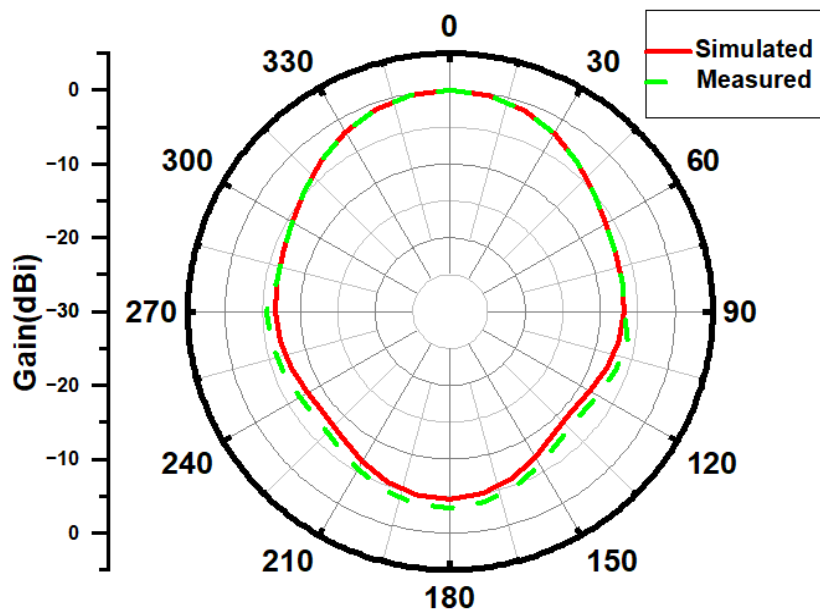
(c)



(d)



(e)



(f)

Figure 4.7 (a) S-parameter measurement by VNA (b) Radiation pattern measurement setup (a) $\Phi = 0^\circ$ Simulated with & without metasurface (b) $\Phi = 90^\circ$ Simulated with and without metasurface (c) $\Phi = 0^\circ$ Measured & Simulated with metasurface (d) $\Phi = 90^\circ$ Measured & Simulated with metasurface.

A comparative analysis between the proposed method and other decoupling techniques is summarized in Table 4.2. It is observed that the proposed method achieves superior decoupling performance with the smallest spacing among the compared methods.

Table 4.2 Comparison of the proposed and other decoupling techniques

Ref.	Method	Frequeny (GHz)	Edge to Edge spacing (λ_0)	 S21 (dB)	Gain (dBi)
[43]	MAAD	5.8	0.02	27	2
[45]	Metasurface	2.5	0.27	25	2.5
[52]	Decoupling surface & defected ground	3.7 & 4.1	0.034	28.4 & 25.9	2.2&0.8
[53]	Parallel coupled-line resonator (PCR)	3.5	0.07	26.2	1.25
[54]	Metal strips and walls	3.5 / 5.7	0.023 & 0.038	18.4 & 22.7	2.7&2.8 & 5
[57]	MDM	2.6/3.5	0.008 & 0.011	25	7.8 & 8.6
This Work	MSB	3.5	0.011	35	3.85

4.5 Conclusion

In this paper, closely integrated MIMO patch antennas operating at 3.5GHz with improved isolation are designed. This design comprises two mirror-symmetrical patch antennas with a metasurface double layer of cut wires used for decoupling of closely coupled two microstrip patch antennas with edge-to-edge distance is $0.011 \lambda_0$. The Simulated and measured results show that the isolation between two patch antennas enhanced from -10dB to -35dB and the gain increased from 1.82 dBi to 3.85 dBi. Currently, the decoupling structure applies only a two-element microstrip antennas but in future, we can use the three and more antenna elements. The MIMO patch antennas is used for 5G wireless communication.

Chapter 5

High-Isolation Circularly Polarized MIMO Antenna for Sub-6 GHz Applications

This chapter introduces a novel circularly polarized MIMO antenna designed for 5G sub-6 GHz applications. The antenna consists of a patch with a unique slot and a circular split ring resonator (SRR) on the ground plane. H-shaped parasitic elements are strategically placed to achieve a minimum isolation of 20 dB between antenna ports.

5.1 Introduction

To enable the new era of the internet of everything, the 5G mobile network system is a new global wireless framework that is designed to provide ubiquity connectivity to everyone and everything at once, including machines, objects, and devices, in a way that is incredibly reliable and reasonably priced. MIMO systems efficiently take advantage of the multipath environment to boost wireless system performance as a whole. Systems using 5G MIMO considerably increase speed and capacity while delivering low latency and excellent dependability. Strong mutual coupling between antenna elements caused by compact MIMO antenna design may lead to a decline in the performance of system diversity overall and inter-element isolation.

In the literature, it is allowed for the 5G sub-6GHz MIMO system to have an isolation level of 10 dB. To improve MIMO performance, however, lower bound isolation of at least 15 dB should be needed. When compared to their linearly polarized (LP) counterparts, circularly polarized MIMO antennas provide several advantages, including the prevention of multipath interference, fading, and quality of service (QoS) [61-64]. Circularly polarized MIMO antennas have so been discussed in the literature in recent years. A compact CP MIMO antenna design in [66] using two truncated corner square patches with parasitic periodic metallic plates. It requires costly Taconic substrate, increasing manufacturing costs. A MIMO antenna proposed in [70] has employed an

inexpensive FR-4 substrate to reduce production cost and to improve the performance of the antenna by applying an eyebrow-shaped strip,

In this chapter, an innovative slot in the patch antenna and a circular split ring resonator at the ground plane makes up the suggested compact two-port CP MIMO antenna. Investigating a special slot at the patch antenna can help to accomplish circular polarization and bandwidth increase. A sequence of parasitic components in the shape of h is placed in the space between the two antenna elements to decouple the two antenna elements. The suggested MIMO CP antenna achieves an impedance bandwidth of 3.3 to 3.6 GHz with impedance matching better than 10 dB and has an axial ratio bandwidth of 3.35 to 3.51 GHz with a steady radiation pattern in both planes over the operating frequency bands.

5.2 Design Procedure of Proposed Antenna

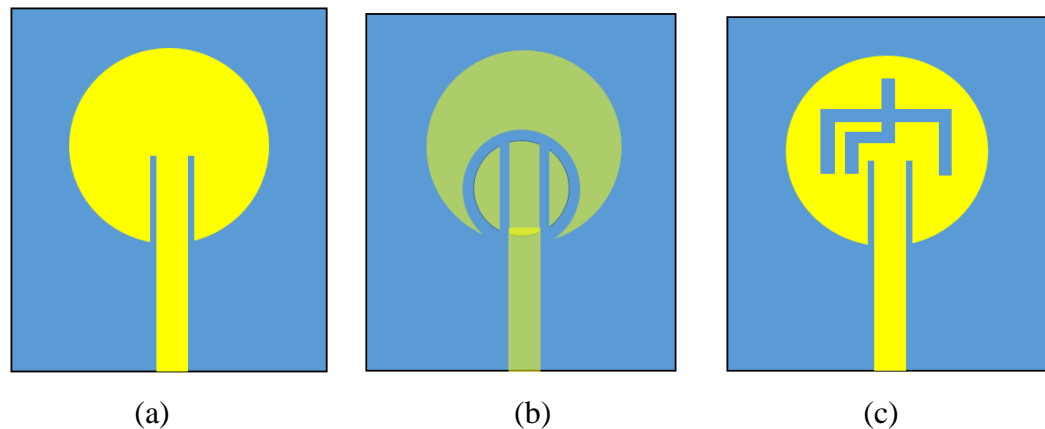
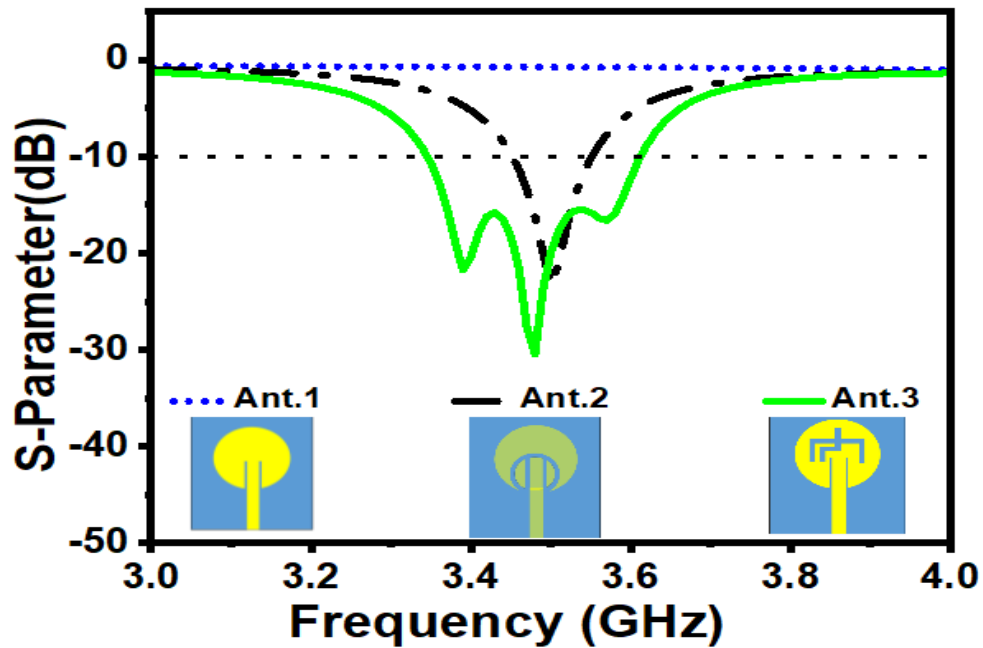
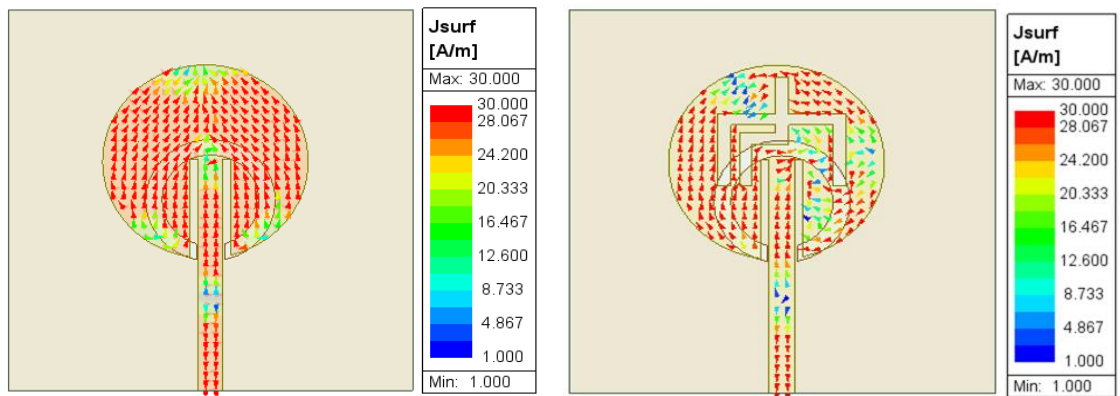


Figure 5.1 Schematics of the single-element antenna to showing step by step design (a) Ant. 1 (b) Ant. 2 (c) Ant. 3

This section will describe the step-wise design and analysis of a novel sub-6 GHz compact patch antenna before moving on to the design and analysis of the proposed CP MIMO antenna. Three prototype antennas, referred to as Ant.1 through Ant.3, serve as a description of the proposed antenna's design step and their corresponding impedance bandwidth and axial ratio bandwidth.



(a)



(b) (i) Ant. 2

(ii) Ant.3

Figure 5.2 (a) Simulated S-parameter of Ant.1 to Ant.3 (b) Surface current density distribution of (i) Ant.2 (ii) Ant.3

First, as seen in Figure 5.1(a), an inset feed circular patch antenna has been created to function at frequencies of about 6 GHz. Figure 5.2(a), depicts the Frequency response of S-parameter Ant.1 to Ant.3, but the resonance frequency is not visible due to the selected frequency range. In Figure 5.1(b) the inset feed circular patch antenna loaded with a circular split ring resonator (Ant.2) has a new resonance frequency of 3.5 GHz as shown

in Figure 5.2(a). The high concentration of current observed around the circular SRR increased the resonance frequency shift towards lower frequency, as shown in Figure 5.2(b)(i).

In Figure 5.1(c), the Ant. 2's bandwidth is increased by the addition of a special slot that combines an L-shaped slot with an inverted fork-shaped slot, and it will occupy a complete 5G Sub-6GHz band. The patch antenna's bandwidth is primarily improved by an inverted fork-shaped slot, which also serves as an impedance matching and an L-shaped slot. Because of this, the unique slot offers good impedance matching and bandwidth enhancement. Along with that, this unique slot is also responsible for the axial ratio bandwidth for the proposed antenna because the introduction of L shape slot perturbed the surface current density distribution of the radiator, as shown in Figure 5.2 (b)(ii).

5.3 Parametric Analysis

Using Ansys HFSS, the simulation of the antenna design across the operational frequency range was conducted, and the design parameters for the antenna structure were fine-tuned. The antenna dimensions were determined through a parametric analysis involving the slot moving in the horizontal direction (parameter Y) and the slot moving in the vertical direction (parameter X). The impact of Y and X on the S_{11} parameters is illustrated in Figure 5.3.

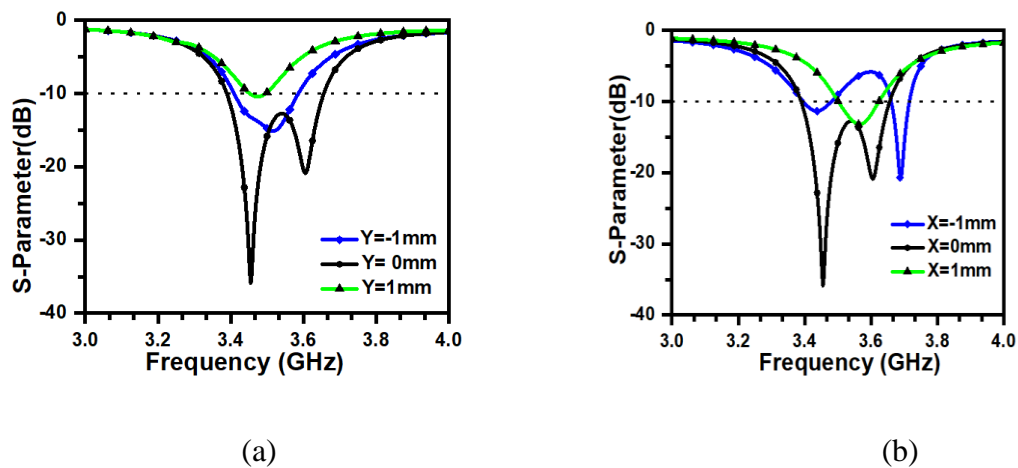
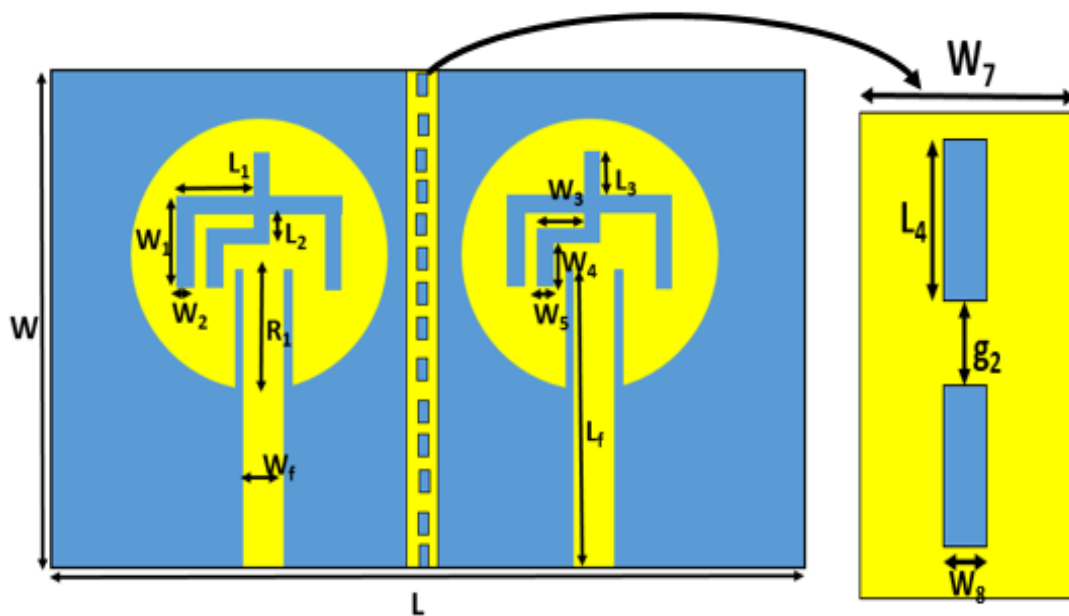


Figure 5.3 Parametric analysis of proposed antenna (a) $|S_{11}|$ with Y (b) $|S_{11}|$ with X

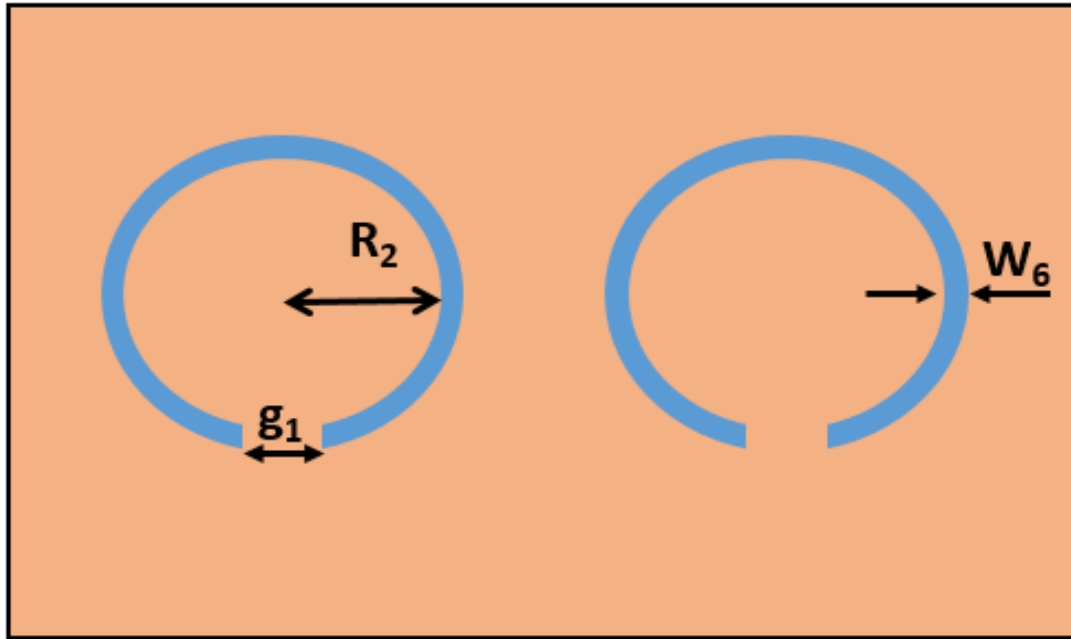
The Y & X varied between -1 to 1 mm. The optimized values were identified as $Y = 0$ mm and $X = 0$ mm, resulting in the desired favourable return loss.

5.4 Proposed MIMO Antenna Design

Figure 5.4(a) & (b) shows the proposed 2-port CP MIMO antenna geometry from our research. The proposed 2-port CP MIMO antenna is created on an FR4 substrate with 0.019 as the loss tangent and 4.4 as the dielectric constant. It has two Ant.3 prototypes that are connected by a succession of h-shaped parasitic element slots to improve isolation in the sub-6GHz band, it has an axial ratio bandwidth of 3.35 to 3.51 GHz and covers the frequency range of 3.3 GHz to 3.6 GHz. The proposed 2-port CP MIMO antenna's final dimensions are summarized in Table 5.1 after some parametric analysis. Figure 5.4(c) will display the proposed antenna's frequency response after the activation of both antennas simultaneously with and without h-shaped parasitic element (strip) and achieve a minimum isolation of 20 dB on its operating band.



(a)



(b)

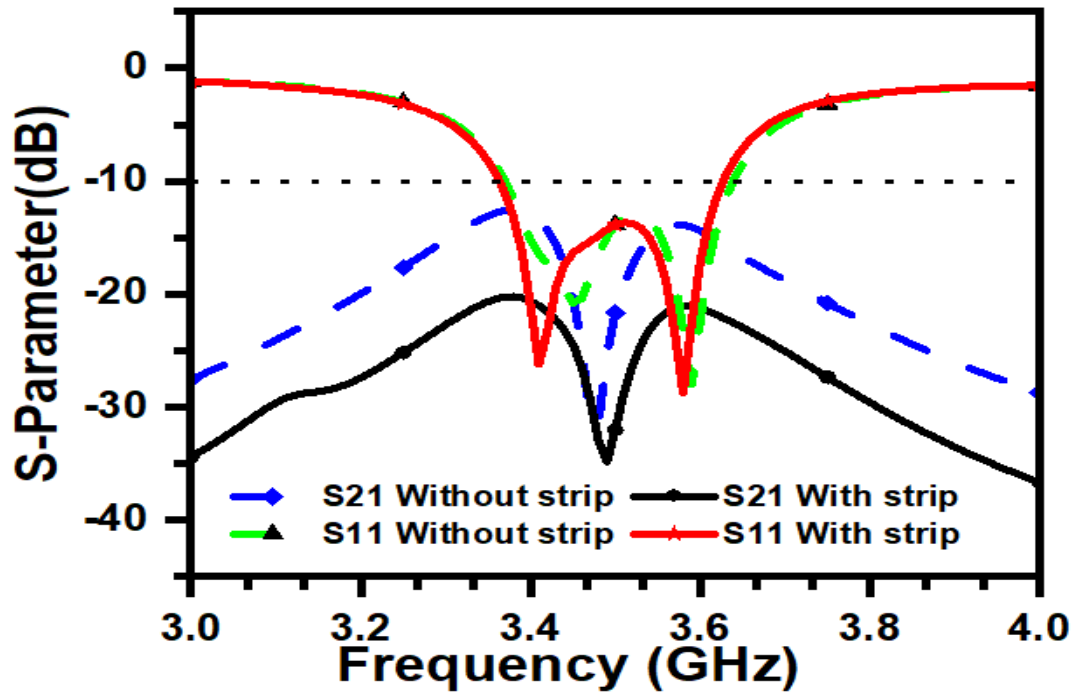


Figure 5.4 Schematics (a) Top View (b) Bottom View (c) S-parameters with & without strip of the proposed 2-port CP MIMO antenna.

Table 5.1 Different parameters of the proposed 2-port CP MIMO antenna

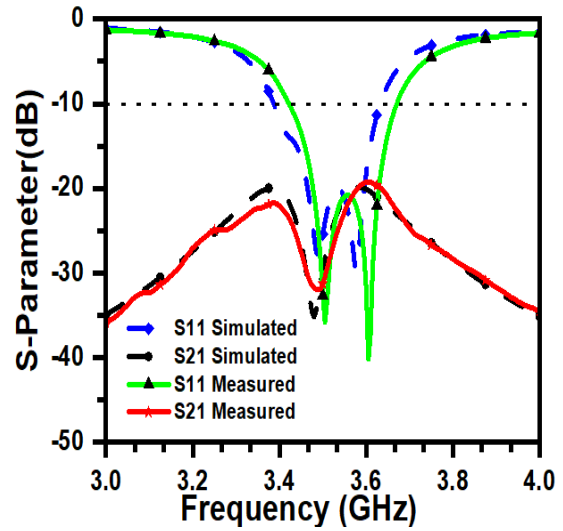
Parameters	L	W	L ₁	W ₁	R ₁	W _f	W ₂	W ₅	W ₇	W ₈
Values (mm)	65	50	6.75	9.5	12.7	3	1.5	1.5	3	1
Parameters	L ₂	W ₃	W ₄	L _f	L ₃	g ₁	g ₂	R ₂	W ₆	L ₄
Values (mm)	2.5	2.5	7	30.41	3.75	3.5	1	6	2	1.5

5.5 Result and Analysis of the Proposed 2-port CP MIMO Antenna

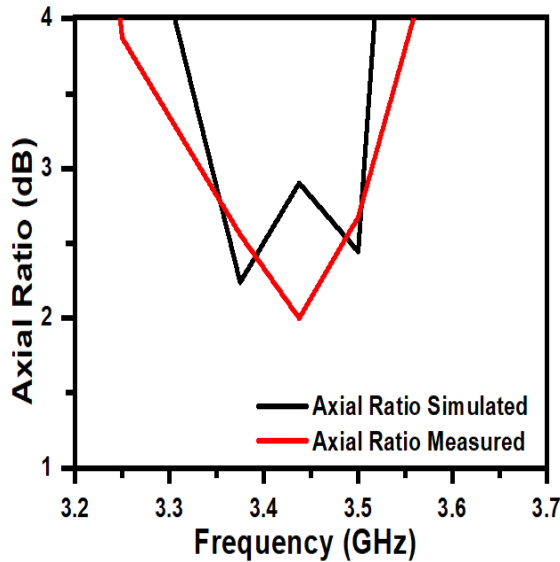
The HFSS tool and a vector network analyser are used to simulate and measure the S-parameters of the proposed 2-port CP MIMO antenna as shown in Figure 5.5(a). According to Figure 5.5(b), the proposed 2-port CP MIMO antenna has the same resonance frequencies in simulation and measurement. The experimental and simulated S_{21} is greater than 20 dB. The proposed 2-port CP MIMO antenna achieves an impedance bandwidth of 3.3 to 3.6 GHz with impedance matching better than 10 dB and has an axial ratio bandwidth of 3.35 to 3.51 GHz, as shown in Figure 5.5(c). Due to manufacturing errors, there are small variations in experimental and simulated measurements. It is also evident that the suggested design results in good isolation and return loss. The gain of the proposed 2-port CP MIMO antenna is shown in Figure 5.5(d), the maximum gain is observed to 3.8 dBi.



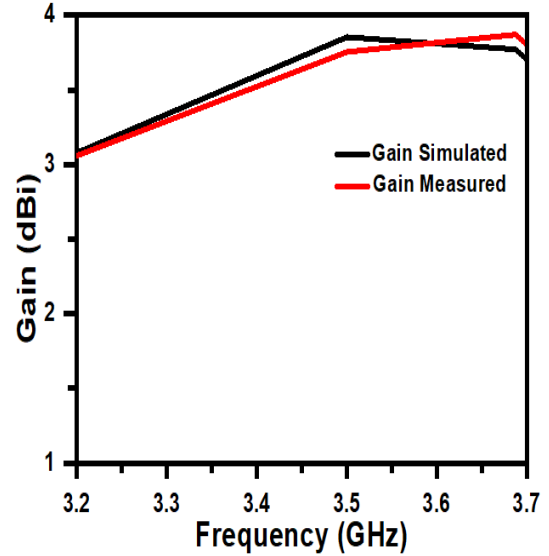
(a)



(b)



(c)



(d)

Figure 5.5 (a) S-parameters (b) Measurement setup of S-parameter by VNA (c) Simulated and Measured axial ratio plot (d) Simulated and Measured gain of the proposed 2-port CP MIMO antenna

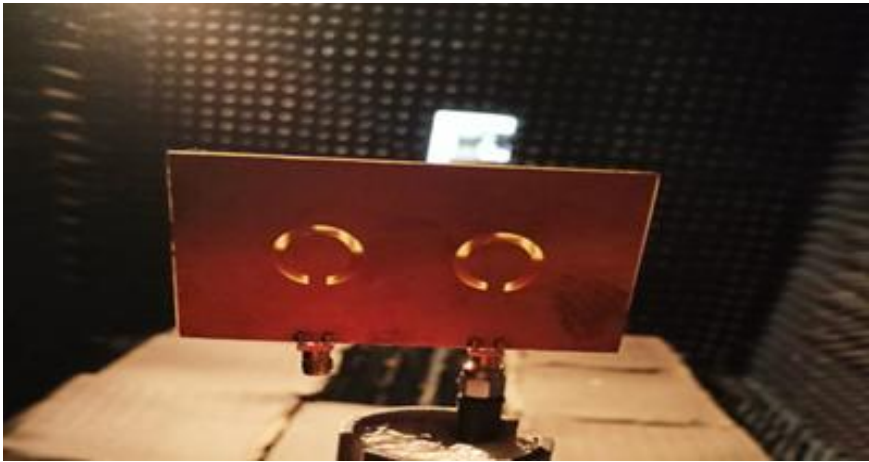
5.5.1 Radiation Characteristics

Figure 5.6(a) & (b), shows the view of the anechoic chamber along with the proposed 2-port CP MIMO antenna used to measure radiation & diversities properties of the antenna.

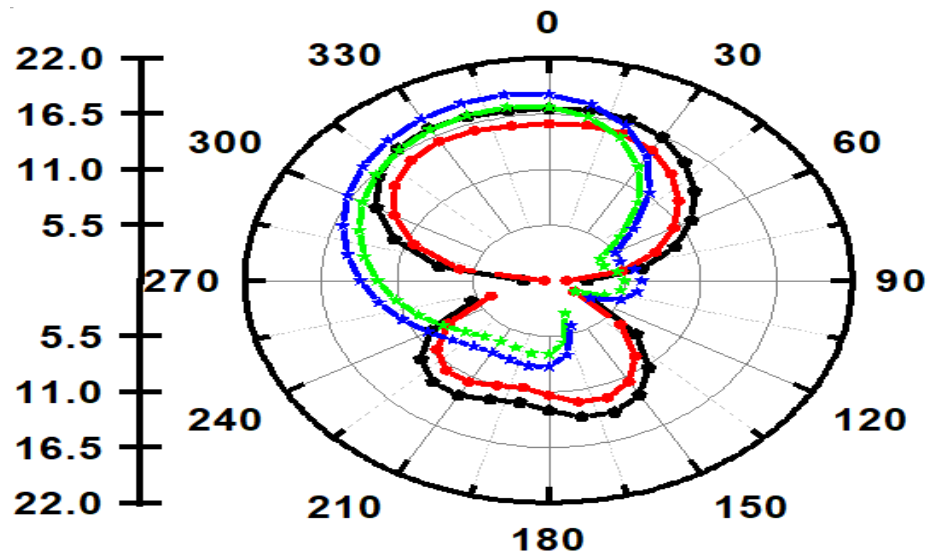
To measure the values of the E and H plane, the antenna was placed horizontally and vertically in an anechoic chamber using positioning equipment.



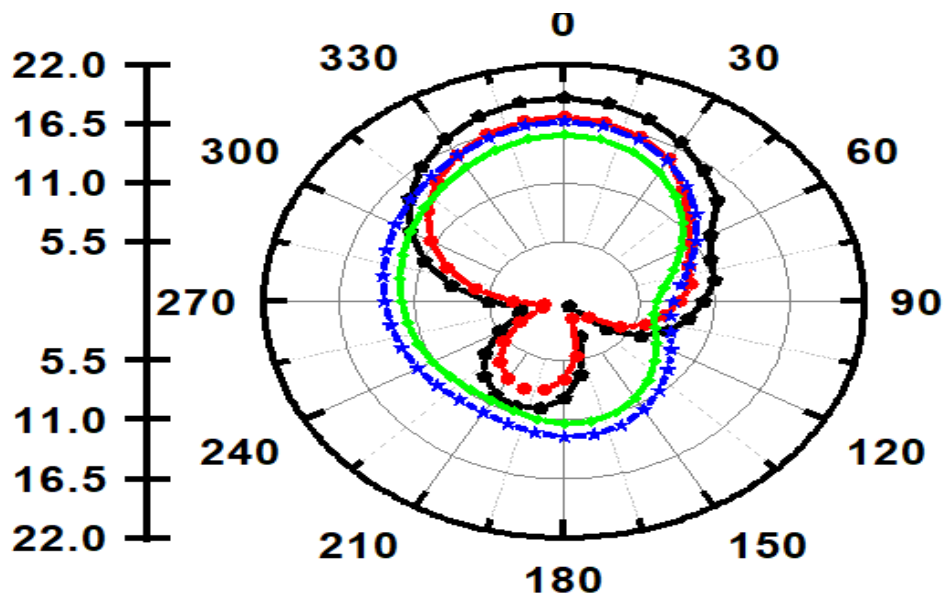
(a)



(b)



(c)



(d)

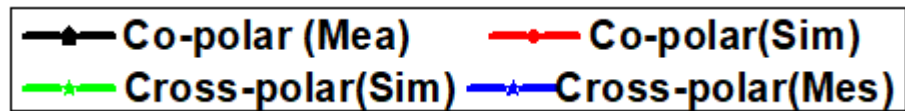
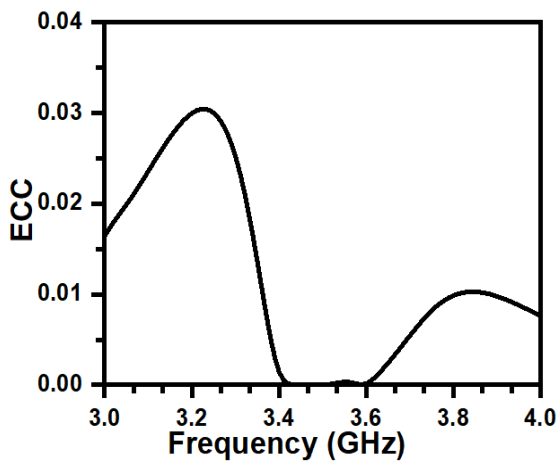


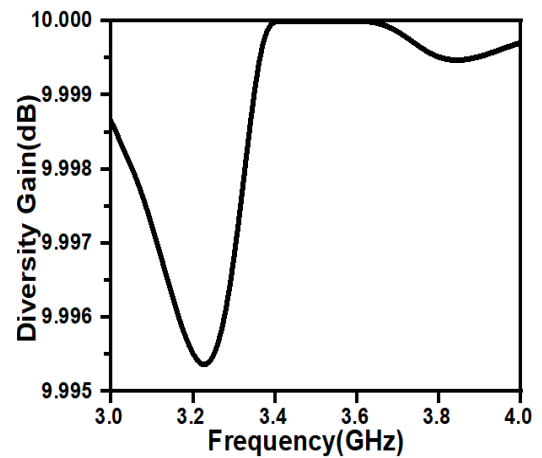
Figure 5.6 Radiation pattern measurement setup (a) Front view (b) Back view (c) E-Plane (d) H-Plane of proposed 2-port CP MIMO antenna

As shown in Figure 5.6(c) & (d), the simulated and measured radiation pattern of the proposed 2-port CP MIMO antenna for the E-& H-Plane is plotted to make comparisons. A very good similarity is obtained between the simulated and measured results while the minor noncompliance is due to manufacturing tolerances and calibration errors during measurements.

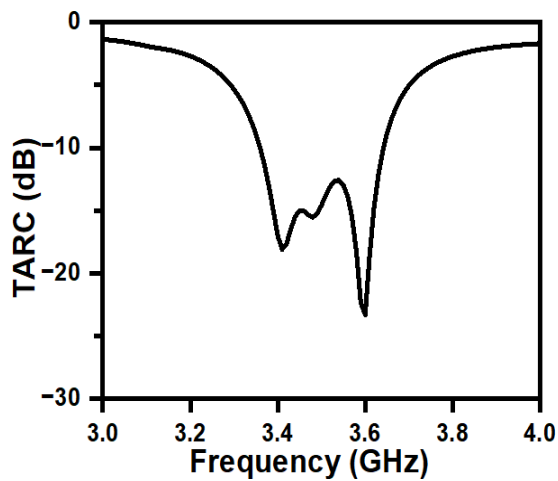
5.6 Diversity Parameter of the MIMO Antenna



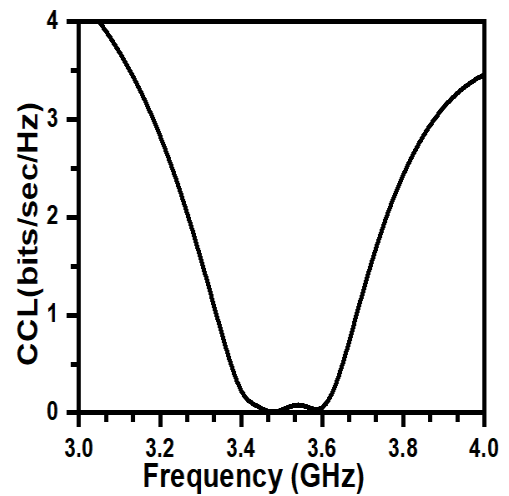
(a)



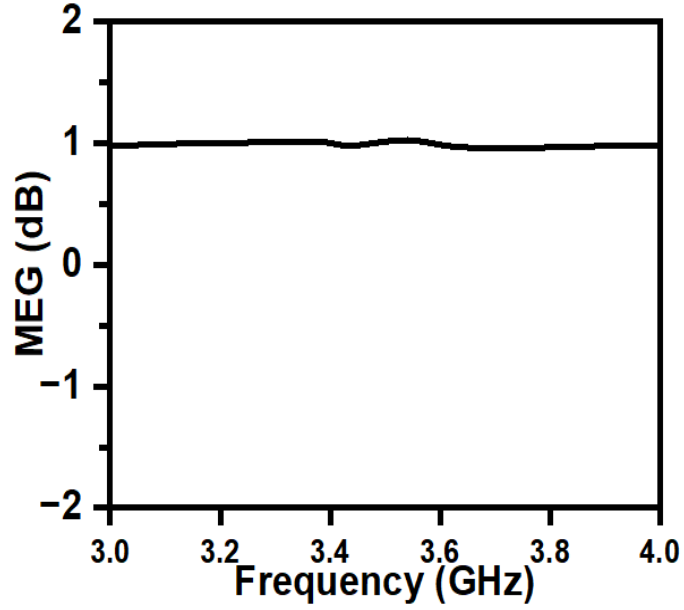
(b)



(c)



(d)



(e)

Figure 5.7. Measured diversity parameters (a) ECC (b) DG (c) TARC (d) CCL (e) MEG of the proposed 2-port CP MIMO antenna

To observe MIMO antenna diversity performance is observed by plotting diversity parameters by using measurement results. The ECC of the proposed 2-port CP MIMO antenna is calculated using (5.1) [9].

$$|\rho_e(i, j, N)| = \frac{\sum_{n=1}^N S_{i,n}^* S_{n,j}}{\prod_{k(=i,j)} [\sum_{n=1}^N S_{i,n}^* S_{n,k}]} \quad (5.1)$$

The ECC of the proposed 2-port CP MIMO antenna are shown in Figure 5.7(a). It is 0.004 throughout the entire spectrum of frequencies, showing that the proposed 2-port CP MIMO antenna successfully provides diversity functions. The ITU (International Telecommunication Union) has set a limit of 0.5. ECC should be less than 0.5 to enhance diversity performance. The outcome of 0.004 shows a very low correlation between the antenna components. The diversity gain demonstrates the differences in time-average SNR signals and provides the communication channel with effective diversity is determined using (5.2).

$$DG = 10\sqrt{1 - ECC^2} \quad (5.2)$$

The proposed antenna's DG values are around 10 dB as illustrated in Figure 5.7(b), and the DG values should ideally be 10 dB. The radiating elements are located close to one another and are used simultaneously in MIMO antenna architecture; however, the interference performance is also influenced by this configuration of radiating antennas which can be calculated by using (5.3).

$$TARC = \frac{\sqrt{(|S_{ii}+S_{ij}e^{j\theta}|)^2+(|S_{ji}+S_{jj}e^{j\theta}|)^2}}{\sqrt{N}} \quad (5.3)$$

Figure 5.7(c) displays the simulated TARC values, which are below 10 dB in the 5G Sub-6GHz band while the predicted values are 0.25 dB. The communication environment's efficient signal transmission without any signal distortion or bit loss is indicated by the channel's capacity. The CCL is a key diversity parameter calculated using the equation (5.4).

$$CCL = -\log_2 \det[\beta^R] \quad (5.4)$$

$$\text{where, } [\beta^R] = \begin{bmatrix} \beta_{ii} & \beta_{ij} \\ \beta_{ji} & \beta_{jj} \end{bmatrix} \quad (5.5)$$

$$\beta_{ii} = 1 - \left(\sum_{j=1}^N |S_{ij}|^2 \right) \quad (5.6)$$

$$\beta_{ij} = -(S_{ii}^* S_{ij} + S_{ji}^* S_{ij}) \quad (5.7)$$

The proposed 2-port CP MIMO antenna has CCL values of 0.10 b/s/Hz, shown in Figure 5.7(d). A MEG is another antenna performance factor that compares the average received signal strength of a MIMO antenna array to its average incident power. MEG can be used to calculate the average received power intensity for each antenna by using (5.8) & (5.9)

$$MEG_i = 0.5 \left[1 - \sum_{j=1}^N |S_{ij}|^2 \right] < -3dB \quad (5.8)$$

$$MEG_j = 0.5 \left[1 - \sum_{i=1}^N |S_{ij}|^2 \right] < -3dB \quad (5.9)$$

$$|MEG_i - MEG_j| < 3dB \quad (5.10)$$

$$\left| \frac{MEG_i}{MEG_j} \right| = \pm 3dB \quad (5.11)$$

In which i, j denote Ant.1 & Ant.2 separately. Figure 5.7(e) displays the MIMO antenna's mean effective gain. The 3.3–3.6 GHz range of the proposed 2- port CP MIMO antenna

comes within the 5G above frequency range. The proposed 2-port CP MIMO antenna is compact and has a wideband, a very low ECC value, high isolation, diversity gain, and MEG.

Table 5.2 Comparison of the proposed 2- port CP MIMO Antenna with other MIMO Antennas

References no.	Antenna Geometry (mm ²)	Material used	B.W @ 10dB, (GHz)	Polarization	Isolation (dB)	ECC	Max. Gain (dBi)
[68]	37 × 30	FR4 ($\epsilon_r = 4.3$, $\tan\delta = 0.019$)	3.3–4.2 GHz	CP	15	0.10	2.5
[73]	21 × 46	FR4 ($\epsilon_r = 4.4$, $\tan\delta = 0.019$)	3.4–3.6 GHz & 4–8 GHz	LP & CP	15	< 0.003	3.25
[74]	55 × 38	FR-4 ($\epsilon_r = 4.3$, $\tan\delta = 0.025$)	3.1–4.5 GHz	LP	20	<0.0004	3.17
[77]	59 × 55	FR4 ($\epsilon_r=4.4$, $\tan\delta=0.02$)	3–7 GHz	LP	18	0.21	3
[78]	82 × 40	FR4 ($\epsilon_r=4.3$, $\tan\delta=0.02$)	3.66–3.7	CP	15	0.05	4.6
[79]	66 × 66	ROGERS3003/0.13	3.2-4.12	LP	.20	<0.05	3
[80]	50 × 100	FR4 4.4/4.5	2.7–3.6	LP	25	----	3
Proposed Antenna	65 × 50	FR4 ($\epsilon_r = 4.4$, $\tan\delta = 0.019$)	3.3–3.6 GHz	CP	20	<0.004	3.8

The proposed 2-port CP MIMO antenna is compared to the most recent state-of-the-art design in this part, which is tabulated in Table 5.2 and is discussed with earlier published work. The proposed 2-port CP MIMO antenna makes use of an FR4 substrate, which

elevates it to the status of a leading candidate for microwave-integrated circuit (MIC) circuit integration. The comparative table also indicates too good diversity performance from the proposed 2-port CP MIMO antenna. The MIMO antenna's innovative design makes it more suited for use in a variety of mobile devices intended for 5G applications.

5.7 Conclusion

The 2-port CP MIMO antenna proposed in this research study uses a distinctive slot and a circular split ring resonator at the ground planes which help to accomplish circular polarization and enhance bandwidth. The proposed 2-port CP MIMO antenna achieves an impedance bandwidth of 3.3 to 3.6 GHz with impedance matching better than 10 dB and has an axial ratio bandwidth of 3.35 to 3.51 GHz with a steady radiation pattern in both planes over the operating frequency bands. The proposed 2-port CP MIMO antenna design with insect fed gives good diversity performance with ECC 0.004, DG 10 dB, CCL 0.40 b/s/Hz, MEG 1.03 dB, and TARC 10 dB. The peak gain for the proposed antenna is 3.8 dBi.

Chapter 6

Dual-Band CPW-Fed MIMO Antenna for 5G Applications

This chapter introduces a novel, integrated dual-band MIMO antenna for global system mobile networks. The antenna's unique orthogonal configuration eliminates the need for isolation elements, simplifying design. Curved radiators enable operation at 3.5 GHz and 5.5 GHz. Fabricated on a low-cost FR-4 substrate, the antenna achieves excellent isolation and low correlation.

6.1 Introduction

MIMO systems utilize multiple transmitting and receiving antennas, capitalizing on the effects of signal propagation via various paths. Nevertheless, the efficiency of antennas and the performance of MIMO systems can be compromised due to heightened mutual interaction when multiple antennas are positioned near. This issue has emerged as a significant challenge requiring attention. Substantial endeavours have been devoted to alleviating this mutual interference.

In the literature, to tackle the above issue and accommodate the constrained space within smartphones, a solution involves integrating 2 or 4 closely positioned or shared-radiator MIMO antenna elements. This approach effectively reduces the overall spatial requirement through spatial reuse [86]. In one instance [87-88], the method of using neutralization lines is employed to mitigate mutual interference among four closely positioned open-slot antenna elements covering the frequency band of 5G. This results in a compressed antenna size for a four-antenna unit. In another study [89], two gap-coupled loop antennas, which are mirror images of each other and function in the frequency range of 5G mid-band, are integrated to create a unique self-decoupled module, antennas employing CPW feeding exhibit several benefits compared to alternative methods such as microstrip and coaxial probe feeding. These advantages encompass cost-effectiveness, reduced dispersion, favourable omnidirectional patterns, minimal surface wave propagation, and streamlined integration with both passive and active components [94].

A MIMO antenna with four ports has been introduced in a suggested chapter using a substrate made of FR-4 material, having a thickness of 1.6 mm, relative permittivity (ϵ_r) of 4.4, and a loss tangent ($\tan \delta$) of 0.02. This antenna design covers two frequency bands. The antenna exhibits effective isolation properties within both of these frequency bands. Every individual component within the MIMO arrangement comprises a monopole antenna characterized by a unique sickle-shaped design. This monopole is connected to an asymmetric CPW feed, a configuration chosen to increase the operational bandwidth. The spacing between these antenna elements is increased by positioning the four elements in a perpendicular orientation relative to each other. Notably, no additional decoupling structures are employed, simplifying the overall design approach. In conclusion, the work presented in the paper offers several advantages and introduces novel concepts, which can be summarized as follows:

- The proposed configuration demonstrates flexibility through the utilization of an FR-4 substrate and attains isolation exceeding 18 dB between ports, all without necessitating an additional decoupling structure. Additionally, the antenna yields a satisfactory gain, thereby bolstering its suitability within dual-band networks.
- The antenna's flexibility and compactness facilitate seamless integration with other components, effectively conserving space.
- Moreover, the antenna exhibits favourable performance in terms of S-parameters, ECC, and diversity gain (DG), reaffirming the stability of the suggested dual-band antenna design."

6.2 Antenna Design

6.2.1 Procedures for Designing a Single Unit Antenna

Figure 6.1 displays the suggested configuration of the dual-band MIMO antenna in a single unit. The antenna configuration comprises a monopole antenna with a distinct sickle-shaped design. This monopole structure takes the form of an 'I' shape with curved extensions, and it is connected to an asymmetric 50Ω coplanar waveguide (CPW) feed. The operational bandwidth is broadened by adjusting parameters such as the distance (g) separating the feed line and the asymmetrical ground, along with the width (W_R) of the

feed line. Both the sickle-shaped monopoles and on the same side as the ground plane of an FR-4 substrate. This substrate possesses specific dimensions, with a thickness of 1.6 mm, a relative permittivity (ϵ_r) of 4.4, and a loss tangent ($\tan \delta$) of 0.02. These components collectively result in an antenna size measuring 32 mm \times 32 mm. The antenna is designed and optimized using the HFSS and its dimensions are tabulated in Table 6.1.

Table 6.1 The dimensions of the single unit dual band antenna.

L_S	W_S	L_g	W_g	L_R	W_R	L_{R1}	W_{g1}	g	W_{R1}	R_L
32	32	14	14.15	23	3	6.3	7	0.35	1.5	11.79

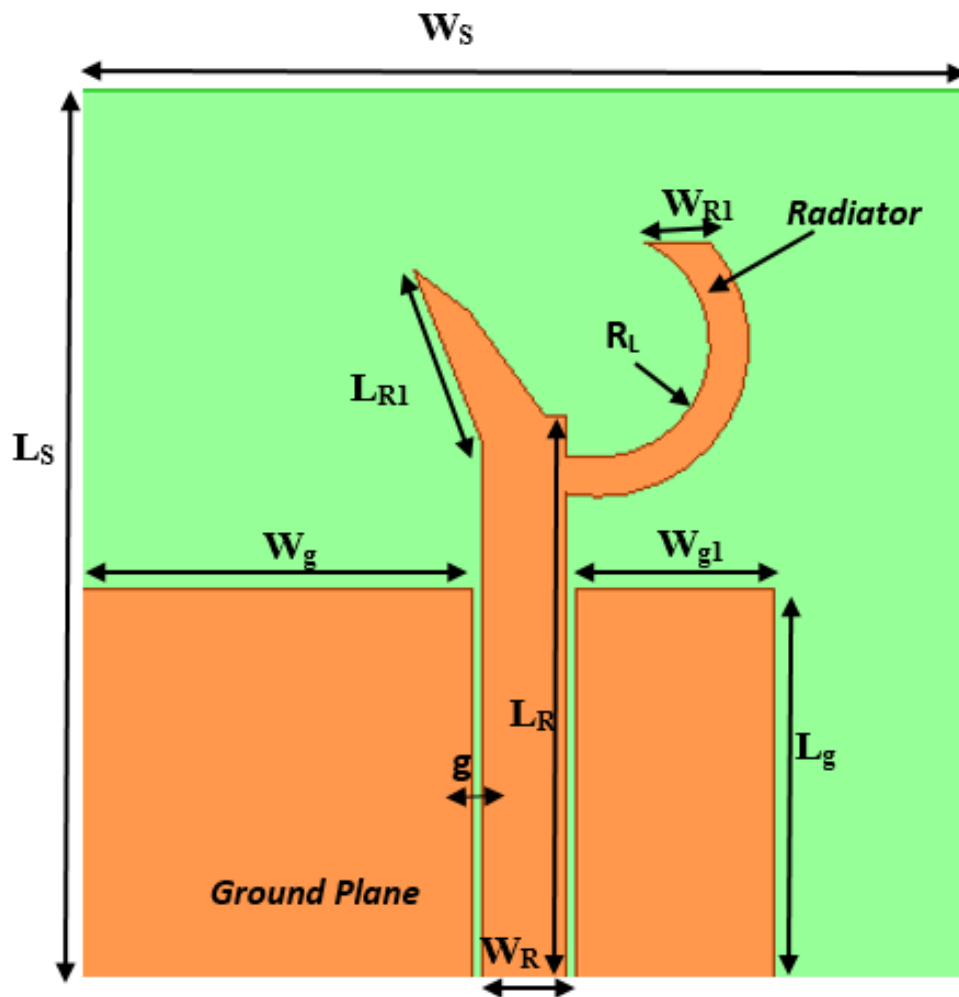


Figure 6.1 Single antenna design

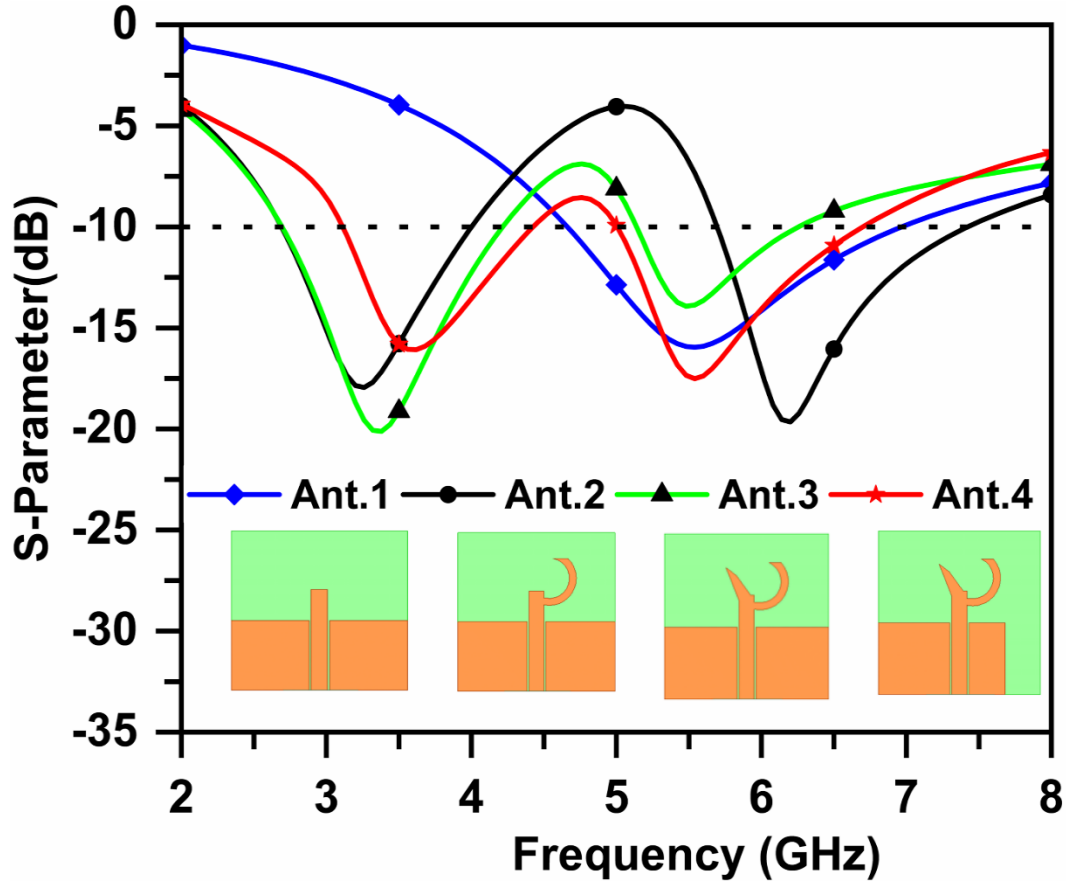


Figure 6.2 Single antenna developments.

Figure 6.2 shows the progression of the antenna unit's evolution, commencing with the original design and culminating in the suggested configuration. Antenna @1 (I-shaped with the symmetric ground) to achieve the desired frequency band at 5.5 GHz. The simulated S₁₁ parameter (depicted by the blue line) demonstrates antenna operation within the frequency range of 4.6 to 7 GHz. The reverse C-shaped radiator configuration is produced, maintaining the same symmetric ground setup (antenna@2). The simulated S₁₁ parameter (indicated by the black line) indicates the antenna's operation across two frequency bands 2.7 to 3.9 GHz and 5.7 to 7.4 GHz. Following this, the sickle-shaped radiator configuration is generated while retaining the same symmetric ground arrangement (antenna@3). The simulated S₁₁ response (shown in green) demonstrates the antenna functioning within two frequency ranges 2.7 to 4.2 GHz and 5.1 to 6.2 GHz. Finally, through the implementation of an asymmetric ground setup (antenna@4),

improvements are observed in the antenna's matching characteristics, particularly within the lower frequency band. The S_{11} parameter (represented by the red colour) achieves a frequency range between 3.0 to 4.4 GHz and 5.0 to 6.6 GHz.

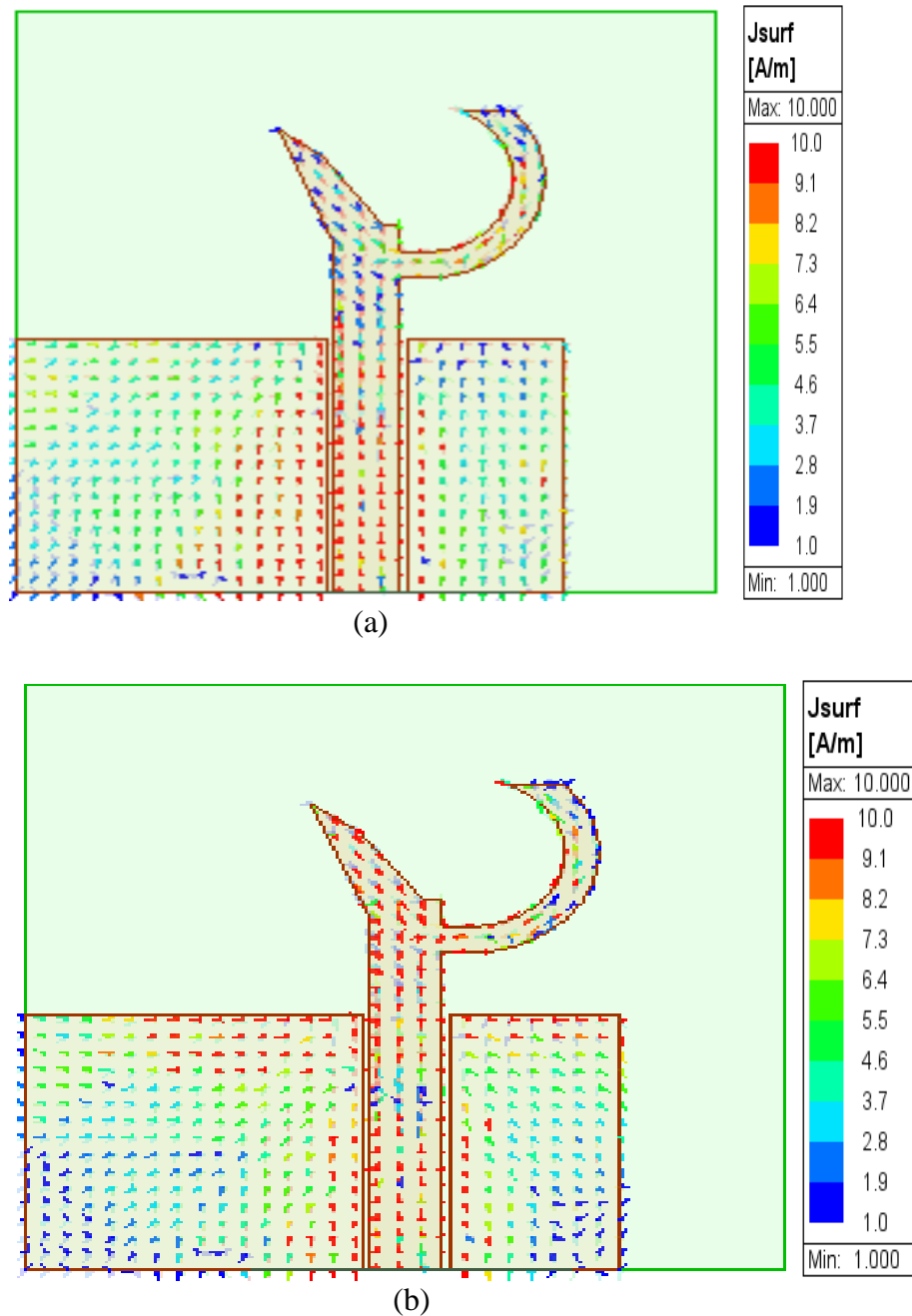
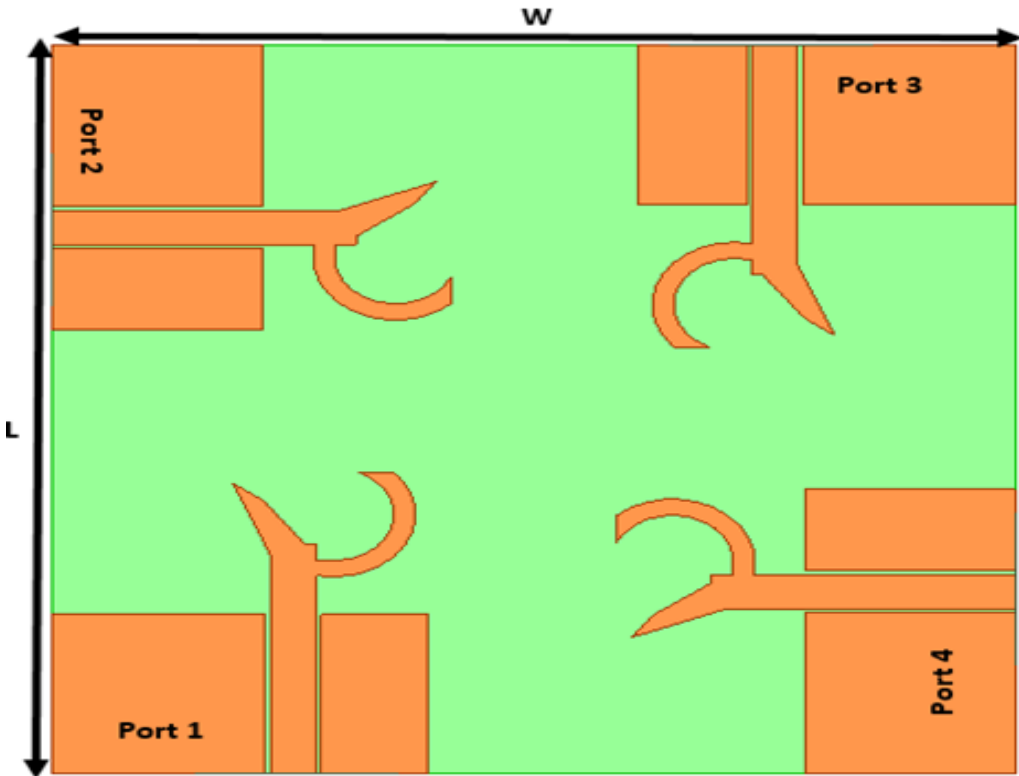


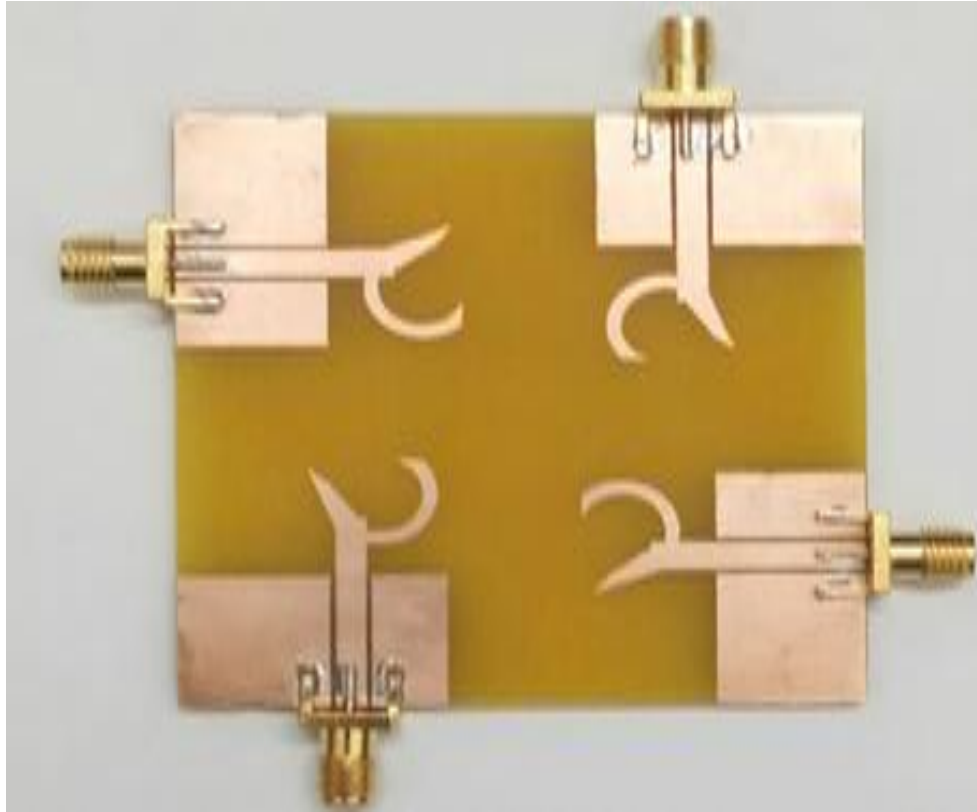
Figure 6.3 The surface current distributions at (a) 3.5 GHz and (b) 5.5 GHz

Figure 6.3(a) illustrates that there was a higher concentration of current near the curved area, which led to the presence of the Wi-MAX band. Likewise, Figure 6.3(b) demonstrates that a significant current followed the I-shaped path, contributing to the generation of WLAN signals. As a result, the antenna successfully exhibited dual-band characteristics.

6.2.2 Suggested Four-Port Configuration



(a)



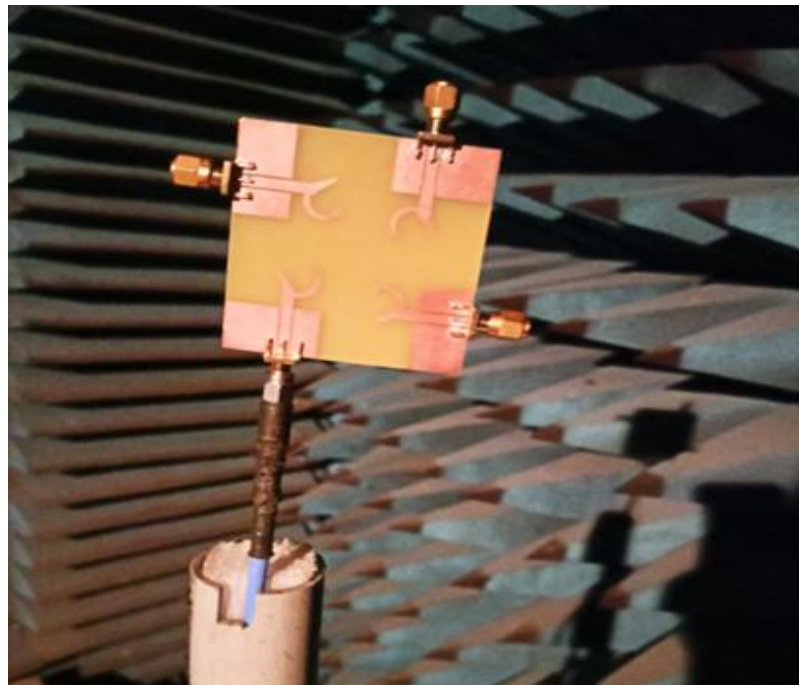
(b)

Figure 6.4 (a) Geometric arrangement (b) physical prototype of MIMO antenna

Figure 6.4(a) displays the spatial arrangement of the MIMO antenna, while Table 1 furnishes the key design measurements. This MIMO configuration employs microstrip-line feeding for four identical sickle-shaped monopole antenna elements. These elements are strategically oriented at right angles to optimize performance. In the layout schematic, the feeding sites for the antenna are identified as ports 1, 2, 3, and 4. The proposed sickle-shaped monopole antenna design is replicated in four instances and strategically positioned in orthogonal orientations. This arrangement aims to enhance the isolation between antenna ports, thereby leading to an overall improvement in the performance of the MIMO system. The four antenna units are placed near one another to minimize the overall size of $L = W = 64 \text{ mm} \times 64 \text{ mm}$. Furthermore, the setup of the fabricated prototype is presented in Figure 6.4(b).



(a)



(b)

Figure 6.5 Measurement setup (a) reflection coefficient in dB (b) radiation pattern

The MIMO is tested using VNA to produce S-parameters as shown in Figure 6.5(a). The proposed antenna is subjected to testing at port 1. These tests are conducted within an anechoic chamber, and depicted in Figure 6.5(b) the configuration of the testing setup.

6.3 Simulated and Measured Results

The MIMO is tested using VNA connected to port 1 and the obtained test results (S_{11} , S_{22} , S_{33} and S_{44}) are shown in Figure 6.6. The antenna exhibits simulated and measured S_{11} results from 3.0 to 4.4 GHz centre at 3.5 GHz and 5.0 to 6.6 GHz centre at 5.5 GHz.

Figure 6.7 depicts the comparison of the results of the MIMO antenna's simulated and tested transmission coefficient. The antenna showcases an isolation level of less than 21 dB within the frequency band of 3 GHz to 4.4 GHz and less than 18 dB within the range of 5.0 to 6.6 GHz. Furthermore, the agreement between the simulated and tested results demonstrates reasonable matching.

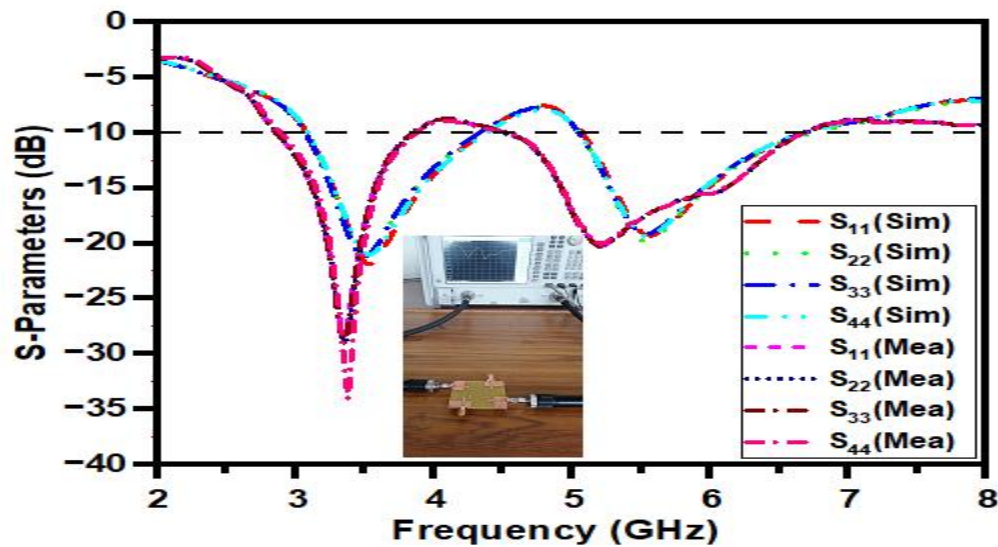
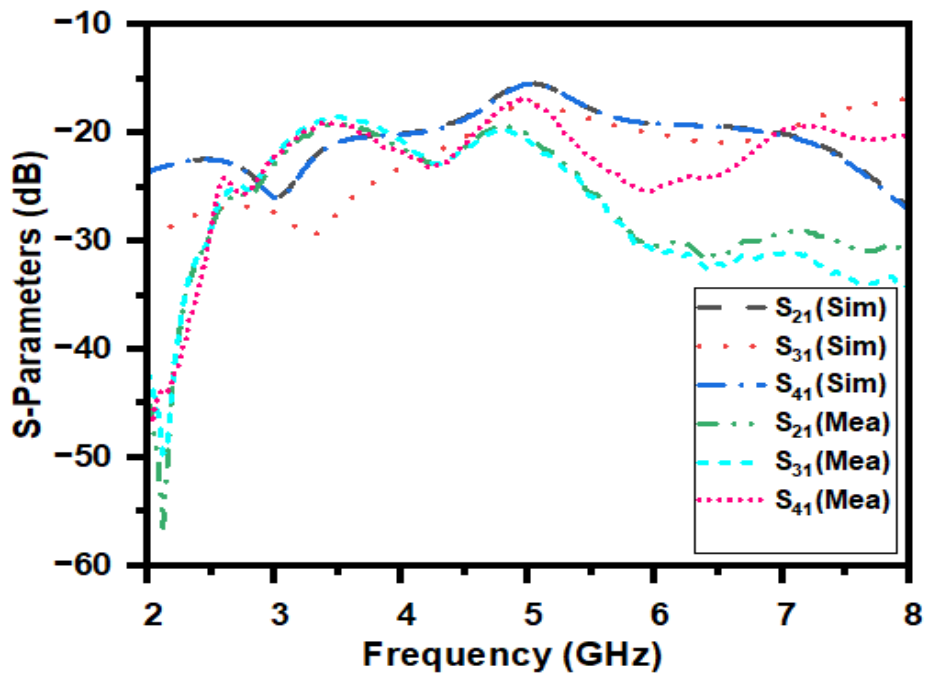
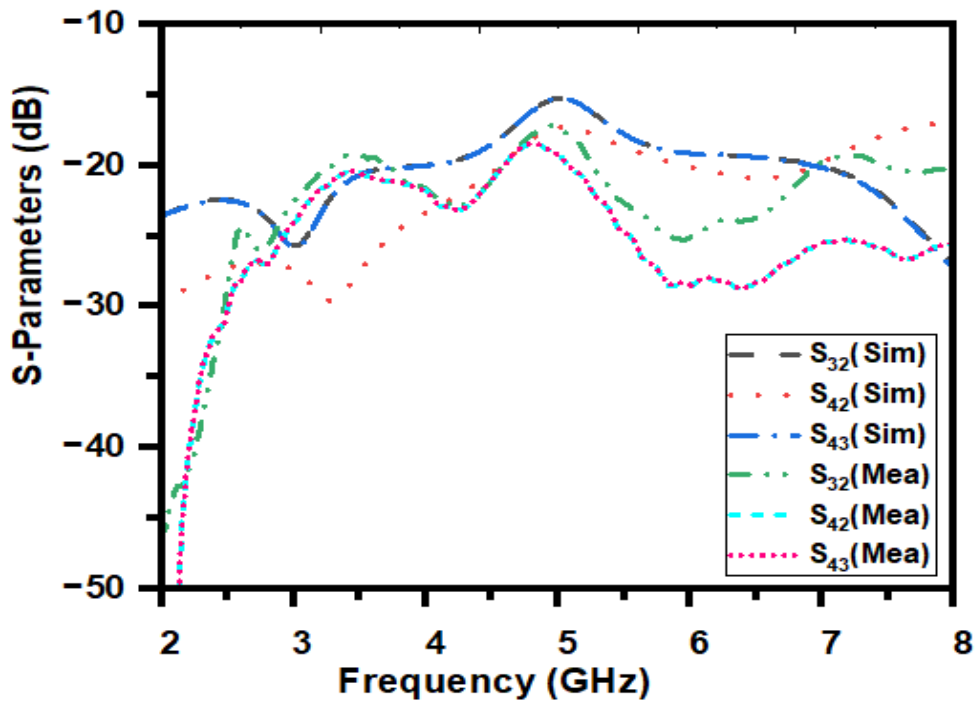


Figure 6.6 S-parameters of the MIMO antenna (Simulated and tested)

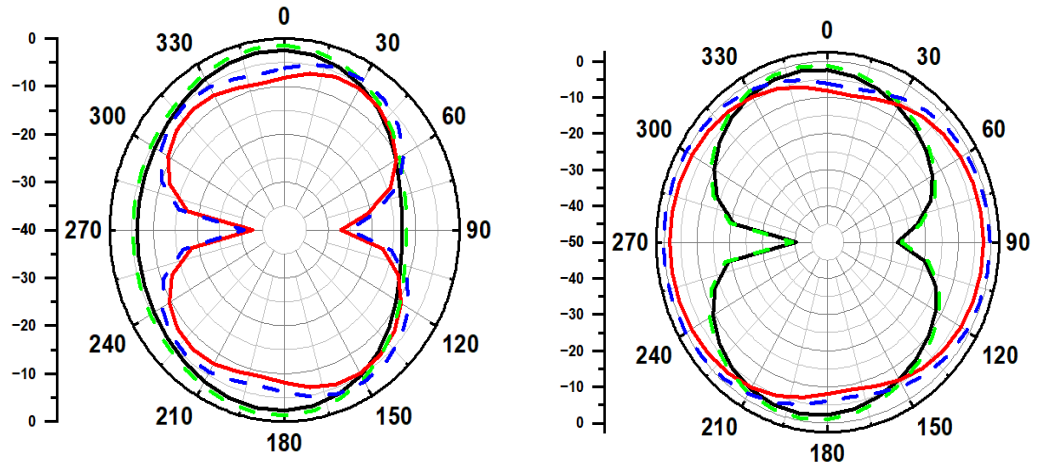


(a)

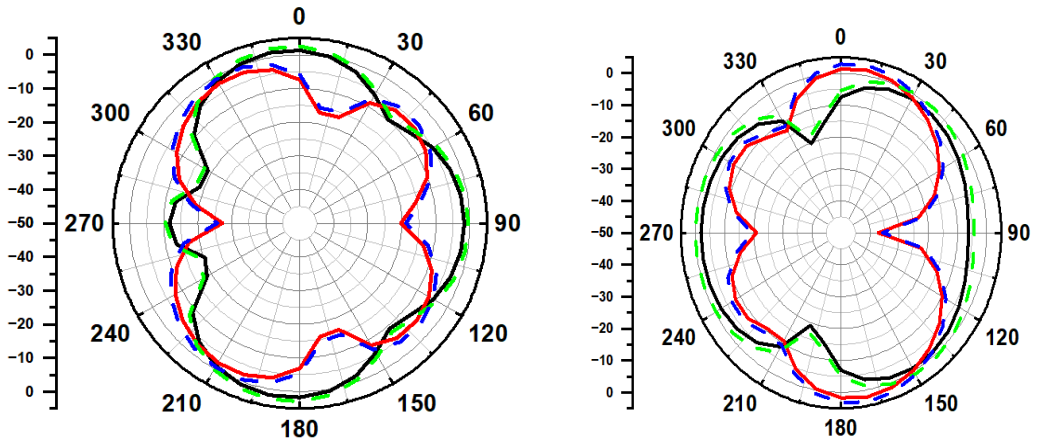


(b)

Figure 6.7 S-parameters (simulated and tested) of the MIMO antenna at (a) port-1 (b) other ports



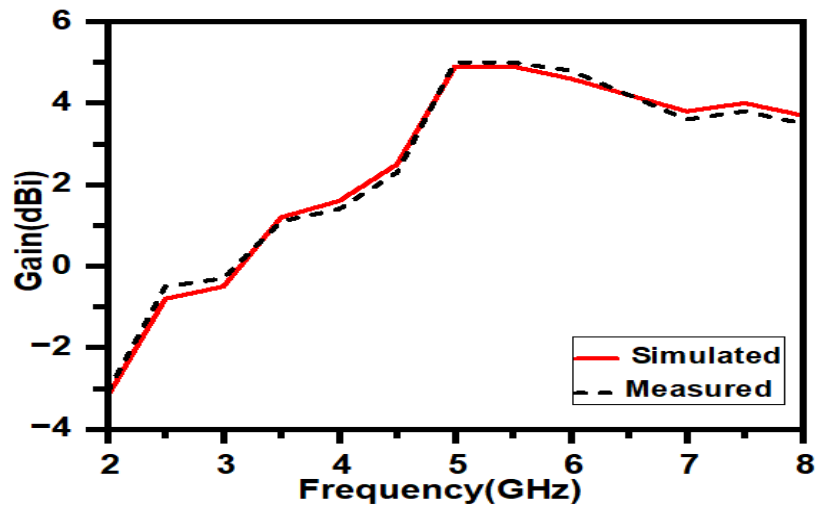
(a)



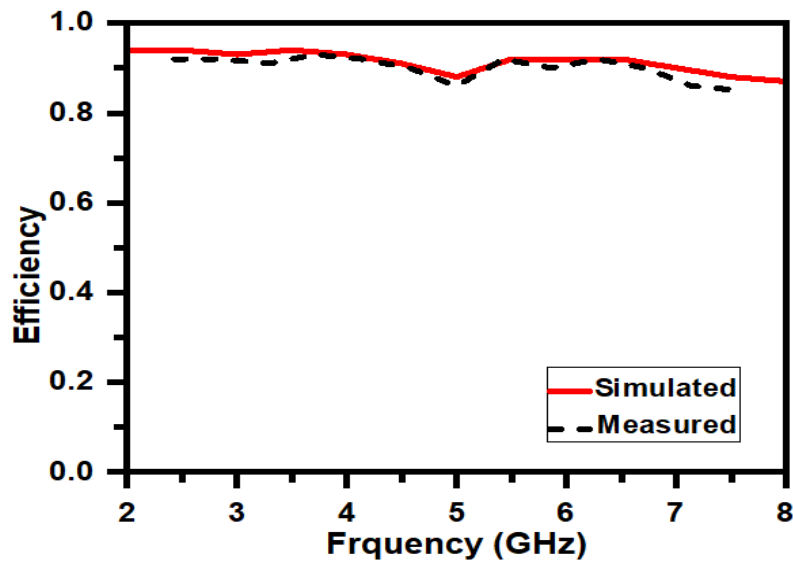
(b)



Figure 6.8 Radiation characteristics of the designed antenna at (a) 3.5 GHz and (b) 5.5 GHz



(a)



(b)

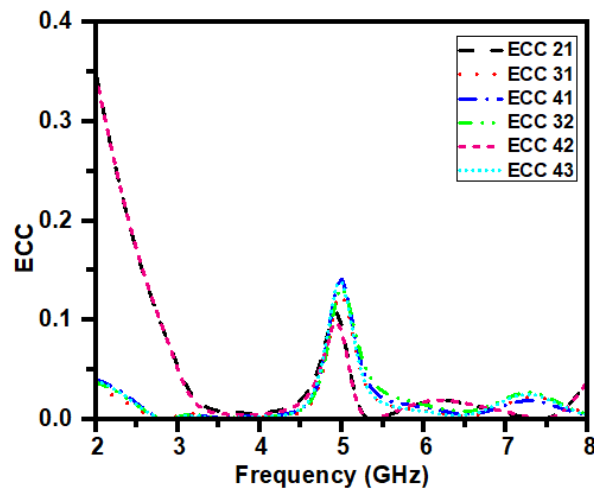
Figure 6.9 Simulated and tested (a) Gain and (b) Efficiency of the proposed MIMO antenna

The antenna's normalized radiation patterns were assessed at frequencies of 3.5 GHz and 5.5 GHz, both in the x-z and y-z planes. In the Co-polar, semi-omnidirectional patterns are introduced, while bidirectional patterns are observed in the Cross-polar. These patterns exhibit reasonable consistency, as depicted in Figure 6.8. Additionally, Figure 6.9(a) displays the comparative results of peak gain from simulation and testing. The antenna's

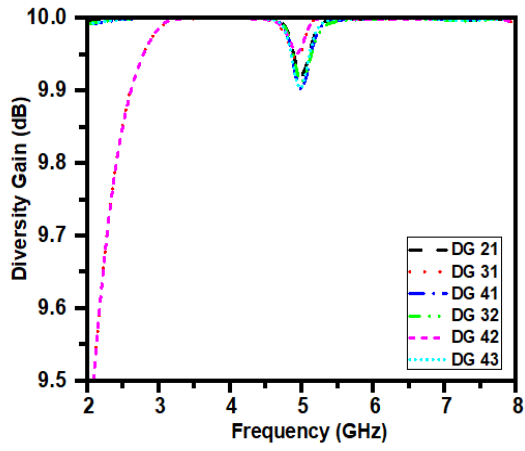
measured gain varies from 1.4 dBi at the lower band to 4.8 dBi at the upper band, demonstrating favourable alignment between the outcomes. Figure 6.9(b) illustrates the overall efficiency at all ports of the proposed antenna design.

6.4 MIMO System Evaluation

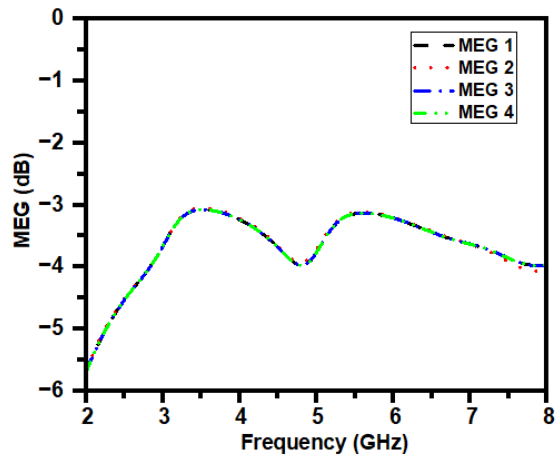
To assess the MIMO system's performance and its diversity characteristics, like ECC, DG, MEG (mean effective gain), TARC (total active reflection coefficient), CCL (channel capacity loss) parameters of the MIMO antenna are computed & analysed. The ECC parameter serves as an indicator of the isolation between ports. Enhanced MIMO effectiveness is indicated by lower ECC values. ECC values below 0.5 are considered favourable for robust MIMO implementation. The value of the ECC is lower than 0.01 from 3.0 to 4.4 GHz and lower than 0.03 from 5.0 to 6.6 GHz as shown in Figure 6.10(a). The simulated and tested DG outcomes are displayed in Figure 6.10(b).



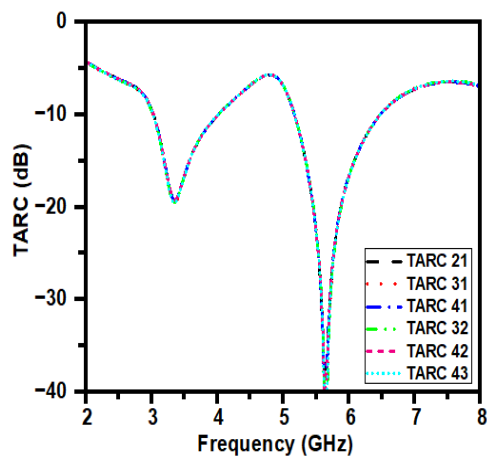
(a)



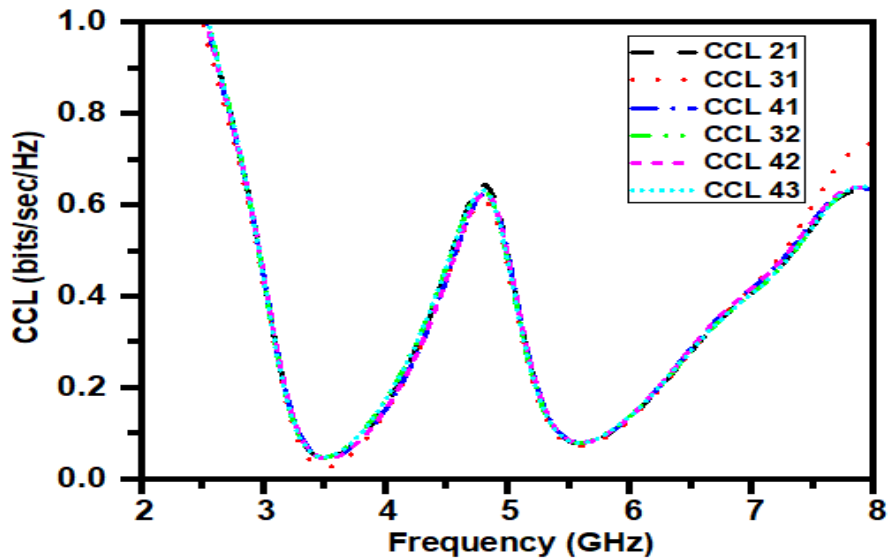
(b)



(c)



(d)



(e)

Figure 6.10 (a) ECC (b) DG (c) MEG (d) TARC (e) CCL of proposed 4-port MIMO

The DG results exhibit values of at least 9.9 dB across the specified operational band configurations. Figure 6.10(c) illustrates the MEG is a performance metric that compares the average received signal strength of a MIMO antenna array to its average incident power. It helps calculate the average received power intensity for each antenna & MEG values for all four antennas defined by industry and standards limit of $-3 \leq \text{MEG (dB)} < -12$. The MIMO antenna architecture utilizes closely spaced radiating elements that operate simultaneously. However, this configuration can impact interference performance, which is quantified by the TARC as shown in Figure 6.10(d) which are below -10 dB. The channel capacity of a communication system reflects its ability to efficiently transmit signals without distortion or loss of bits. In the case of the proposed MIMO antennas, a CCL value below 0.10 b/s/Hz as

shown in Figure 6.10(e). A comparative analysis between the proposed MIMO antenna and other designs is presented in Table 6.2 to validate its performance. The suggested MIMO antenna stands out with its compact dimensions while maintaining favorable levels of isolation, gain, and ECC values. These characteristics make it well-suited for applications in dual-band network scenarios.

Table 6.2 Comparing the MIMO antenna presented here with previously documented MIMO antenna designs.

Reference no.	Antenna dimension (mm ³)	MIMO antenna Elements	Frequency bands (GHz)	Isolation (dB)	Peak Gain(dBi)	Efficiency	ECC
[86]	100×100×1.6	4	3.5,5.5	> 20	-	-	<0.1
[101]	58×58×0.8	4	3.5,5.5	> 18	7	-	<0.07
[84]	81×87×1.6	4	4.8,7.7	≥ 20	5	60%,87%	<0.1
[83]	110×97×1.4	4	2.4,5.8	25-33	4	60%,70%	<0.1
[102]	54×54×0.13	4	4.5,8.5	> 17	4.5	-	<0.03
[100]	60×65×1.6	4	3.5,4.5	> 15	4.85	80%	<0.13
[99]	140×70×9.55	4	2.7,3.5	> 20	2.1,3.7	70%	<0.5
[98]	65×65×1.6	4	3.5,5.9	> 20	2.9,3.7	80%	<0.01
[103]	200×150×0.76	4	-	> 15	4.2	95%	<0.01
[104]	100×50×4.5	4	3	> 25	3	80%	<0.01
[105]	120×65×1.6	4	3.5,4.8	> 18	4.71	-	<0.14
[106]	145×75×0.8	8	3.4,4.9	-	-	85%	<0.15
[107]	150×70×0.8	8	3.5,5	> 17	4.4,5.5	61%	<0.01
[108]	45×38×0.2	4	2.5,3.6,5.5	> 20	4	-	<0.04
[109]	100×80×1.6	4	3,5,4.3	> 20	5.42	-	<0.1
[110]	55×55×0.2	4	3.6,4.75,9.1	> 15	4	-	<0.17
[111]	90×90×1.57	4	3.56,5.28	> 22	4.2,2.8	88%,79%	<0.05
[112]	40×40×1.6	4	3.4,4.8	> 16	2.6,4	93%	-
[113]	36×27×1.6	4	8.5	>18	3.55	70%	<0.01
[114]	66×66×0.13	4	3.5	>20	3	99%	<0.05
[115]	30×40×1.6	4	4.5	>17	3.5	85%	<0.05
[116]	100×60×1.6	4	2.6,3.2	> 20	5.3	-	<0.01
Proposed Antenna	64×64×1.6	4	3.5,5.5	> 18	1.4, 4.9	94%,92%	<0.03

6.5 Conclusions

This chapter explores a compact four-port MIMO antenna featuring dual-band capabilities. The suggested design comprises four resonators of matching shapes, organized in an orthogonal arrangement, with the diagonal components arranged in an anti-parallel pattern. The antenna successfully exhibited an isolation of ≥ 18 dB for both Wi-MAX and WLAN frequency bands (3.5 GHz and 5.5 GHz, respectively). The study encompassed simulations and practical measurements of gain, S-parameters, isolation, ECC, and radiation patterns. The outcomes proved that the decoupling worked without any element being achieved and a favorable diversity response was attained. The results obtained showcase the capacity utility of the suggested MIMO antenna for dual-band applications.

Chapter 7

Triple Band Self-Decoupled MIMO Antenna Pair for 5G Communication

This chapter introduces a new two-port MIMO antenna designed for 5G mobile phones. Its unique self-decoupling feature eliminates the need for additional decoupling components. By using a mode-cancellation technique, the antenna achieves excellent isolation (over 22 dB) across three frequency bands: 2.58-2.84 GHz, 3.4-3.9 GHz, and 4.3-4.6 GHz. Experimental results show high isolation between ports and good overall gain (1.9 dBi, 3.77 dBi, and 2.9 dBi). This design offers a promising approach for highly integrated 5G MIMO antennas due to its simplicity, efficiency, and self-decoupling capabilities.

7.1 Introduction

Multiple-Input-Multiple-Output (MIMO) technology is a wireless communication technique that uses multiple transmitting and receiving antennas to improve the performance of wireless systems. MIMO takes advantage of the multipath propagation phenomenon, where signals sent from a transmitter reach the receiver through multiple paths due to reflections, diffractions, and scattering in the environment. MIMO has been widely adopted in various wireless communication standards, including Wi-Fi (802.11n/ac/ax), cellular networks (4G LTE, 5G), and wireless point-to-point links. Its effectiveness in increasing data rates and system capacity has made it a fundamental technology for addressing the ever-increasing demand for more data speeds in modern wireless networks.

In the literature, A licensed band of frequencies between 4.40 and 5.01 GHz, 3.30 and 3.80 GHz, and 3.30 and 4.20 GHz is needed for the Sub-6 GHz 5G. While Wi-Fi 6E 5G provides quality of service (QoS) suitable for Industrial Internet of Things (IoT) applications, which require low latency and high capacity, and has become the standard networking technology for both households and businesses, including robotics [116]. To enable independent usage of Wi-Fi 6E and 5G bands in indoor networks and seamless transition between them, the aim of a compact MIMO antenna capable of functioning

across multiple frequency bands. One particular issue with the MIMO antenna design is the mutual interaction between components of densely positioned antennas, lowering the MIMO antenna's efficiency in terms of effective spectrum utilization and high-speed data transmission [102]. When a large number of antennae group together the mutual couplings increased and it reduces antenna efficiency and MIMO performance. It is a serious issue in the MIMO technology-based antenna system [125].

This chapter presents, a triple-band monopole MIMO antenna with improved isolation. The proposed design is created and evaluated to confirm the simulation and measured results by analysing the S-parameter, radiation pattern, efficiency & peak gain using HFSS. The overall dimension of the entire model is 70 mm × 31 mm. Measured outcomes for the combined antenna indicate that the proposed antenna functions within three frequency bands, achieving S_{11} values of less than or equal to 10 dB from 2.58 GHz to 2.84 GHz, 3.4 GHz to 3.9 GHz and 4.3 GHz to 4.6 GHz. Furthermore, peak gain at three bands is 1.9 dBi, 3.77 dBi and 2.9 dBi. Two symmetric feeding strips are used to individually excite the individual radiator, which has a diameter of 35 mm by 18.5 mm. The distance between the two feeding ports is $D_0=10$ mm, which is an essential requirement for port isolation of more than 22 dB.

7.2 Antenna Design and Decoupled Structure

7.2.1 Triple-Band Antenna Design

The evolution of the suggested triple-band antenna is depicted in Figure 7.1. To reach the suggested 50 Ω of impedance, microstrip lines having a width of 3 mm for transmission and a ground plane-to-transmission line gap of 1.6 mm provide fed. Figure 7.2 shows the simulated S_{11} results for each configuration. The radiator shape for antenna 1 is a rectangular patch, as seen in Figure 7.1a. The operating bandwidth is affected by the ground plane's length. The antenna is used in the frequency range from 3.3 GHz to 3.6 GHz when the ground plane measures 31 mm, as illustrated in Figure 7.2 red dotted line (antenna 1).

By making adjustments to the radiator's design, utilizing a conventional two-triangle cut on the antenna (illustrated in Figure 7.1b), an antenna slanted to the left is generated, exhibiting resonance across two frequency bands. Figure 7.2 (antenna 2, indicated by the blue dotted line) demonstrates a band with an S_{11} level below 19 dB, centred at 3.47 GHz. The bandwidth of this band extends from 3.3 GHz to 3.6 GHz, with S_{11} levels ≤ 10 dB. Additionally, a second band is observed between 4.7 GHz and 4.9 GHz, featuring an S_{11} level ≤ 10 dB.

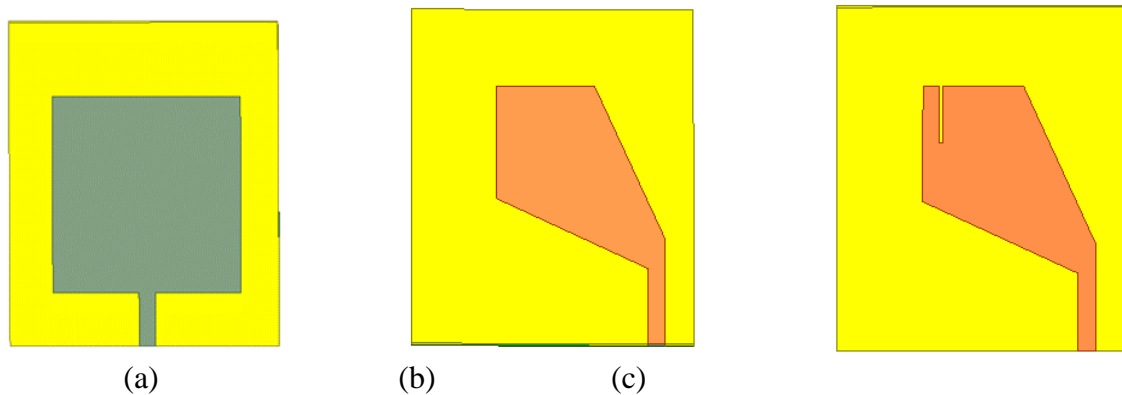


Figure 7.1 Evolution of the microstrip-fed monopole antenna (a) Antenna_1 (b) Antenna_2 (c) Antenna_3

Moreover, the introduction of a rectangular slot, illustrated in Figure 7.1c and also observable in Figure 7.2 (a) (depicted by the solid black line for antenna 3), leads to a transformation of the dual-band antenna into a triple-band configuration. This transformation occurs due to modifications in the current distribution within the antenna's structure, resulting in the emergence of novel resonant frequencies encompassing the 2.5 GHz to 2.8 GHz bands. In this revised arrangement, the initial band functions within the 2.5 GHz to 2.8 GHz frequency range (260 MHz) with a central frequency of 2.7 GHz. Subsequently, the second band, centred at 3.6 GHz, from 3.4 GHz to 3.9 GHz (500 MHz). Lastly, the third band operates with a central frequency of 4.5 GHz and covers the 4.3 GHz to 4.6 GHz frequency range (300 MHz).

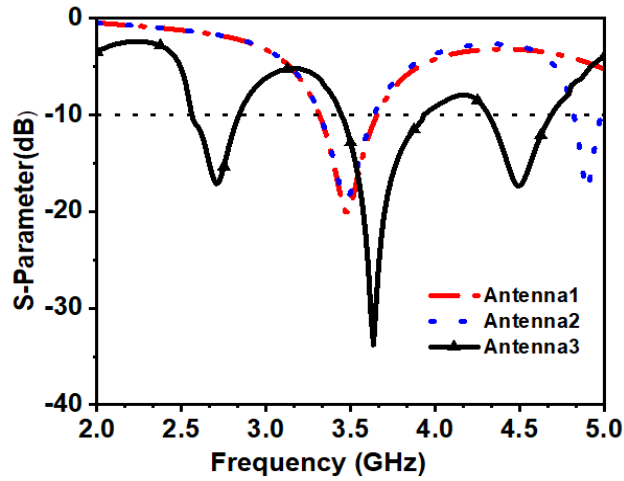


Figure 7.2 Simulated S-parameter of single antenna

7.2.2 Parametric Analysis

Using Ansys HFSS, the simulation of the antenna design across the operational frequency range was conducted, and the design parameters for the antenna structure were fine-tuned. The antenna's dimensions were determined through a parametric analysis involving the length of the slot (parameter W_2). The impact of W_2 on the S_{11} parameters is illustrated in Figure 7.3. The W_2 varied between 9 to 11 mm. The optimized values were $W_2 = 10$ mm, resulting in the desired favourable return loss.

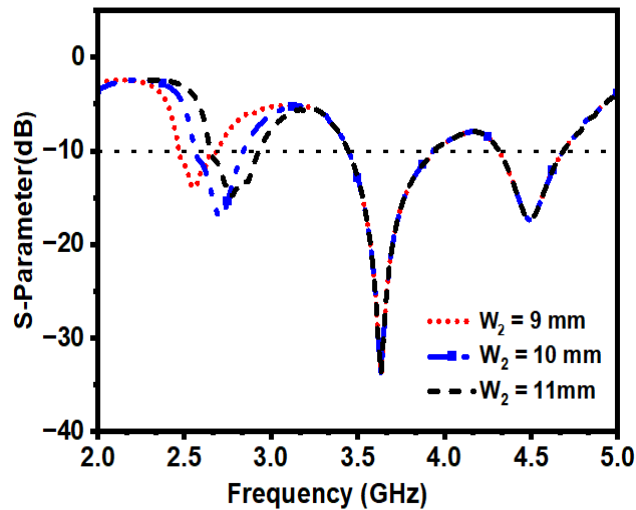


Figure 7.3 Parametric analysis of single antenna

7.2.3 Proposed Self-Decoupled Antenna Pair

Figure 7.4 shows the design of the proposed two symmetrically mirrored tilted monopoles whose dimension is $70 \text{ mm} \times 31 \text{ mm}$, which is located above the ground plane with the substrate on a 1.6 mm thick RT-Duroid ($\epsilon_r = 2.2$, $\tan\delta = 0.009$) without using any the isolating structure. As indicated in Figure 7.4(a), the two comparable monopole-tilted radiators are placed 10 mm apart from one another in a horizontal orientation. The parameters of the tilted monopoles MIMO antenna are $L=70 \text{ mm}$, $W=31 \text{ mm}$, $L_1=17.5 \text{ mm}$, $W_1=20.5 \text{ mm}$, $L_2=0.8 \text{ mm}$, $W_2=10 \text{ mm}$, $L_{S1}=30 \text{ mm}$, $L_{S2}=30 \text{ mm}$, $g_1=10 \text{ mm}$, $W_3=8 \text{ mm}$.

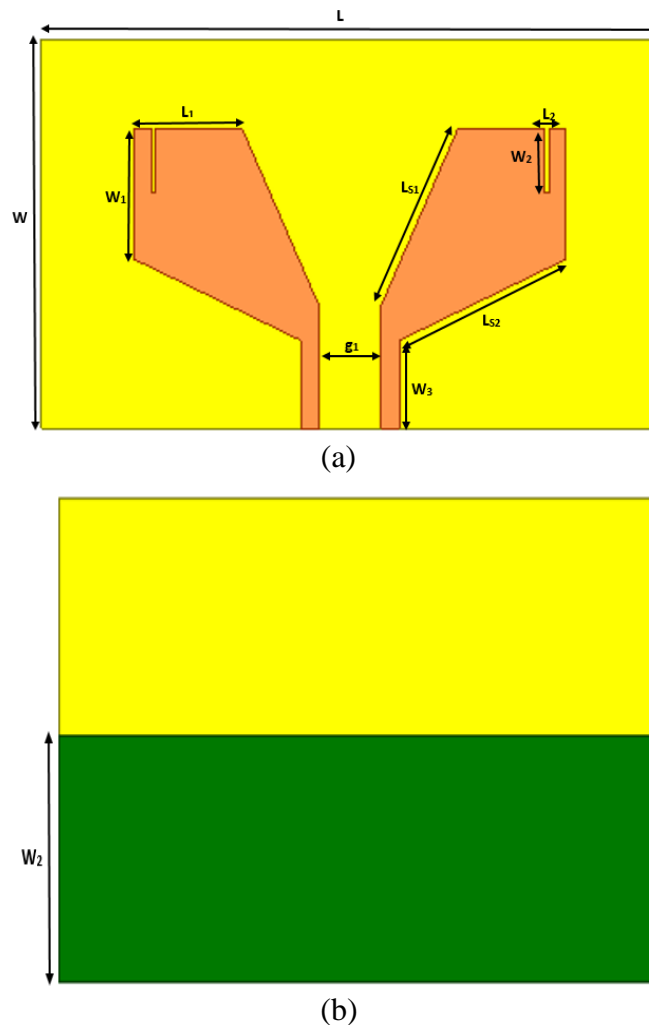


Figure 7.4 Layout and design of self-decoupled MIMO antenna, (a) top view (b) bottom view

7.2.4 Decoupling Analysis

The active reflection coefficients for the common-mode (CM) and differential-mode (DM) signals in a symmetric and reciprocal 2-port network are calculated and simplified using the theory of microwave networks. The S-parameters of the network satisfy $S_{11} = S_{22}$ and $S_{12} = S_{21}$ under this condition. The ratio of the reflected incident signal is known as the active reflection coefficient S_{CM} for the CM signal, & the incident signal to the reflected signal is known as the active reflection coefficient S_{DM} for the DM signal. The greater the isolation between ports 1 and 2 the smaller the difference between these coefficients.

The Euclidean distance in the Smith chart makes it simple to determine the distinction between the CM and DM complex reflection coefficients. $S_{CM} = S_{DM}$, which means that just the CM and DM reflection coefficients are equivalent & If port 1 and port 2 are properly isolated, the opposing currents in common mode (CM) and differential mode (DM) can be eliminated through flawless self-isolation (i.e., $S_{21} = 0$). For instance, if the isolation between ports 1 and 2 in S_{21} is less than $-10 \text{ dB} = 0.316$, then $|S_{CM} - S_{DM}|$ is less than 0.632 (The Smith chart's radius is normalized to a value of one). To establish good isolation between port 1 and port 2, it is essential to adjust the CM and DM signals' active reflection coefficients must be similar (or as close in the Smith chart) as possible.

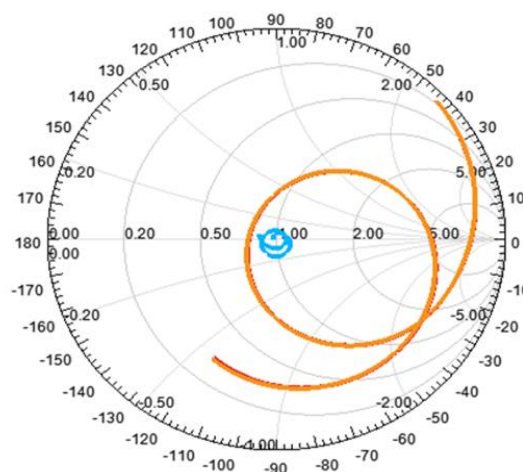
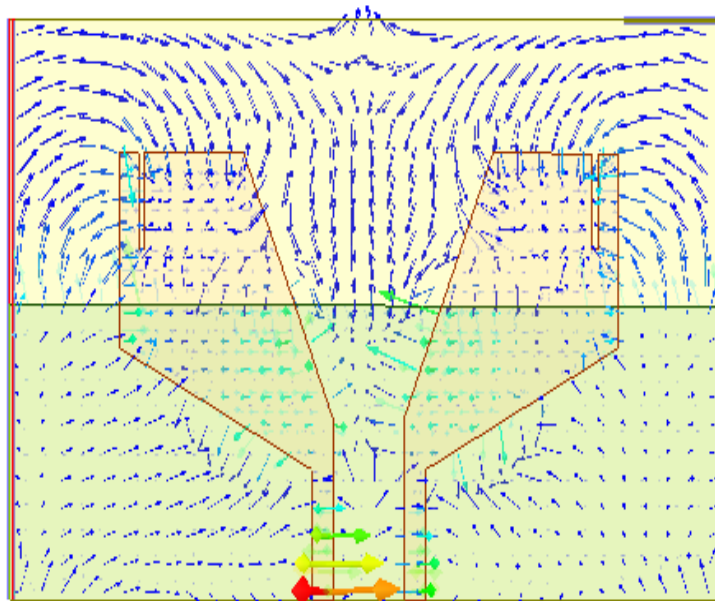


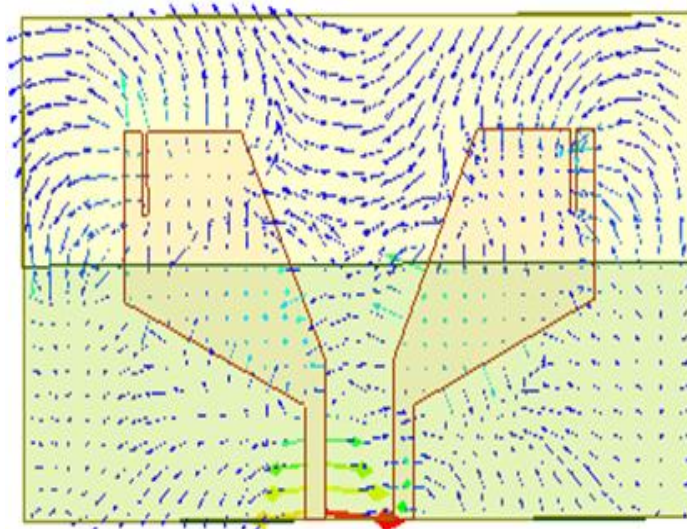
Figure 7.5 Simulated Smith chart showing the feeding distance $D_o=10\text{mm}$ and the CM and DM reflection coefficients

Figure 7.5 shows the Smith chart to create good isolation by adjusting the impedances of two ports, CM and DM, and their active reflection coefficients. The feeding distance D_0 , or distance between these ports, is an important factor that can be changed to enhance their performance. Based on the information given, it is possible to get an optimised self-isolation performance when D_0 is equal to 10 mm. Figure 4 depicts the Smith chart for the DM impedance, which has a longer curve and is less uniform than the CM impedance. Because of the influence of the horizontal dipole-like mode's inverse ground mirror current. To achieve good results, both impedances can be changed to a comparable status.

The CM and DM-fed antenna pair vector current distributions as shown in Figure 7.6. Two folded monopole-like current distributions in the antenna cause the current to be out of phase when the antenna is supplied using a common mode (CM) signal, as illustrated in Figure 7.6(a). This indicates that the current on either side of the antenna runs in opposing directions. The antenna's current distribution resembles a horizontal dipole and is in a phase when the antenna is supplied using the differential mode (DM) signal, as illustrated in Figure 7.6(b). This shows that the current flows in the same direction through the antenna on both sides. When designing and analysing antennas with CM and DM feeding, it's essential to take these current distributions into account because they may have an impact on the antenna's performance and radiation pattern.



(a)



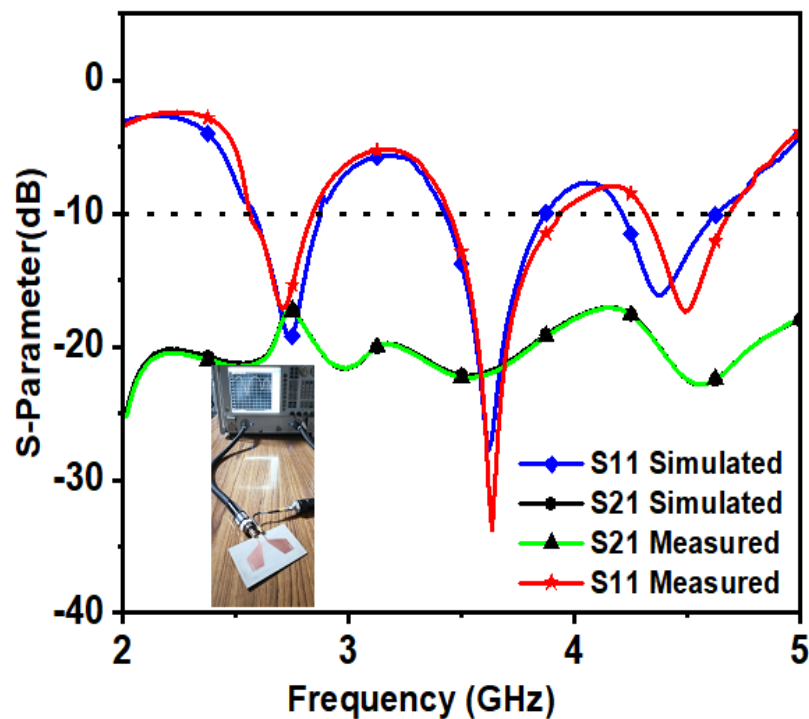
(b)

Figure 7.6 Self-decoupled antenna pair's vector current distributions at 3.6GHz (a) CM fed. (b) DM.

7.3 Simulated and Measured Results

The simulated and measured MIMO antenna's S-parameters for ports 1 and 2 such as S_{11} , S_{22} , S_{12} , and S_{21} are shown in Figure 7.7 (a) & (b). The simulation results indicate an isolation of over 22 dB between ports 1 and 2 of the MIMO antenna and operates at three

bands 2.7 GHz, 3.6 GHz and 4.5 GHz, a bandwidth ranging from 2.5 GHz to 2.8 GHz and computed at $S_{11} \leq 10$ dB for the first band, 3.4 GHz to 3.9 GHz for the second band and 4.3 GHz to 4.5 GHz for the third band, respectively. The results exhibit identical frequency ranges to those observed in the simulated and measured results, as seen in Figure 7.7 (blue and red curve). The measurements indicate the antenna operates in three bands with a centred on 2.7 GHz, 3.6 GHz and 4.5 GHz, with bandwidths ranging from 2.5 GHz to 2.8 GHz, 3.4 GHz to 3.9 GHz and 4.36 GHz to 4.57 GHz for three bands. Here measured and simulated outcomes are nearly identical, with only a minor difference between the two. This is due to the fabrication step and simulation impact. The S-parameter measurement setup can be shown in the Figure 7.7(c).



(a)

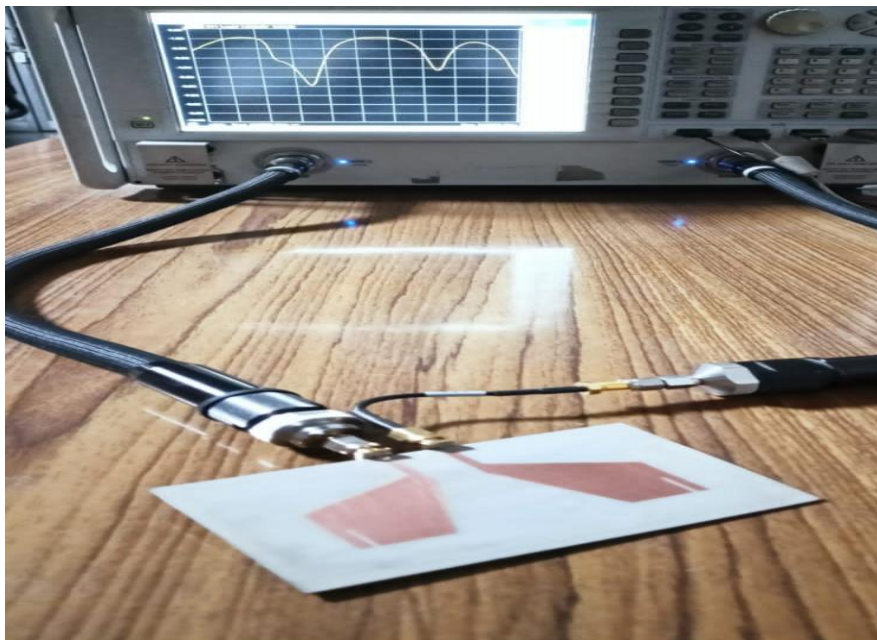
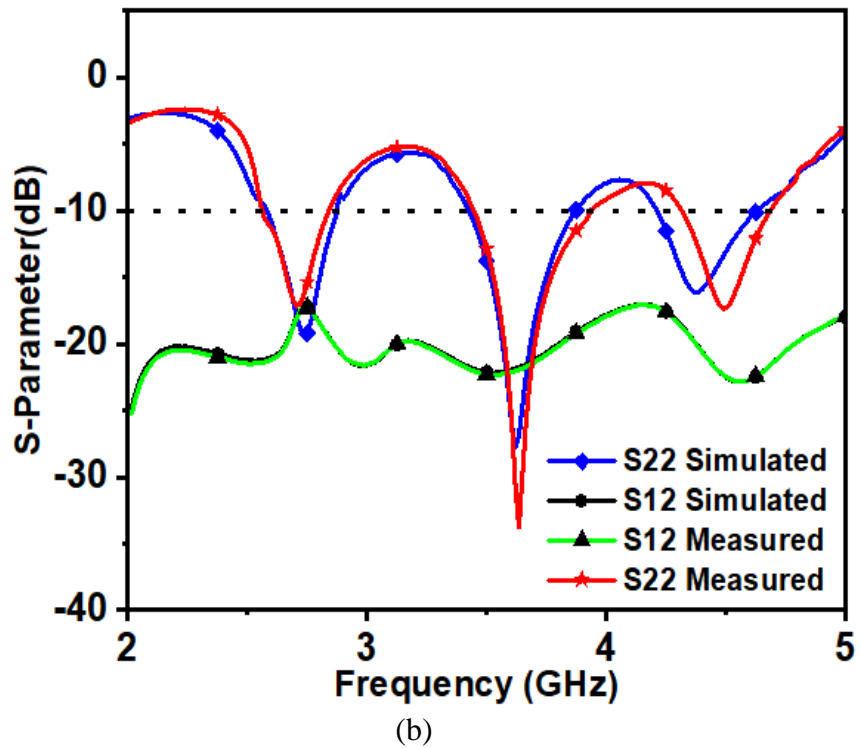
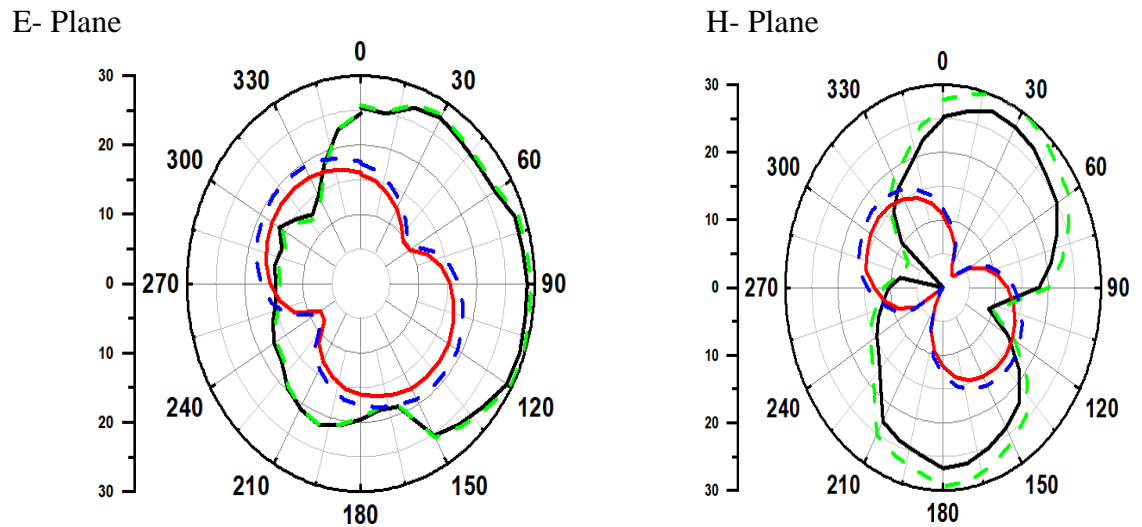


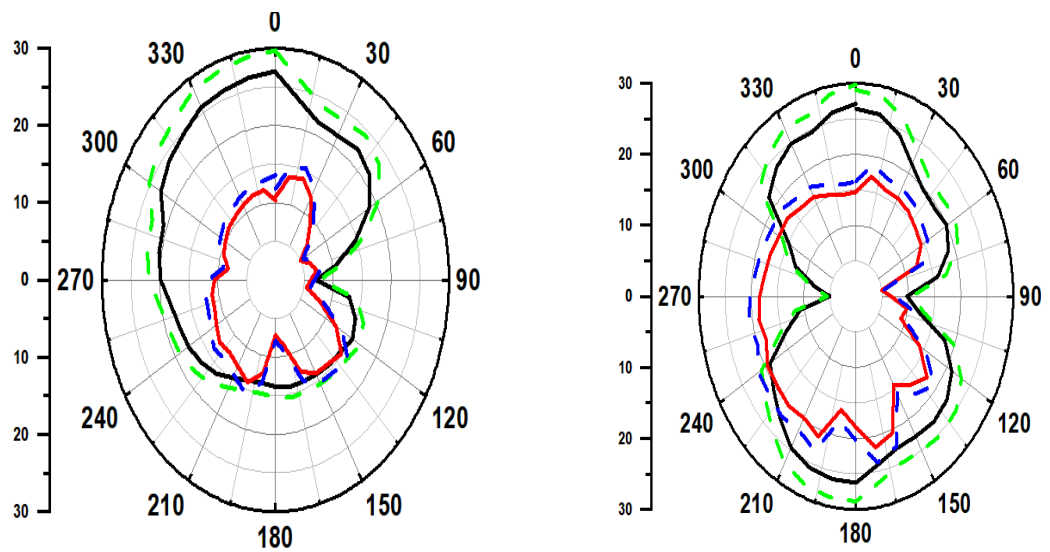
Figure 7.7 Self-decoupled MIMO antenna pair (a) S_{11} & S_{21} (b) S_{22} & S_{12} simulated and measured results (c) experimental test bench setup

7.3.1 Radiation Pattern

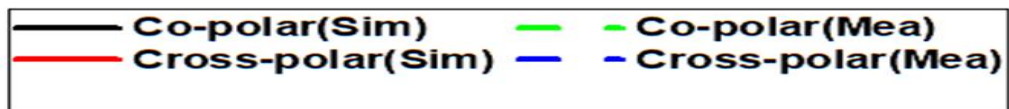
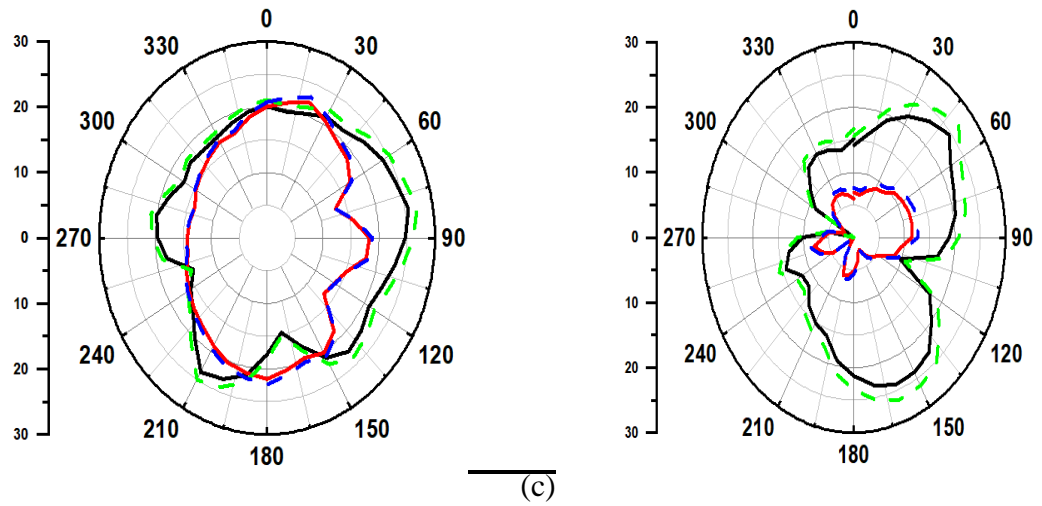
Figure 7.8(a, b, c) depicts the simulated and measured radiation patterns in the E and H planes at frequencies of 2.7 GHz, 3.6 GHz, and 4.5 GHz. An anechoic chamber is being used to test the antenna, as shown in Figure 7.8 (d). The antenna exhibits a bidirectional pattern in the H-plane.



(a)



(b)

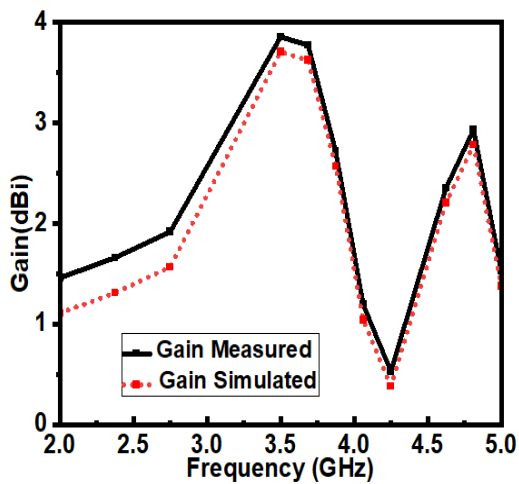


(d)

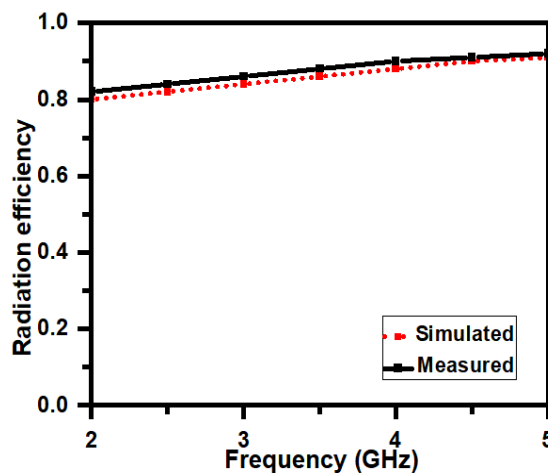
Figure 7.8 Radiation patterns of self-decoupled MIMO antenna (a) at 2.7GHz (b) at 3.6GHz (c) at 4.5GHz (d) Measurement in anechoic chamber

7.3.2 Peak Gain & Efficiency

Figure 7.9 (a) displays the antenna's peak gain as observed in simulations and measurements. The antenna simulated the peak gain of 1.9 dBi, 3.77 dBi and 2.9 dBi for three bands and measured the peak gain of about 2 dBi, 3.8dBi, and 3 dBi. Figure 7.9(b) illustrates the overall radiation efficiency of proposed antenna design. The efficiency of the antenna at three different resonances are 83 %, 86 % and 89 % respectively.



(a)



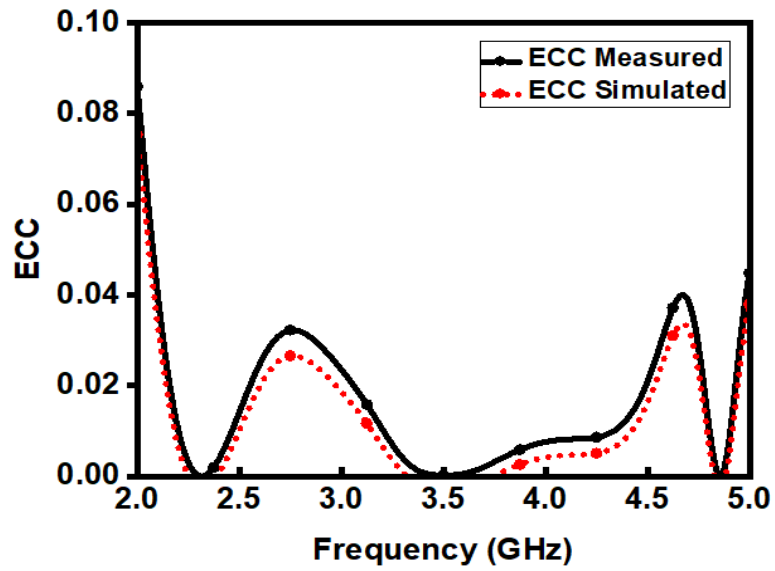
(b)

Figure 7.9 Self-decoupled MIMO antenna pair (a) Peak gain (b) Radiation efficiency

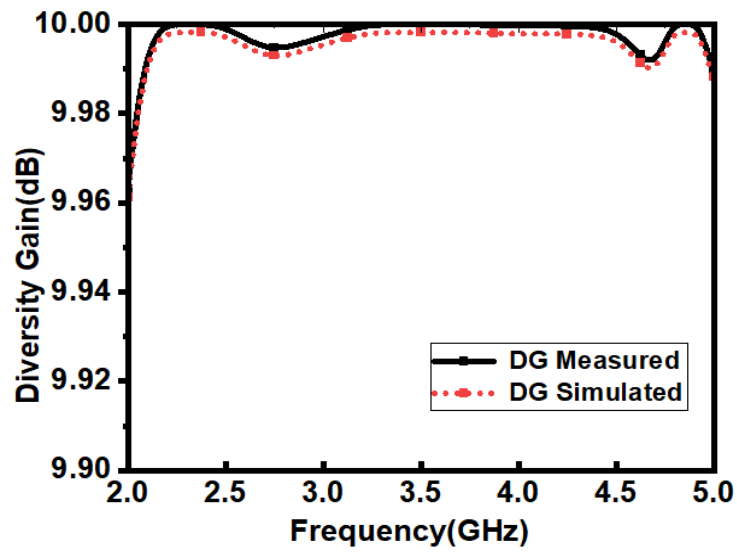
7.3.3 Diversity Performance Analysis

The diversity evaluation (ECC, DG, TARC, CCL and MEG) has significance for confirming the two-port MIMO antenna's performance, which was examined through simulations and experiments. The envelop correlation coefficient (ECC) graph for the specified frequency ranges is shown in Figure 7.10 (a). The ECC of the two-port MIMO antenna was less than 0.04 across the whole band, confirming that this MIMO antenna performs similarly to whatever is necessary for MIMO diversity performance. Figure 7.10 (b) illustrates the diversity gain (DG) of a dual-port MIMO antenna. The measured and simulated DG results for the far-field radiation patterns closely align with the target value of 10 dB.

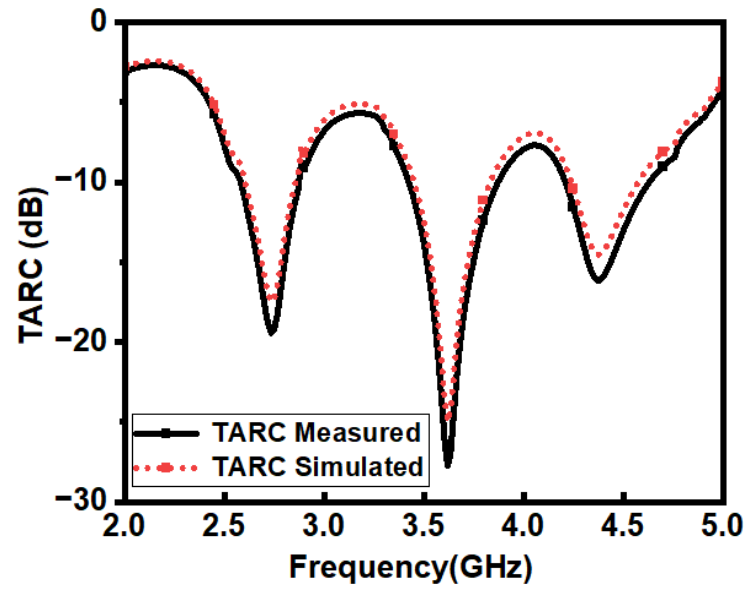
The radiating elements are located close to one another and are used simultaneously in the MIMO antenna architecture; however, the interference performance is also influenced by this configuration of radiating antennas which can be calculated by TARC (Total Active Reflection Coefficient) Figure 7.10 (c) displays the TARC values, which are below 10 dB. Channel capacity loss (CCL) is a critical factor in evaluating the effectiveness of a MIMO antenna in high-data-rate communication systems, as it directly impacts the ability to transmit signals and information reliably and without distortion. Figure 7.10 (d) demonstrates that the CCL value is lower than the practical limit (0.4 bits/s/Hz), indicating that it meets the requirement for communication. In Figure 7.10 (e) shows mean effective gain (MEG) of the antenna, when powered by ports 1 and 2 respectively, shows a consistent value of below 3 dB across the entire frequency band. The MEG1/MEG2 is nearly one. These findings indicate that the radiating elements in the MIMO design maintain a stable gain performance.



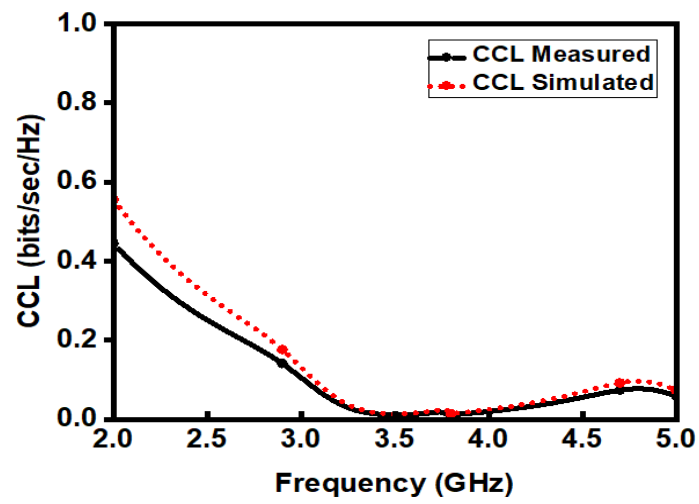
(a)



(b)



(c)



(d)

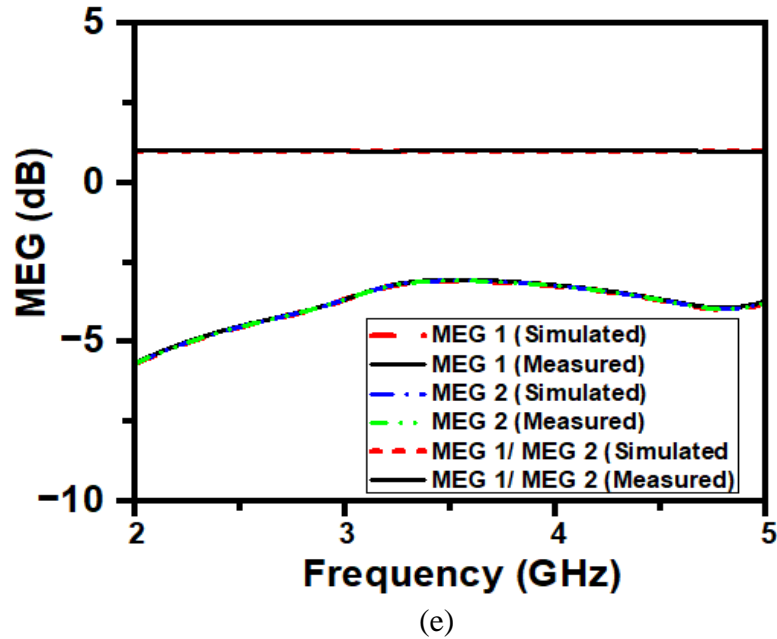


Figure 7.10 Self-decoupled MIMO antenna measured (a) ECC (b) DG (c) TARC (d) CCL (e) MEG

7.4 SAR Analysis

The SAR analysis setup is displayed in Figure 7.11, phantom model consisting of skin 2mm, fat 3.5mm, muscles 10mm, and bone 10mm [23] is placed at a distance of 3mm from the antenna. The maximum value of SAR is 0.497W/kg at 100mW which is less than the prescribed 1.6W/kg. Therefore, the antenna is suitable as well as safe to be used in near human body for 5G communication system.

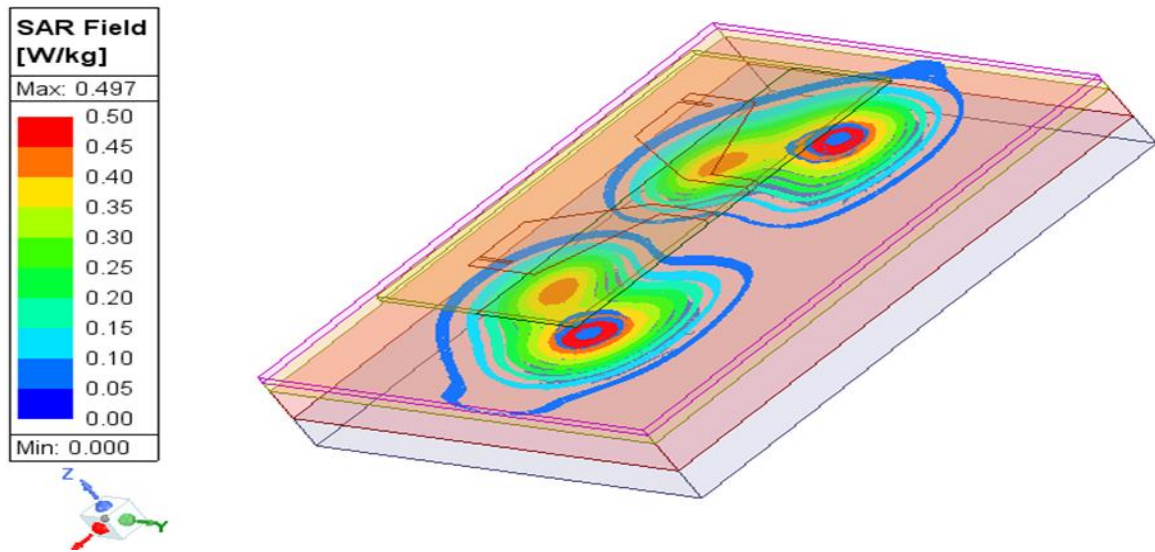


Figure 7.11 SAR of the proposed antenna

These findings indicate that the two MIMO antennas with self-isolation are effectively decoupled from each other, making them well-suited for applications involving MIMO technology. To validate the design's novelty, the proposed design is compared to previous works, as seen in Table 7.1. From Table 7.1 it's clear that our proposed antenna has better isolation and compact size. Similarly, ECC & DG are comparable with the other references. The proposed antenna is the ideal design for triple-band wireless applications since it offers outstanding performance and a small footprint.

Table 7.1 Comparisons of the decoupled antenna pair for recent literature

Ref.	Element	Decoupling Mechanism	-10dB S_{11}	Size of antenna	Isolation	Distance between feed	ECC	DG
[129]	8	Self	3.3-4.2	150×75×0.8	>10.5	9mm	<0.2	-
[130]	4	Coupled CPW	3.7-7.3	-	>20	5.6mm	<0.03	-
[131]	2	-	1.46-1.52	120×120×0.3	>16.3	2mm	-	-
[132]	8	Asymmetrically mirrored	3.4-3.6	10×7×1	>10		<0.1	-
[133]	4	Orthogonal mode	3.4-3.6	25×7×1.5	>20.1	-	<0.008	-

[134]	4	-	4.3–6.45	100 × 60 × 0.76	> 15	15mm	< 0.004	-
[135]	4	Parasitic resonant strip	2.6-2.8, 3.4-3.6	140×70×9.5	>20	-	-	-
[136]	4	Orthogonal mode	4.8, 7.7	81 × 87 × 1.6	>20	-	< 0.15	>9.9
[137]	4	Parasitic Meandering Resonator	3-5	65×60×1.6	>15	-	<0.05	>9.7
[138]	4	orthogonal	3.5, 5.9	65 × 65 × 1.6	>20	-	< 0.01	>9.9
[139]	2	Defected ground	2.99 – 3.61, 4.53-4.92	62×25.6×1.524	<16	-	-	-
[140]	2	Slotted ground plane	2.4,3.5, 5.5	48×31×1.6	<20	-	<0.003	>9.9
Proposed	2	Self	2.5-2.8,3.4-3.9,4.3-4.5	70×31×1.6	>22	10 mm	<0.04	>9.9

7.5 Conclusion

The efficient development, exploration, and assessment of the design have resulted in a dual-port MIMO antenna that meets the bandwidth needs of both the Sub-6 GHz and 5G. The dual-pair MIMO antenna demonstrates operation across three bands with impedance bandwidths: 2.5 GHz to 2.8 GHz, 3.4 GHz to 3.9 GHz, and 4.3 GHz to 4.5 GHz. Additionally, it achieves a peak gain of 1.9 dBi, 3.77 dBi and 2.9 dBi. To make sure that the MIMO antennas closely spaced have an effective mutual coupling of over -21 dB, a self-decoupling structure is implemented antenna. The ECC value of 0.04 and DG measurement of greater than 9.98 dB have been established to comfortably meet practical standards. The dual-port MIMO antenna can be seamlessly integrated into contemporary Sub-6 GHz 5G improved diversity analysis, and compact design. Furthermore, it is highly

suitable for constructing extensive antenna arrays that improve the quality of wireless communication transmission and reception. Additionally, its design simplifies and enhances effortless internet accessibility.

Chapter 8

Conclusion and Future Scope

This chapter is divided into two primary sections. (i) A comprehensive summary of the key findings and accomplishments presented throughout the thesis, and (ii) Potential avenues for further exploration and development based on the research conducted. The presented thesis is mainly focused on the high gain, beam scanning, MIMO antenna and diversity parameters.

8.1 Conclusion of the Presented Work

The first chapter provides an overview of 5G technology and the anticipated frequency bands. It then examines the future needs for various types of antennas like microstrip patch, MIMO antennas. Additionally, it explores bandwidth, isolation, gain and diversity parameters. This introduction establishes the groundwork necessary to understand the research presented in the thesis.

In the second chapter, a design for a coplanar waveguide (CPW)-fed patch antenna integrated with a metasurface superstrate. The metasurface layer, positioned above the antenna, is designed to reflect the radiated electromagnetic waves in phase, resulting in enhanced gain and beam-scanning capabilities. By employing the CPW feeding technique, we have achieved significant improvements in bandwidth and overall antenna performance. The proposed antenna exhibits a -10 dB bandwidth of 3.86-4.49 GHz, a realized gain of 6.06 dBi, an efficiency of 92%, and a scanning capability of -4 degrees. These promising results demonstrate the potential of this antenna design for 5G wireless communication applications, offering enhanced performance and flexibility.

In the third chapter, 5G patch antenna design incorporating a metasurface superstrate. The metasurface layer, positioned above the antenna, functions as a Fabry-Perot cavity, reflecting the radiated energy in phase and thereby enhancing both gain and bandwidth. The realized antenna achieved a -10 dB bandwidth of 3.44-3.61 GHz, a realized gain of

6.8 dBi, and an efficiency of 69%. These results demonstrate the potential of the proposed antenna design for 5G applications, offering improved performance and efficiency.

In the fourth chapter, This paper presents a novel design for closely integrated multiple-input multiple-output (MIMO) patch antennas operating at 3.5 GHz. To improve isolation between the antennas, a double-layer metasurface composed of cut wires is incorporated between the two mirror-symmetrical patch elements. This configuration effectively decouples the closely spaced antennas, which are separated by a distance of $0.011 \lambda_0$ (where λ_0 is the wavelength at 3.5 GHz). Simulation and measurement results demonstrate a significant enhancement in isolation from -10 dB to -35 dB, while simultaneously increasing the antenna gain from 1.82 dBi to 3.85 dBi. The proposed decoupling structure is currently applied to a two-element MIMO antenna, but its design can be extended to accommodate three or more antenna elements in future applications. The enhanced isolation and improved gain achieved in this design make these MIMO patch antennas well-suited for 5G wireless communication systems.

In the fifth chapter, 2-port circularly polarized (CP) MIMO antenna design incorporating a unique slot and circular split ring resonator (CSRR) at the ground plane. These elements contribute to achieving circular polarization and improving the antenna's bandwidth. The proposed antenna demonstrates an impedance bandwidth of 3.3 to 3.6 GHz with an impedance matching better than 10 dB. Additionally, it exhibits an axial ratio bandwidth of 3.35 to 3.51 GHz while maintaining a stable radiation pattern in both planes across the operating frequency range. When fed using an insect antenna, the proposed 2-port CP MIMO antenna delivers excellent diversity performance. Key diversity metrics include an envelope correlation coefficient (ECC) of 0.004, a diversity gain (DG) of 10 dB, a channel capacity (CCL) of 0.40 b/s/Hz, a maximum eigenvalue gain (MEG) of 1.03 dB, and a total average correlation (TARC) of 10 dB. The antenna's peak gain is 3.8 dBi.

In the sixth chapter, a compact four-port MIMO antenna design operating in dual-band mode. The proposed design features four identically shaped resonators arranged in an

orthogonal configuration, with the diagonal elements positioned in an anti-parallel arrangement. The antenna demonstrated an isolation of ≥ 18 dB for both Wi-MAX (3.5 GHz) and WLAN (5.5 GHz) frequency bands. Comprehensive simulations and measurements were conducted to evaluate gain, S-parameters, isolation, envelope correlation coefficient (ECC), and radiation patterns. The results confirmed the effectiveness of the decoupling mechanism without the need for any additional elements and demonstrated favorable diversity performance. These findings highlight the suitability of the proposed MIMO antenna for dual-band applications, offering compact size and robust performance.

In the seventh chapter, a dual-port MIMO antenna design that effectively supports both Sub-6 GHz and 5G frequency bands. The antenna operates across three bands with impedance bandwidths of 2.5-2.8 GHz, 3.4-3.9 GHz, and 4.3-4.5 GHz, achieving peak gains of 1.9 dBi, 3.77 dBi, and 2.9 dBi, respectively. To ensure minimal mutual coupling between the closely spaced MIMO antennas, a self-decoupling structure is incorporated. This design achieves an effective mutual coupling of over -21 dB, with an envelope correlation coefficient (ECC) of 0.04 and a diversity gain (DG) exceeding 9.98 dB, comfortably meeting practical standards. The dual-port MIMO antenna is well-suited for integration into modern Sub-6 GHz 5G systems, offering enhanced diversity performance and a compact design. Its versatility enables the construction of large-scale antenna arrays, leading to improved wireless communication quality and seamless internet access.

8.2 Future Scope of the Presented Work

The thesis presents a comprehensive study of MIMO antenna systems, focusing on various key parameters such as high gain, efficiency, radiation pattern, and diversity parameter. The research explores single-band, dual-band, and triple-band MIMO antennas, as well as metasurface-based single-band MIMO antennas. It establishes specific limits for conventional parameters like impedance, bandwidth, isolation, gain, and efficiency to ensure optimal performance. Additionally, the thesis addresses the challenges of integrating MIMO antennas into transceiver systems while maintaining their performance.

Future research may involve techniques to enhance conventional parameters and overcome the limitations of MIMO antennas.

The thesis primarily focused on the foundational design principles of MIMO antennas. While it provides a comprehensive understanding of single-band, dual-band, and triple-band configurations, it's important to note that the field of MIMO antenna design is continually evolving. Exploring alternative design methodologies can potentially lead to innovative solutions for achieving multiband applications, expanding the versatility and capabilities of MIMO technology.

Multi-antenna systems are indispensable for 5G and future wireless technologies like 6G, particularly given the higher frequency ranges employed in millimeter-wave and terahertz bands. These frequencies face challenging propagation conditions due to factors like atmospheric absorption and blockage. Multi-antenna configurations and beamforming techniques can effectively address these issues. Furthermore, there is a growing emphasis on circular polarization, which offers advantages in 5G and 6G systems, such as improved signal quality and reduced interference

This thesis could be extended to investigate the integration of filtering capabilities into MIMO antenna systems, which could enhance their performance in microwave and millimeter-wave applications.

Publications

List of Publications in SCI/SCIE Journals (Published)

1. Kansal, P., Mandpura, A. K., & Kumar, N. (2024). *A dual band CPW-fed MIMO antenna for fifth generation application*. Physica Scripta, 99(5), 055548.
2. Kansal, P., Mandpura, A. K., & Kumar, N. (2024). *Triple band self-decoupled MIMO antenna pair for 5G communication*. Physica Scripta, 99(9), 095532.
3. Kansal, P., Mandpura, A. K., & Kumar, N. (2024). *Investigation of circularly polarized MIMO antenna with enhanced isolation for sub-6 GHz application*. Physica Scripta, 99(10), 105536.

List of Publications in SCI/SCIE Journals (Communicated)

1. Kansal, P., Mandpura, A. K., & Kumar, N. *Metasurface Based (MSB) Decoupling Method for Closely Coupled MIMO Patch Antennas for 5G*, IETE Journal of Research , Taylor and francis (Under Review).

List of Publications in National / International Conferences

1. Kansal, P., Mandpura, A. K., & Kumar, N., *High Gain Microstrip Patch Antenna based on Fabry Perot Cavity for 5G Communication*, IEEE International Conference (ICMNBC), organized by Department of Electronics and Telecommunication Engineering, Sri Siddhartha Institute Of Technology, Tumkur, India, pp. 1-5, 03-04 December 2021.
2. Kansal, P., Mandpura, A. K., & Kumar, N., *CPW Fed Microstrip Patch Antenna for 5G Communication*, IEEE International Conference (SILCON), organized by National Institute of Technology (NIT), Silchar, Assam, India, pp.1-4, 04-06 November 2022.

List of Patents

1. Kansal, P., Mandpura, A. K., & Kumar, N. (2024, February). *Next-Generation Leaky Wave Antenna for 5G Deployment*. , Design no. 6346272, Grant Date. 21 February 2024, Certificate of Registration for UK design.

References

- [1] M. Agiwal, A. Roy, and N. Saxena, "Next Generation 5G Wireless Networks: A Comprehensive Survey," *IEEE Commun. Surv. Tutor.*, vol. 18, no. 3, pp. 1617–1655, 2016, doi: 10.1109/COMST.2016.2532458.
- [2] "5G Evolution: A View on 5G Cellular Technology Beyond 3GPP Release 15 | IEEE Journals & Magazine | IEEE Xplore." Accessed: Aug. 31, 2024. [Online]. Available: <https://ieeexplore.ieee.org/abstract/document/8826541>
- [3] "5G-Spectrum-Positions.pdf." Accessed: Aug. 31, 2024. [Online]. Available: <https://www.gsma.com/connectivity-for-good/spectrum/wp-content/uploads/2022/06/5G-Spectrum-Positions.pdf>
- [4] J. D. Kraus, "Antennas McGraw-Hill," N. Y., 1988.
- [5] "Sub-6G and mmWave Tech Cuts Through the Haze of 5G Antenna Design - News." Accessed: Aug. 31, 2024. [Online]. Available: <https://www.allaboutcircuits.com/news/sub6g-and-mmwave-solutions-cut-through-haze-of-5g-antenna-design/>
- [6] T. Ohishi, N. Oodachi, S. Sekine, and H. Shoki, "A method to improve the correlation coefficient and the mutual coupling for diversity antenna," in 2005 IEEE Antennas and Propagation Society International Symposium, Jul. 2005, pp. 507-510 Vol. 1A. doi: 10.1109/APS.2005.1551365.
- [7] "2014-12-08-c88a32b3c59a11944a9c4e544fee7770.pdf." Accessed: Aug. 31, 2024. [Online]. Available: <https://www.gsma.com/solutions-and-impact/technologies/networks/wp-content/uploads/2015/01/2014-12-08-c88a32b3c59a11944a9c4e544fee7770.pdf>
- [8] Y.-L. Ban, C. Li, G. Wu, and K.-L. Wong, "4G/5G multiple antennas for future multi-mode smartphone applications," *IEEE Access*, vol. 4, pp. 2981–2988, 2016.
- [9] T. Barnett, A. Sumits, S. Jain, U. Andra, and T. Khurana, "Cisco Visual Networking Index (VNI) Complete IP Traffic & Service Adoption Forecasts Global Update, 2014–2019".

- [10] R. Azim, M. T. Islam, and N. Misran, "Microstrip Line-fed Printed Planar Monopole Antenna for UWB Applications," *Arab. J. Sci. Eng.*, vol. 38, no. 9, pp. 2415–2422, Sep. 2013, doi: 10.1007/s13369-013-0553-x.
- [11] Y. Ding, Z. Du, K. Gong, and Z. Feng, "A novel dual-band printed diversity antenna for mobile terminals," *IEEE Trans. Antennas Propag.*, vol. 55, no. 7, pp. 2088–2096, 2007.
- [12] J.-W. Wu, H.-M. Hsiao, J.-H. Lu, and S.-H. Chang, "Dual broadband design of rectangular slot antenna for 2.4 and 5 GHz wireless communication," *Electron. Lett.*, vol. 40, no. 23, pp. 1461–1463, 2004.
- [13] M. J. Ammann and Z. N. Chen, "A wide-band shorted planar monopole with bevel," *IEEE Trans. Antennas Propag.*, vol. 51, no. 4, pp. 901–903, Apr. 2003, doi: 10.1109/TAP.2003.811061.
- [14] Q. C. Li, H. Niu, A. T. Papathanassiou, and G. Wu, "5G network capacity: Key elements and technologies," *IEEE Veh. Technol. Mag.*, vol. 9, no. 1, pp. 71–78, 2014.
- [15] S. Sinha, B. Rana, C. K. Ghosh, and S. K. Parui, "A CPW-Fed Microstrip Antenna for WLAN Application," *Procedia Technol.*, vol. 4, pp. 417–420, Jan. 2012, doi: 10.1016/j.protcy.2012.05.065.
- [16] C.-Y. Pan, T.-S. Horng, W.-S. Chen, and C.-H. Huang, "Dual wideband printed monopole antenna for WLAN/WiMAX applications," *IEEE Antennas Wirel. Propag. Lett.*, vol. 6, pp. 149–151, 2007.
- [17] R. Karli and H. Ammor, "Rectangular Patch Antenna for Dual-Band RFID and WLAN Applications," *Wirel. Pers. Commun.*, vol. 83, no. 2, pp. 995–1007, Jul. 2015, doi: 10.1007/s11277-015-2436-9.
- [18] J.-Y. Jan, C.-Y. Pan, K.-Y. Chiu, and H.-M. Chen, "Broadband CPW-fed circularly-polarized slot antenna with an open slot," *IEEE Trans. Antennas Propag.*, vol. 61, no. 3, pp. 1418–1422, 2012.
- [19] D. Wen, Y. Hao, H. Wang, and H. Zhou, "Design of a wideband antenna with stable omnidirectional radiation pattern using the theory of characteristic modes," *IEEE Trans. Antennas Propag.*, vol. 65, no. 5, pp. 2671–2676, 2017.

- [20] J. Joubert, J. C. Vardaxoglou, W. G. Whittow, and J. W. Odendaal, "CPW-fed cavity-backed slot radiator loaded with an AMC reflector," *IEEE Trans. Antennas Propag.*, vol. 60, no. 2, pp. 735–742, 2011.
- [21] A. Bagwari, R. Tiwari, and V. S. Kushwah, "CPW-Fed micro-strip patch antenna for wireless communication," in *2020 Global Conference on Wireless and optical technologies (GCWOT)*, IEEE, 2020, pp. 1–5. Accessed: Aug. 14, 2024. [Online]. Available: <https://ieeexplore.ieee.org/abstract/document/9391602/>
- [22] C. A. Balanis, *Antenna theory: analysis and design*. John wiley & sons, 2016. Accessed: Aug. 13, 2024. [Online]. Available: https://books.google.com/books?hl=en&lr=&id=iFEBCgAAQBAJ&oi=fnd&pg=PR13&dq=Antenna+Theory:+Analysis+and+Design&ots=Cm-_srQ7wn&sig=3pXSlrUoAKSqfjhdIAoSmIPs88
- [23] Z. H. Jiang, D. E. Brocker, P. E. Sieber, and D. H. Werner, "A compact, low-profile metasurface-enabled antenna for wearable medical body-area network devices," *IEEE Trans. Antennas Propag.*, vol. 62, no. 8, pp. 4021–4030, 2014.
- [24] S. Ghosh, T.-N. Tran, and T. Le-Ngoc, "A dual-layer EBG-based miniaturized patch multi-antenna structure," in *2011 IEEE International Symposium on Antennas and Propagation (APSURSI)*, IEEE, 2011, pp. 1828–1831. Accessed: Aug. 13, 2024. [Online]. Available: <https://ieeexplore.ieee.org/abstract/document/5996852/>
- [25] Y.-S. Chen and T.-Y. Ku, "A low-profile wearable antenna using a miniature high impedance surface for smartwatch applications," *IEEE Antennas Wirel. Propag. Lett.*, vol. 15, pp. 1144–1147, 2015.
- [26] J. Zuo, X. Chen, G. Han, L. Li, and W. Zhang, "An integrated approach to RF antenna-filter co-design," *IEEE Antennas Wirel. Propag. Lett.*, vol. 8, pp. 141–144, 2009.
- [27] D. Wen, Y. Hao, H. Wang, and H. Zhou, "Design of a wideband antenna with stable omnidirectional radiation pattern using the theory of characteristic modes," *IEEE Trans. Antennas Propag.*, vol. 65, no. 5, pp. 2671–2676, 2017.

- [28] S. B. Yeap and Z. N. Chen, "Microstrip patch antennas with enhanced gain by partial substrate removal," *IEEE Trans. Antennas Propag.*, vol. 58, no. 9, pp. 2811–2816, 2010.
- [29] N.-W. Liu, L. Zhu, and W.-W. Choi, "A differential-fed microstrip patch antenna with bandwidth enhancement under operation of TM₁₀ and TM₃₀ modes," *IEEE Trans. Antennas Propag.*, vol. 65, no. 4, pp. 1607–1614, 2017.
- [30] J. Wu, Z. Zhao, Z. Nie, and Q.-H. Liu, "A printed unidirectional antenna with improved upper band-edge selectivity using a parasitic loop," *IEEE Trans. Antennas Propag.*, vol. 63, no. 4, pp. 1832–1837, 2015.
- [31] T. O. Olawoye and P. Kumar, "A high gain microstrip patch antenna with slotted ground plane for sub-6 GHz 5G communications," in *2020 International Conference on Artificial Intelligence, Big Data, Computing and Data Communication Systems (icABCD)*, IEEE, 2020, pp. 1–6. Accessed: Aug. 13, 2024. [Online]. Available: <https://ieeexplore.ieee.org/abstract/document/9183820/>
- [32] Q. L. Li, S. W. Cheung, D. Wu, and T. I. Yuk, "Microwave lens using periodic dielectric sheets for antenna-gain enhancement," *IEEE Trans. Antennas Propag.*, vol. 65, no. 4, pp. 2068–2073, 2017.
- [33] A. Zaidi, A. Baghdad, A. Ballouk, and A. Badri, "High gain microstrip patch antenna, with PBG substrate and PBG cover, for millimeter wave applications," in *2018 4th International Conference on Optimization and Applications (ICOA)*, IEEE, 2018, pp. 1–6. Accessed: Aug. 13, 2024. [Online]. Available: <https://ieeexplore.ieee.org/abstract/document/8370528/>
- [34] Y. Li and J. Chen, "Improved High Gain Miniaturized Bow-Tie Antenna with AMC," in *2020 IEEE MTT-S International Conference on Numerical Electromagnetic and Multiphysics Modeling and Optimization (NEMO)*, IEEE, 2020, pp. 1–4. Accessed: Aug. 13, 2024. [Online]. Available: <https://ieeexplore.ieee.org/abstract/document/9343523/>
- [35] A. Y. Grinev and A. A. Izmaylov, "Dual-Band Antenna System Based on a Metastructure with the Property of an Artificial Magnetic Conductor," in *2021 Systems*

- of Signals Generating and Processing in the Field of on Board Communications, IEEE, 2021, pp. 1–4. Accessed: Aug. 13, 2024. [Online]. Available: <https://ieeexplore.ieee.org/abstract/document/9416054/>
- [36] E. G. Larsson, O. Edfors, F. Tufvesson, and T. L. Marzetta, “Massive MIMO for next generation wireless systems,” *IEEE Commun. Mag.*, vol. 52, no. 2, pp. 186–195, Feb. 2014, doi: 10.1109/MCOM.2014.6736761.
- [37] M. A. Jensen and J. W. Wallace, “A review of antennas and propagation for MIMO wireless communications,” *IEEE Trans. Antennas Propag.*, vol. 52, no. 11, pp. 2810–2824, Nov. 2004, doi: 10.1109/TAP.2004.835272.
- [38] L. Zhao and K.-L. Wu, “A Dual-Band Coupled Resonator Decoupling Network for Two Coupled Antennas,” *IEEE Trans. Antennas Propag.*, vol. 63, no. 7, pp. 2843–2850, Jul. 2015, doi: 10.1109/TAP.2015.2421973.
- [39] Y. Wang and Z. Du, “A Wideband Printed Dual-Antenna System With a Novel Neutralization Line for Mobile Terminals,” *IEEE Antennas Wirel. Propag. Lett.*, vol. 12, pp. 1428–1431, 2013, doi: 10.1109/LAWP.2013.2287199.
- [40] J.-Y. Chung, T. Yang, and J. Lee, “Low correlation MIMO antennas with negative group delay,” *Prog. Electromagn. Res. C*, vol. 22, pp. 151–163, 2011.
- [41] M. S. Khan, M. F. Shafique, A. Naqvi, A.-D. Capobianco, B. Ijaz, and B. D. Braaten, “A miniaturized dual-band MIMO antenna for WLAN applications,” *IEEE Antennas Wirel. Propag. Lett.*, vol. 14, pp. 958–961, 2015.
- [42] R. Karimian, A. Kesavan, M. Nedil, and T. A. Denidni, “Low-mutual-coupling 60-GHz MIMO antenna system with frequency selective surface wall,” *IEEE Antennas Wirel. Propag. Lett.*, vol. 16, pp. 373–376, 2016.
- [43] Z. Wang, L. Zhao, Y. Cai, S. Zheng, and Y. Yin, “A meta-surface antenna array decoupling (MAAD) method for mutual coupling reduction in a MIMO antenna system,” *Sci. Rep.*, vol. 8, no. 1, p. 3152, 2018.
- [44] M. S. Khan, A.-D. Capobianco, S. M. Asif, D. E. Anagnostou, R. M. Shubair, and B. D. Braaten, “A compact CSRR-enabled UWB diversity antenna,” *IEEE Antennas Wirel. Propag. Lett.*, vol. 16, pp. 808–812, 2016.

- [45] F. Liu, J. Guo, L. Zhao, X. Shen, and Y. Yin, "A Meta-Surface Decoupling Method for Two Linear Polarized Antenna Array in Sub-6 GHz Base Station Applications," *IEEE Access*, vol. 7, pp. 2759–2768, 2019, doi: 10.1109/ACCESS.2018.2886641.
- [46] S. Blanch, J. Romeu, and I. Corbella, "Exact representation of antenna system diversity performance from input parameter description," *Electron. Lett.*, vol. 39, no. 9, pp. 705–707, 2003.
- [47] S. M. Mikki and Y. M. Antar, "On cross correlation in antenna arrays with applications to spatial diversity and MIMO systems," *IEEE Trans. Antennas Propag.*, vol. 63, no. 4, pp. 1798–1810, 2015.
- [48] M. S. Sharawi, A. T. Hassan, and M. U. Khan, "Correlation coefficient calculations for MIMO antenna systems: A comparative study," *Int. J. Microw. Wirel. Technol.*, vol. 9, no. 10, pp. 1991–2004, 2017.
- [49] M. S. Sharawi, "Current misuses and future prospects for printed multiple-input, multiple-output antenna systems [wireless corner]," *IEEE Antennas Propag. Mag.*, vol. 59, no. 2, pp. 162–170, 2017.
- [50] S. Soltani, P. Lotfi, and R. D. Murch, "A dual-band multiport MIMO slot antenna for WLAN applications," *IEEE Antennas Wirel. Propag. Lett.*, vol. 16, pp. 529–532, 2016.
- [51] M. S. Sharawi, A. B. Numan, M. U. Khan, and D. N. Aloï, "A dual-element dual-band MIMO antenna system with enhanced isolation for mobile terminals," *IEEE Antennas Wirel. Propag. Lett.*, vol. 11, pp. 1006–1009, 2012.
- [52] Z. Niu, H. Zhang, Q. Chen, and T. Zhong, "Isolation enhancement in closely coupled dual-band MIMO patch antennas," *IEEE Antennas Wirel. Propag. Lett.*, vol. 18, no. 8, pp. 1686–1690, 2019.
- [53] K. S. Vishvakshenan, K. Mithra, R. Kalaiarasan, and K. S. Raj, "Mutual coupling reduction in microstrip patch antenna arrays using parallel coupled-line resonators," *IEEE Antennas Wirel. Propag. Lett.*, vol. 16, pp. 2146–2149, 2017.
- [54] A. Boukarkar, X. Q. Lin, Y. Jiang, L. Y. Nie, P. Mei, and Y. Q. Yu, "A miniaturized extremely close-spaced four-element dual-band MIMO antenna system with

polarization and pattern diversity,” *IEEE Antennas Wirel. Propag. Lett.*, vol. 17, no. 1, pp. 134–137, 2017.

[55] B. L. Dhevi, K. S. Vishvakshenan, and K. Rajakani, “Isolation enhancement in dual-band microstrip antenna array using asymmetric loop resonator,” *IEEE Antennas Wirel. Propag. Lett.*, vol. 17, no. 2, pp. 238–241, 2017.

[56] J. Deng, J. Li, L. Zhao, and L. Guo, “A dual-band inverted-F MIMO antenna with enhanced isolation for WLAN applications,” *IEEE Antennas Wirel. Propag. Lett.*, vol. 16, pp. 2270–2273, 2017.

[57] F. Liu, J. Guo, L. Zhao, G.-L. Huang, Y. Li, and Y. Yin, “Dual-band metasurface-based decoupling method for two closely packed dual-band antennas,” *IEEE Trans. Antennas Propag.*, vol. 68, no. 1, pp. 552–557, 2019.

[58] J. G. Andrews et al., “What will 5G be?,” *IEEE J. Sel. Areas Commun.*, vol. 32, no. 6, pp. 1065–1082, 2014.

[59] U. Banerjee, A. Karmakar, and A. Saha, “A review on circularly polarized antennas, trends and advances,” *Int. J. Microw. Wirel. Technol.*, vol. 12, no. 9, pp. 922–943, 2020.

[60] M. Samsuzzaman and M. T. Islam, “Circularly polarized broadband printed antenna for wireless applications,” *Sensors*, vol. 18, no. 12, p. 4261, 2018.

[61] J. Kulkarni, A. Desai, and C. Sim, “Two port CPW-fed MIMO antenna with wide bandwidth and high isolation for future wireless applications,” *Int. J. RF Microw. Comput.-Aided Eng.*, vol. 31, no. 8, Aug. 2021, doi: 10.1002/mmce.22700.

[62] N. O. Parchin, H. J. Basherlou, and R. A. Abd-Alhameed, “Dual circularly polarized crescent-shaped slot antenna for 5G front-end systems,” *Prog. Electromagn. Res. Lett.*, vol. 91, pp. 41–48, 2020.

[63] H. H. Tran, N. Hussain, and T. T. Le, “Low-profile wideband circularly polarized MIMO antenna with polarization diversity for WLAN applications,” *AEU-Int. J. Electron. Commun.*, vol. 108, pp. 172–180, 2019.

- [64] M. Jalali, M. Naser-Moghadasi, and R. A. Sadeghzadeh, "Dual circularly polarized multilayer MIMO antenna array with an enhanced SR-feeding network for C-band application," *Int. J. Microw. Wirel. Technol.*, vol. 9, no. 8, pp. 1741–1748, 2017.
- [65] L. Malviya, R. K. Panigrahi, and M. Kartikeyan, "Circularly polarized 2\times 2 MIMO antenna for WLAN applications," *Prog. Electromagn. Res. C*, vol. 66, pp. 97–107, 2016.
- [66] A. K. Singh, S. K. Mahto, and R. Sinha, "Quad element MIMO antenna for LTE/5G (sub-6 GHz) applications," *J. Electromagn. Waves Appl.*, vol. 36, no. 16, pp. 2357–2372, Nov. 2022, doi: 10.1080/09205071.2022.2076618.
- [67] S. S. Singhwal, B. K. Kanaujia, A. Singh, J. Kishor, and L. Matekovits, "Multiple input multiple output dielectric resonator antenna with circular polarized adaptability for 5G applications," *J. Electromagn. Waves Appl.*, vol. 34, no. 9, pp. 1180–1194, Jun. 2020, doi: 10.1080/09205071.2020.1730984.
- [68] A. K. Dwivedi, A. Sharma, A. K. Pandey, and V. Singh, "Two Port Circularly Polarized MIMO Antenna Design and Investigation for 5G Communication Systems," *Wirel. Pers. Commun.*, vol. 120, no. 3, pp. 2085–2099, Oct. 2021, doi: 10.1007/s11277-021-08461-9.
- [69] S. Saxena, B. K. Kanaujia, S. Dwari, S. Kumar, and R. Tiwari, "MIMO antenna with built-in circular shaped isolator for sub-6 GHz 5G applications," *Electron. Lett.*, vol. 54, no. 8, pp. 478–480, Apr. 2018, doi: 10.1049/el.2017.4514.
- [70] R. N. Tiwari, P. Singh, B. K. Kanaujia, and P. Kumar, "Compact circularly polarized MIMO printed antenna with novel ground structure for wideband applications," *Int. J. RF Microw. Comput.-Aided Eng.*, vol. 31, no. 8, Aug. 2021, doi: 10.1002/mmce.22737.
- [71] A. Kumar, A. Q. Ansari, B. K. Kanaujia, J. Kishor, and L. Matekovits, "A review on different techniques of mutual coupling reduction between elements of any MIMO antenna. Part 1: DGSs and parasitic structures," *Radio Sci.*, vol. 56, no. 3, pp. 1–25, 2021.

- [72] A. Kumar, A. Q. Ansari, B. K. Kanaujia, J. Kishor, and L. Matekovits, "A review on different techniques of mutual coupling reduction between elements of any MIMO antenna. Part 1: DGSs and parasitic structures," *Radio Sci.*, vol. 56, no. 3, pp. 1–25, 2021.
- [73] M. Ameen, O. Ahmad, and R. K. Chaudhary, "Single split-ring resonator loaded self-decoupled dual-polarized MIMO antenna for mid-band 5G and C-band applications," *AEU-Int. J. Electron. Commun.*, vol. 124, p. 153336, 2020.
- [74] N. Agrawal, M. Gupta, and S. Chouhan, "Modified ground and slotted MIMO antennas for 5G sub-6 GHz frequency bands," *Int. J. Microw. Wirel. Technol.*, vol. 15, no. 5, pp. 817–825, 2023.
- [75] R. K. Jaiswal, K. Kumari, A. K. Ojha, and K. V. Srivastava, "Five-port MIMO antenna for n79-5G band with improved isolation by diversity and decoupling techniques," *J. Electromagn. Waves Appl.*, vol. 36, no. 4, pp. 542–556, Mar. 2022, doi: 10.1080/09205071.2021.1975315.
- [76] G. Liu, C. Zhang, Z. Chen, and B. Chen, "A compact dual band MIMO antenna for 5G/WLAN applications," *Int. J. Microw. Wirel. Technol.*, vol. 14, no. 10, pp. 1347–1352, 2022.
- [77] T. Kumari, G. Das, A. Sharma, and R. K. Gangwar, "Design approach for dual element hybrid MIMO antenna arrangement for wideband applications," *Int. J. RF Microw. Comput.-Aided Eng.*, vol. 29, no. 1, p. e21486, Jan. 2019, doi: 10.1002/mmce.21486.
- [78] S. Rajkumar, N. Vivek Sivaraman, S. Murali, and K. T. Selvan, "Heptaband swastik arm antenna for MIMO applications," *IET Microw. Antennas Propag.*, vol. 11, no. 9, pp. 1255–1261, Jul. 2017, doi: 10.1049/iet-map.2016.1098.
- [79] M. A. Abdelghany, A. A. Ibrahim, H. A. Mohamed, and E. Tammam, "Compact sub-6 GHz four-element flexible antenna for 5G applications," *Electronics*, vol. 13, no. 3, p. 537, 2024.
- [80] H. T. Chattha, "4-port 2-element MIMO antenna for 5G portable applications," *IEEE Access*, vol. 7, pp. 96516–96520, 2019.

- [81] Z. Zhang, *Antenna design for mobile devices*. John Wiley & Sons, 2017. Accessed: Aug. 16, 2024. [Online]. Available: https://books.google.com/books?hl=en&lr=&id=tKJtDgAAQBAJ&oi=fnd&pg=PP10&dq=Antenna+Design+for+Mobile+Devices&ots=Rp9CUELSdq&sig=ZaSjbMDIE8waVqdev_Ga_UFRHLU
- [82] H. Li and B. K. Lau, "MIMO systems and antennas for terminals," in *Handbook of Antenna Technologies*, Springer, 2016, pp. 2347–2388. Accessed: Aug. 16, 2024. [Online]. Available: <https://portal.research.lu.se/en/publications/mimo-systems-and-antennas-for-terminals>
- [83] S. Roy, S. Ghosh, S. S. Pattanayak, and U. Chakarborty, "Dual-polarized textile-based two/four element MIMO antenna with improved isolation for dual wideband application," *Int. J. RF Microw. Comput.-Aided Eng.*, vol. 30, no. 9, Sep. 2020, doi: 10.1002/mmce.22292.
- [84] K. Srivastava, A. Kumar, B. K. Kanaujia, S. Dwari, and S. Kumar, "A CPW-fed UWB MIMO antenna with integrated GSM band and dual band notches," *Int. J. RF Microw. Comput.-Aided Eng.*, vol. 29, no. 1, p. e21433, Jan. 2019, doi: 10.1002/mmce.21433.
- [85] M. Li, Z. Xu, Y. Ban, C. Sim, and Z. Yu, "Eight-port orthogonally dual-polarised MIMO antennas using loop structures for 5G smartphone," *IET Microw. Antennas Propag.*, vol. 11, no. 12, pp. 1810–1816, Sep. 2017, doi: 10.1049/iet-map.2017.0230.
- [86] M. Shehata, M. S. Said, and H. Mostafa, "Dual notched band quad-element MIMO antenna with multitone interference suppression for IR-UWB wireless applications," *IEEE Trans. Antennas Propag.*, vol. 66, no. 11, pp. 5737–5746, 2018.
- [87] K.-L. Wong, J.-Y. Lu, L.-Y. Chen, W.-Y. Li, and Y.-L. Ban, "8-antenna and 16-antenna arrays using the quad-antenna linear array as a building block for the 3.5-GHz LTE MIMO operation in the smartphone," *Microw. Opt. Technol. Lett.*, vol. 58, no. 1, pp. 174–181, Jan. 2016, doi: 10.1002/mop.29527.

- [88] M. Saravanan, R. Kalidoss, B. Partibane, and K. S. Vishvaksenan, "Design of an interlocked four-port MIMO antenna for UWB automotive communications," *Int. J. Microw. Wirel. Technol.*, vol. 14, no. 2, pp. 239–246, 2022.
- [89] K.-L. Wong, C.-Y. Tsai, and J.-Y. Lu, "Two asymmetrically mirrored gap-coupled loop antennas as a compact building block for eight-antenna MIMO array in the future smartphone," *IEEE Trans. Antennas Propag.*, vol. 65, no. 4, pp. 1765–1778, 2017.
- [90] Z. Ren, A. Zhao, and S. Wu, "MIMO antenna with compact decoupled antenna pairs for 5G mobile terminals," *IEEE Antennas Wirel. Propag. Lett.*, vol. 18, no. 7, pp. 1367–1371, 2019.
- [91] C. Deng, D. Liu, and X. Lv, "Tightly arranged four-element MIMO antennas for 5G mobile terminals," *IEEE Trans. Antennas Propag.*, vol. 67, no. 10, pp. 6353–6361, 2019.
- [92] L. Sun, H. Feng, Y. Li, and Z. Zhang, "Tightly arranged orthogonal mode antenna for 5G MIMO mobile terminal," *Microw. Opt. Technol. Lett.*, vol. 60, no. 7, pp. 1751–1756, Jul. 2018, doi: 10.1002/mop.31240.
- [93] L. Sun, H. Feng, Y. Li, and Z. Zhang, "Compact 5G MIMO mobile phone antennas with tightly arranged orthogonal-mode pairs," *IEEE Trans. Antennas Propag.*, vol. 66, no. 11, pp. 6364–6369, 2018.
- [94] L. Chang, Y. Yu, K. Wei, and H. Wang, "Polarization-orthogonal co-frequency dual antenna pair suitable for 5G MIMO smartphone with metallic bezels," *IEEE Trans. Antennas Propag.*, vol. 67, no. 8, pp. 5212–5220, 2019.
- [95] R. Pandeewari and S. Raghavan, "A CPW -fed triple band OCSRR embedded monopole antenna with modified ground for WLAN and WIMAX applications," *Microw. Opt. Technol. Lett.*, vol. 57, no. 10, pp. 2413–2418, Oct. 2015, doi: 10.1002/mop.29352.
- [96] A. Karimbu Vallappil, B. A. Khawaja, I. Khan, and M. Mustaqim, "Dual-band Minkowski–Sierpinski fractal antenna for next generation satellite communications and wireless body area networks," *Microw. Opt. Technol. Lett.*, vol. 60, no. 1, pp. 171–178, Jan. 2018, doi: 10.1002/mop.30931.

- [97] J. Guo, L. Cui, C. Li, and B. Sun, "Side-edge frame printed eight-port dual-band antenna array for 5G smartphone applications," *IEEE Trans. Antennas Propag.*, vol. 66, no. 12, pp. 7412–7417, 2018.
- [98] K. G. Sujanth Narayan, J. A. Baskaradas, and D. Rajesh Kumar, "Design of a CPW-Fed Compact MIMO Antenna for Next Generation Vehicle to Everything (V2X) Communication," *Wirel. Pers. Commun.*, vol. 120, no. 3, pp. 2179–2200, Oct. 2021, doi: 10.1007/s11277-021-08922-1.
- [99] G. Li, H. Zhai, Z. Ma, C. Liang, R. Yu, and S. Liu, "Isolation-improved dual-band MIMO antenna array for LTE/WiMAX mobile terminals," *IEEE Antennas Wirel. Propag. Lett.*, vol. 13, pp. 1128–1131, 2014.
- [100] D. Thangarasu, S. K. Palaniswamy, and R. R. Thipparaju, "Quad Port Multipolarized Reconfigurable MIMO Antenna for Sub 6 GHz Applications," *Int. J. Antennas Propag.*, vol. 2023, pp. 1–17, Mar. 2023, doi: 10.1155/2023/8882866.
- [101] P. Kumar, S. Urooj, and F. Alrowais, "Design and implementation of quad-port MIMO antenna with dual-band elimination characteristics for ultra-wideband applications," *Appl. Sci.*, vol. 10, no. 5, p. 1715, 2020.
- [102] A. A. Ibrahim, M. I. Ahmed, and M. F. Ahmed, "A systematic investigation of four ports MIMO antenna depending on flexible material for UWB networks," *Sci. Rep.*, vol. 12, no. 1, p. 14351, 2022.
- [103] R. Hussain and M. S. Sharawi, "An integrated slot-based frequency-agile and UWB multifunction MIMO antenna system," *IEEE Antennas Wirel. Propag. Lett.*, vol. 18, no. 10, pp. 2150–2154, 2019.
- [104] H. T. Chattha, "4-port 2-element MIMO antenna for 5G portable applications," *IEEE Access*, vol. 7, pp. 96516–96520, 2019.
- [105] A. Biswas and V. R. Gupta, "Design and Development of Low Profile MIMO Antenna for 5G New Radio Smartphone Applications," *Wirel. Pers. Commun.*, vol. 111, no. 3, pp. 1695–1706, Apr. 2020, doi: 10.1007/s11277-019-06949-z.
- [106] K. Yan, P. Yang, F. Yang, L. Y. Zeng, and S. Huang, "Eight-antenna array in the 5G smartphone for the dual-band MIMO system," in 2018 IEEE International Symposium

- on Antennas and Propagation & USNC/URSI National Radio Science Meeting, IEEE, 2018, pp. 41–42. Accessed: Aug. 16, 2024. [Online]. Available: <https://ieeexplore.ieee.org/abstract/document/8608394/>
- [107] G. Wei and Q. Feng, “Dual-band MIMO antenna array for compact 5G smartphones,” *Prog. Electromagn. Res. C*, vol. 99, pp. 157–165, 2020.
- [108] J. Kulkarni, A. G. Alharbi, I. Elfergani, J. Anguera, C. Zebiri, and J. Rodriguez, “Dual polarized, multiband four-port decagon shaped flexible MIMO antenna for next generation wireless applications,” *IEEE Access*, vol. 10, pp. 128132–128150, 2022.
- [109] A. Armghan, S. Lavadiya, P. Udayaraju, M. Alsharari, K. Aliqab, and S. K. Patel, “Sickle-shaped high gain and low profile based four port MIMO antenna for 5G and aeronautical mobile communication,” *Sci. Rep.*, vol. 13, no. 1, p. 15700, 2023.
- [110] N. P. Kulkarni, N. B. Bahadure, P. D. Patil, and J. S. Kulkarni, “Flexible interconnected 4-port MIMO antenna for sub-6 GHz 5G and X band applications,” *AEU-Int. J. Electron. Commun.*, vol. 152, p. 154243, 2022.
- [111] T. Upadhyaya et al., “Quad-port MIMO antenna with high isolation characteristics for sub 6-GHz 5G NR communication,” *Sci. Rep.*, vol. 13, no. 1, p. 19088, 2023.
- [112] N. Sheriff, S. Kamal, H. Tariq Chattha, T. Kim Geok, and B. A. Khawaja, “Compact wideband four-port MIMO Antenna for Sub-6 GHz and internet of things applications,” *Micromachines*, vol. 13, no. 12, p. 2202, 2022.
- [113] J. Kulkarni, B. Garner, and Y. Li, “A dual-CP quad-port MIMO antenna with reduced mutual coupling for X-band application,” *IEEE Antennas Wirel. Propag. Lett.*, vol. 22, no. 9, pp. 2085–2089, 2023.
- [114] M. A. Abdelghany, A. A. Ibrahim, H. A. Mohamed, and E. Tammam, “Compact sub-6 GHz four-element flexible antenna for 5G applications,” *Electronics*, vol. 13, no. 3, p. 537, 2024.
- [115] J. Kulkarni, A. Desai, and C.-Y. D. Sim, “Wideband four-port MIMO antenna array with high isolation for future wireless systems,” *AEU-Int. J. Electron. Commun.*, vol. 128, p. 153507, 2021.

- [116] M. A. Salamin, A. Zugari, M. Alibakhshikenari, C. H. See, R. Abd-Alhameed, and E. Limiti, "Compact highly isolated dual-band 4-port MIMO antenna for sub-6 GHz applications," *J. Electromagn. Waves Appl.*, vol. 37, no. 10–12, pp. 1023–1043, Aug. 2023, doi: 10.1080/09205071.2023.2220145.
- [117] M. A. Jensen and J. W. Wallace, "A review of antennas and propagation for MIMO wireless communications," *IEEE Trans. Antennas Propag.*, vol. 52, no. 11, pp. 2810–2824, 2004.
- [118] S. S. Singhwal, B. K. Kanaujia, A. Singh, and J. Kishor, "Dual-port MIMO dielectric resonator antenna for WLAN applications," *Int. J. RF Microw. Comput.-Aided Eng.*, vol. 30, no. 4, Apr. 2020, doi: 10.1002/mmce.22108.
- [119] I. Adam et al., "Mutual coupling reduction of a wideband circularly polarized microstrip MIMO antenna," *IEEE Access*, vol. 7, pp. 97838–97845, 2019.
- [120] L. Malviya, R. K. Panigrahi, and M. V. Kartikeyan, "MIMO antennas with diversity and mutual coupling reduction techniques: a review," *Int. J. Microw. Wirel. Technol.*, vol. 9, no. 8, pp. 1763–1780, 2017.
- [121] X. Chen, S. Zhang, and Q. Li, "A review of mutual coupling in MIMO systems," *Ieee Access*, vol. 6, pp. 24706–24719, 2018.
- [122] S. Padmanathan et al., "Compact multiband reconfigurable MIMO antenna for sub-6GHz 5G mobile terminal," *IEEE Access*, vol. 10, pp. 60241–60252, 2022.
- [123] T. Addepalli and V. R. Anitha, "Compact two-port MIMO antenna with high isolation using parasitic reflectors for UWB, X and Ku band applications," *Prog. Electromagn. Res. C*, vol. 102, pp. 63–77, 2020.
- [124] P. Ranjan, M. Patil, S. Chand, A. Ranjan, S. Singh, and A. Sharma, "Investigation on dual-port printed MIMO antenna with reduced RCS for C-band radar application," *Int. J. RF Microw. Comput.-Aided Eng.*, vol. 30, no. 3, Mar. 2020, doi: 10.1002/mmce.22092.
- [125] J. Kulkarni, A. Desai, and C. Sim, "Two port CPW-fed MIMO antenna with wide bandwidth and high isolation for future wireless applications," *Int. J. RF Microw. Comput.-Aided Eng.*, vol. 31, no. 8, Aug. 2021, doi: 10.1002/mmce.22700.

- [126] Y. Dou, Z. Chen, J. Bai, Q. Cai, and G. Liu, “Two-Port CPW-Fed Dual-Band MIMO Antenna for IEEE 802.11 a/b/g Applications,” *Int. J. Antennas Propag.*, vol. 2021, pp. 1–8, Jun. 2021, doi: 10.1155/2021/5572887.
- [127] H. Li and B. K. Lau, “MIMO systems and antennas for terminals,” in *Handbook of Antenna Technologies*, Springer, 2016, pp. 2347–2388. Accessed: Aug. 17, 2024. [Online]. Available: <https://portal.research.lu.se/en/publications/mimo-systems-and-antennas-for-terminals>
- [128] Z. Zhang, *Antenna design for mobile devices*. John Wiley & Sons, 2017. Accessed: Aug. 17, 2024. [Online]. Available: https://books.google.com/books?hl=en&lr=&id=tKJtDgAAQBAJ&oi=fnd&pg=PP10&dq=12.%09Z.+Zhang,+Antenna+Design+for+Mobile+Devices.+John+Wiley+%26+Sons,+2017.&ots=Rp9CUKOXfn&sig=K__I3nM-KW18APch-KpB5250yeo
- [129] L. Sun, Y. Li, Z. Zhang, and H. Wang, “Self-decoupled MIMO antenna pair with shared radiator for 5G smartphones,” *IEEE Trans. Antennas Propag.*, vol. 68, no. 5, pp. 3423–3432, 2020.
- [130] Z. Zhou, Y. Ge, J. Yuan, Z. Xu, and Z. D. Chen, “Wideband MIMO antennas with enhanced isolation using coupled CPW transmission lines,” *IEEE Trans. Antennas Propag.*, vol. 71, no. 2, pp. 1414–1423, 2023.
- [131] L. Sun, Y. Li, Z. Zhang, and H. Wang, “Antenna decoupling by common and differential modes cancellation,” *IEEE Trans. Antennas Propag.*, vol. 69, no. 2, pp. 672–682, 2020.
- [132] K.-L. Wong, C.-Y. Tsai, and J.-Y. Lu, “Two asymmetrically mirrored gap-coupled loop antennas as a compact building block for eight-antenna MIMO array in the future smartphone,” *IEEE Trans. Antennas Propag.*, vol. 65, no. 4, pp. 1765–1778, 2017.
- [133] A. M. Saadh, K. Ashwath, P. Ramaswamy, T. Ali, and J. Anguera, “A uniquely shaped MIMO antenna on FR4 material to enhance isolation and bandwidth for wireless applications,” *AEU-Int. J. Electron. Commun.*, vol. 123, p. 153316, 2020.

- [134] G. Li, H. Zhai, Z. Ma, C. Liang, R. Yu, and S. Liu, "Isolation-improved dual-band MIMO antenna array for LTE/WiMAX mobile terminals," *IEEE Antennas Wirel. Propag. Lett.*, vol. 13, pp. 1128–1131, 2014.
- [135] K. Srivastava, A. Kumar, B. K. Kanaujia, S. Dwari, and S. Kumar, "A CPW-fed UWB MIMO antenna with integrated GSM band and dual band notches," *Int. J. RF Microw. Comput.-Aided Eng.*, vol. 29, no. 1, p. e21433, Jan. 2019, doi: 10.1002/mmce.21433.
- [136] D. Thangarasu, S. K. Palaniswamy, and R. R. Thipparaju, "Quad Port Multipolarized Reconfigurable MIMO Antenna for Sub 6 GHz Applications," *Int. J. Antennas Propag.*, vol. 2023, pp. 1–17, Mar. 2023, doi: 10.1155/2023/8882866.
- [137] K. G. Sujanth Narayan, J. A. Baskaradas, and D. Rajesh Kumar, "Design of a CPW-Fed Compact MIMO Antenna for Next Generation Vehicle to Everything (V2X) Communication," *Wirel. Pers. Commun.*, vol. 120, no. 3, pp. 2179–2200, Oct. 2021, doi: 10.1007/s11277-021-08922-1.
- [138] N. Sharma, A. Kumar, A. De, and R. K. Jain, "Isolation enhancement using CSRR slot in the ground for compact two-element textile MIMO antenna," *Appl. Comput. Electromagn. Soc. J. ACES*, pp. 535–545, 2022.
- [139] P. Sharma, R. N. Tiwari, P. Singh, and B. K. Kanaujia, "Dual-band trident shaped MIMO antenna with novel ground plane for 5G applications," *AEU-Int. J. Electron. Commun.*, vol. 155, p. 154364, 2022.
- [140] B. Bayarzaya et al., "A compact MIMO antenna with improved isolation for ISM, sub-6 GHz, and WLAN application," *Micromachines*, vol. 13, no. 8, p. 1355, 2022.